ENERGY-BALANCE MODELS OF THE SOLAR CORONA

M. A. Wragg

A Thesis Submitted for the Degree of PhD
at the
University of St Andrews

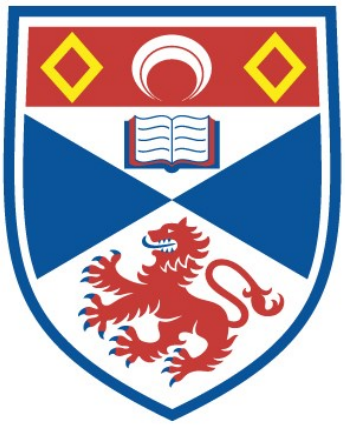

1982

ENERGY-BALANCE MODELS OF THE SOLAR CORONA

M. A. WRAGG

THESIS SUBMITTED FOR THE DEGREE OF DOCTOR OF PHILOSOPHY

OF THE UNIVERSITY OF ST. ANDREWS

ENERGY-BALANCE MODELS OF THE SOLAR CORONA

ABSTRACT

Solar coronal observations have shown that the corona has a highly complex structure which pressumably owes its existence to the magnetic field. Models in thermal and hydrostatic equilibrium are here calculated in order to try and explain many of these observations.

Coronal holes occur where open field lines reach out into space. The model of McWhirter, et al. (1975) for the inner corona in such a configuration is generalised to allow different types and magnitudes of heating as well as different area divergences and flows. It is found that hot, fast upflows cannot always exist in thermal equilibrium. The choice of boundary conditions can appreciably alter the results, and so different choices are compared.

Most of the corona, especially in active regions, appears to consist of coronal loops. Subtle relations for energy balance models of such loops are found to exist between the physical parameters of a loop's length, base density, and heat input. No solution exists at coronal temperatures in certain cases, which may explain the observations of very cool loops. The effect of a loop's geometry and field line divergence on the structure is found. Results predicted from scaling laws are compared, and the uniqueness of the solution for a loop with a fixed

mass is studied. The error in the predicted emission measure through assuming uniform pressure is shown to be considerable.

The life-time of a loop can often be many days, suggesting the existence of a thermally stable state. A global stability analysis is performed, and it is found that a loop's stability may depend critically upon its length. Thermally isolated loops, which are the most unstable type, can be thermally stable, provided their pressure falls off sufficiently rapidly with height (due to hydrostatic equilibrium).

ACKNOWLEDGEMENTS

I have pleasure in thanking Dr. Eric Priest for his encouragement, help and supervision during my period as a research student.

I wish also to thank Dr. Bernard Roberts and fellow research students at St. Andrews; Alan Hood, Peter Cargill, Andrew Webb and Alex Milne, for many interesting and helpful discussions.

I am grateful to the University of St. Andrews for financial support.

CERTIFICATE

I certify that Michael A. Wragg has satisfied the conditions of the Ordinance and Regulations and is thus qualified to submit the accompanying application for the degree of Doctor of Philosophy.

POSTGRADUATE CAREER

I was admitted into the University of St. Andrews as a research student under Ordinance General No. 12 in October 1977 to work on Energy-balance models of the solar corona under the supervision of Dr. E. R. Priest. I was admitted under the above resolution as a candidate for the degree of Ph.D. in October 1978.

DECLARATION

I declare that the following thesis is a record of research work carried out by me, that the thesis is my own composition, and that it has not been previously presented in application for a higher degree.

(MICHAEL A. WRAGG)

CONTENTS

1. INTRODUCTION

'And God said, "Let there be light"; and there was light.' For us that source of light is the Sun, and from the beginning man, in his infinite curiosity, has tried to comprehend it. This thesis seeks to add a small part to that conquest. It describes the construction of energy-balance models that may be used to investigate and explain the numerous observations that have been reaped, particularly from the recent Skylab missions. These models, together with the aims of this thesis, are summarised in Section 1.3, but first some of the observations are presented (Section 1.1) and the equations to be used in the following chapters are set out (Section 1.2).

1.1 OBSERVATIONS

To look casually at the Sun in white light shows deceptively little - perhaps just a few sunspots, but with more effort the structure of the outer layers of the solar atmosphere can be discerned. Above the photosphere there lies the chromosphere which extends upwards until the temperature reaches about 2×10^4 K. Thereafter it rises through a very narrow transition region to the corona at about 10^6 K (Gibson, 1973).

Though some observations can be done from the Earth

of, for instance, the outer corona in white light or the low chromosphere in Hα, most of the chromosphere and all of the lower corona may be observed most readily in UV and X-rays from space-borne instruments. Although there had been many rockets in earlier years, it was Skylab in 1973/4 which gave both better and more extensive observations of the corona, while it devoted more time to Solar Physics than any other project. (For a review of Skylab and its results see Stuhlinger, 1976.) Though the mission occurred during the "quiet" period of the Sun's 11-year cycle, it soon became clear that even then the Sun is far from quiet.

The solar atmosphere has often been divided into three types of region, namely active regions, quiet regions and coronal holes. Each is a consequence of the magnetic field structure.

An active region consists, most simply, of a bipolar magnetic region (Sheeley, et al., 1975). It forms typically near latitudes of $\pm 25^{\circ}$ or 30° at the beginning of a new solar cycle, and nearer $\pm 10^{\circ}$ at the end of a cycle. Usually, in each hemisphere the preceeding polarity of a region has a lower latitude, while the following one is of the same sign as the respective pole.

The evolution of coronal holes, apart from those at the poles, is influenced also by the presence of bipolar magnetic regions. They seem to be born as a result of two or more bipolar magnetic regions forming sufficiently close together that their respective preceeding and following magnetic fields (of like sign) cannot achieve

flux balance (Timothy, et al., 1975). The resulting region (or cell) of unipolar flux must be about 30^{o} or more across before a hole can develop (Bohlin and Sheeley, 1978). The following polarity of a pair, being closer to the pole and having the same sign may sometimes attach itself to the pole (Bohlin and Sheeley, 1978).

Once active regions or coronal holes have formed, they eventually disperse away, leaving behind the relatively quiet and more homogeneous corona termed quiet regions, which are, in fact, still highly structured, and closed (Vaiana, et al., 1973a). At any one time, most of the corona (typically about four fifths) consists of quiet regions. Coronal plasma is highly ionised and is seen to trace out the magnetic field configuration (Vaiana, et al., 1973a). Active regions are seen to be hotter and some 5 or 10 times more dense than quiet regions (Noyes, et al., 1970; Dupree, et al., 1973; Vaiana and Rosner, 1978), possibly because they are heated more strongly, while coronal holes are cooler and less dense (Maxson and Vaiana, 1977; Vernazza and Mason, 1978; Vernazza and Raymond, 1979), presumably because matter escapes into the solar wind taking energy with it (e.g. Vaiana, et al., 1973b). The magnetic field strength is enhanced over quiet-region values in active regions, but it is not necessarily depreciated in coronal holes (Bohlin and Sheeley, 1978).

1.1.1 Coronal Holes

Coronal holes gained their name from appearing devoid

of X-ray emission due to density deficiency of about a third of quiet Sun values (Maxson and Vaiana, 1977). Because of reduced density X-ray bright points are more noticeable within them, but overall there is little notable structure. The magnetic field lines diverge with height. Typical temperatures are not much in excess of 10^6 K e.g. 1.3 x 10^6 K was found by Timothy, et al., (1975) for one particular hole. Constraints on the temperature in the inner corona have been calculated by Leer and Holzer (1979) by using both the observed values of the proton flux at 1 A.U. and the pressure at the base of the corona. They suggested that the maximum and mean temperature could be at most 3.1 x 10^6 K and 2.6 x 10^6 K but would more likely be 2.5 x 10^6 K and 2.0 x 10^6 K or less.

The birth of a coronal hole takes place in less than a day, and is always the result of (magnetic) activity (Levine, 1978). Most holes are associated with active regions for most of their lives, although usually with different active regions at different times, since the lifetime of an active region is typically shorter than that of a coronal hole (Levine, 1977; Harvey and Sheeley, 1979). The decay of a hole may be associated with the number of bright points occurring within the hole, which increases with the age of the hole (Nolte, et al., 1978), or it could be caused by differential rotation, although this is rather less pronounced than would be expected; while equatorial parts of large holes rotate at their local rotation rate, parts at higher latitudes rotate at a rate between the equatorial

rotation rate and the rotation rate at the higher latitude (Timothy, et al., 1975). The boundaries of a hole can be severely disrupted by neighbouring activity; whole loop systems at the boundary can fall into a hole (Bohlin and Sheeley, 1978). Also differential rotation can help to form large new holes by carrying smaller, high and low latitude holes past each other, where they can merge if they have the same polarity (Sheeley and Harvey, 1980). During the Skylab period their lifetime (excluding the polar holes) had a range of 3 to 20 rotations (one rotation is about 26 days) with a mean of 6, but near sunspot minimum many small, short-lived holes were produced and the mean lifetime was then only one or two rotations (Sheeley and Harvey, 1978).

The solar cycle has a great effect on the polar holes, which can extend from a latitude of roughly 60° or 70° polewards, each about 8% of the surface area, but they wane and eventually change polarity every 11 years (Sheeley, 1980; Sheeley and Harvey, 1980). Recently (during the period of small, waning polar holes) the mid-latitude holes have begun to violate the usual rule of having the same polarity as the respective polar hole.

Holes can be divided into two types, namely small, compact holes well away from the poles, and those nearer the poles, which tend to connect with polar holes of like polarity. These form a north-south extension often as much as 120° in latitude (Timothy, et al., 1975).

Coronal holes have, broadly speaking, been equated

with open fields, although there are exceptions in both directions. It is now believed that although all (non-polar) open field lines are associated with activity, i.e. do not originate from the quiet Sun, active regions may have pockets of open field coming from within them (Švestka, et al., 1977b). Conversely, a significant portion of a coronal hole may well possess closed fields. Observationally, some active-region remnants may be seen within a hole, while theoretically, from the strength of the magnetic field at 1 A.U., it seems likely that some of the field must be closed (Levine, et al., 1977). This is thought to be true especially in young holes when the field strength is a maximum (Levine, 1977); it later decreases with time, perhaps by a factor of two per rotation. The field can be spatially very non-uniform in a hole, varying by as much as a factor of 5 (Bohlin and Sheeley, 1978), and being generally weaker in the centre.

1.1.2 Active Regions

In X-rays active regions are characterised by their greatly enhanced emission. They are the largest bipolar magnetic features on the Sun, and most often emerge along global neutral lines. When resolved, it is seen that an active region consists mostly of coronal loops (as does, in fact, much of the Sun), although a more overall structure is also evident. Temperatures and densities are both larger than in quiet regions. Whereas quiet regions have

values of $1 - 2 \times 10^6$ K and $2 - 8 \times 10^{14}$ m^{-3} (e.g. Withbroe and Noyes, 1977; Maxson and Vaiana, 1977), an active region usually has a temperature of $2 - 4 \times 10^6$ K (occasionally up to 7×10^6 K), and a density of $5 \times 10^{14} - 1.8 \times 10^{16}$ m^{-3} (e.g. Parkinson, 1973; Brabban, 1974; Davis, et al., 1975; Pick, et al., 1979). Usually, a hot, dense core is seen, perhaps from 20 Mm to 30 Mm above the surface, with a less impressive outer portion sometimes up to some 150 Mm high (Gabriel and Jordan, 1975). Thus the emission measure is found to be a decreasing function of temperature above about 2×10^6 K because of the much smaller amounts of plasma at higher temperatures.

A useful measurement of length, here, is the megametre (Mm), = 10^6 m. A 1 Mm long coronal loop would stretch nicely from St. Andrews down to London. The solar radius, $R_\odot$, is then 696 Mm.

1.1.3 Coronal Loops

Loop-shaped areas of enhanced emission are frequently seen on the Sun. It is assumed that these features trace the magnetic field lines. They connect points on the solar surface of opposite magnetic polarity and cross the neutral line. The hot corona consists almost entirely of closed loops while the cool corona shows fewer closed loops and most of the open field (Sheeley et al., 1975; Priest, 1978).

Loops occur within active regions, between active

regions, and on a larger scale, span great distances over the solar surface. There are many observations giving examples of loop temperatures, densities, lengths and lifetimes (e.g. Krieger, et al., 1971; Vaiana, et al., 1973b; Underwood, et al., 1974; Chapman and Broussard, 1977; Pye, et al., 1978; Cheng, et al., 1980). Generally speaking, individual loops live for between a few hours to a few tens of hours, occasionally very much longer. Apart from so-called flare loops, most loops do not go through striking changes during this time. Active-region loops have temperatures typically between 2 and 3 x 10^6 K, occasionally up to 6 x 10^6 K, densities of 5 x 10^{14} to 7 x 10^{15} m^{-3} and lengths of 10 to 200 Mm, although 400 Mm long loops are not uncommon. The hotter, denser, shorter ones usually comprise the core of an active region. Joining active regions are interconnecting loops. These possess temperatures around 2 x 10^6 K, densities within 5 x 10^{14} to 2 x 10^{15} m^{-3} and lengths 20 to 700 Mm. Hotter temperatures are sometimes seen in loops which have brightened. Without active regions, there are also loops as large as interconnecting loops, occasionally even longer, but these are cooler (down to 10^6K) and less dense, 2 x 10^{14} to 10^{15} m^{-3}. Flows, usually downflows, have sometimes been interpreted in the transition region (Doschek, et al., 1976; November, et al., 1976; Foukal, 1978).

Underwood, et al., (1974) described several interesting events from the Skylab period. The evolution of one active-region complex (McMath 12703 and 12706) showed individual

loops of an arcade disappearing after a lifetime of a few hours. As the loops faded, bright regions appeared at their feet, probably indicating the outflow of mass. Other occurrences of parts of loop structures brightening were also seen. Underwood, et al. suggested that one example observed near a summit was due to magnetic field reconnection, whereas a different event which showed a prominent brightening at one footpoint was probably due to an injection of mass. One large loop seen was a month old.

Chase, et al. (1976) observed a hundred loops interconnecting different active regions detectable in soft X-rays during the Skylab mission. They found that these interconnections occurred predominantly over short distances; all close active regions (tens of megametres apart) were connected. As larger separations were compared so the proportion of connected regions reduced, with the longest connection spanning 37 heliographic degrees. Assuming a semi-circular loop geometry this loop would have been 700 Mm long. Chase, et al. postulated that this is indeed an upper limit, since for the temperature and densities they observed (typically 2.3×10^6 K and 2×10^{15} m^{-3}) the radiative loss becomes as large as conduction at this length. However, less dense loops can reach further and are occasionally seen, even in excess of 1000 Mm.

Of those observed by Chase, et al., loops contained within a single hemisphere seemed to be roughly half as long as those crossing the equator. This suggests that

most single hemisphere loops may be born merely by brightening, the magnetic configuration being previously present and occasionally detectable. On the other hand, most transequatorial loops begin by magnetic flux reconnecting near the centre as new flux is thrust out from one of the active regions in question. Alternatively, part of the reason why short interconnections are usually confined to one hemisphere may simply be that the latitudes within 10 degrees of the equator are usually devoid of active regions (Withbroe, 1970).

Interconnecting loops are often seen to brighten and remain bright for a few hours or a day. Švestka, et al., (1977a); Švestka and Howard (1979) studied these brightenings and found temperatures of $3 - 4 \times 10^6$ K and densities $< 2 \times 10^{15}$ m^{-3}, less in some old loops. They suggested enhancements in young loops are due to the emergence of new flux near the footpoints, though they may be triggered by outside disturbances in some old loops. Whatever the cause it would have to result in at least one of the following: an increased temperature (inflow of additional energy); or increase in density (inflow of mass); a compression of the loop radially; or an increase in the thickness of the loop in the line of sight.

Howard and Švestka (1977) studied the evolution of centres of activity and the interconnections between them. Although individual loops rarely remain unchanged for more than a day or so, whole systems are seen from one rotation

to the next.

Although active regions are characterised by loops with temperatures in excess of a million degrees in the corona, there are notable exceptions which have been termed cool loops, having temperatures more than an order of magnitude lower (Foukal, 1975, 1976, 1978; Jordan, 1975; Gabriel and Jordan, 1975; Levine and Withbroe, 1977). The density within cool loops is not significantly different from that of hot loops, which implies a greatly reduced pressure. This, for a radial (static) pressure balance, implies that the magnetic field inside cool loops would need to be stronger, but because of the dominance of the field over the plasma (some two orders of magnitude) the predicted difference is too small to be measured. Some hot loops always occur close to, but significantly displaced from, the axis of the cool loops, and observations are best explained in terms of hot material outside a slender cool core (throughout the whole length of the loop). Consequently, great temperature and pressure variations exist over only 10 or 20 Mm. Foukal (1976, 1978) said these cool loops cannot be explained by a static model and suggested coronal material is continuously flowing across the field lines near the summit, from the hot annulus into the cool core. This could be caused by a density gradient into the cool tube due to a smaller pressure scale height. Once inside the cool loop, the new hot material would tend to cool, condense and fall down each leg of the loop.

An interesting event was observed by Levine and

Withbroe (1977) on 24 November 1973 in active region McMath 12628. A loop structure in apparent equilibrium was seen to have most ($\sim$70 %) of its mass suddenly drain out, from the top down through both footpoints, and yet, only 12 hours later, it refilled to assume its initial configuration. The evacuation time and the radiative cooling time for the loop were similar (about 15 min) which suggests that the heating may have been switched off or the static equilibrium state may have ceased to exist. The loop pressure, in units of NT was about 2×10^{21} $m^{-3}K$. This loop possessed a cool core (or perhaps several cool cores of only a hundred kilometres in radius). The cores reached all the way down to the footpoints, within a common hot sheath, and the draining effect was seen to be greater within them.

Loops can, sometimes, be gigantic. About 60 loops comparable with the size of the Sun were observed on Skylab. After a relatively fast rise, with expansion velocities of 400 - 500 km s^{-1}, they may persist for many weeks (Stuhlinger, 1976). McIntosh, et al. (1976) noted loop systems from old active-region remnants of various ages from a week to a year, with corresponding sizes ranging from 175 Mm to over 1000 Mm long.

1.2 EQUATIONS

The four fundamental equations of electromagnetism are Maxwell's equations. Written in terms of the magnetic induction $\mathbf{B}$, and electric field intensity $\mathbf{E}$, they are

$$\nabla . \mathbf{E} = \rho_c / \varepsilon , \qquad (1.2.1)$$

$$\nabla . \mathbf{B} = 0 , \qquad (1.2.2)$$

$$\nabla \times \mathbf{E} + \frac{\partial \mathbf{B}}{\partial t} = 0 , \qquad (1.2.3)$$

$$\nabla \times \mathbf{B} - \frac{1}{c^2} \frac{\partial \mathbf{E}}{\partial t} = \mu \mathbf{j} , \qquad (1.2.4)$$

in terms of the permeability μ, permittivity ε, the velocity of light $c = (\mu\varepsilon)^{-\frac{1}{2}}$, the volume current density $\mathbf{j}$ in matter, and the volume charge density ρ_c. M.K.S. units are used throughout.

For solar applications, the magnetohydrodynamic (MHD) equations can be used. These are based on the assumptions that length scales of interest are sufficiently large that a macroscopic description is valid, and that velocities are much less than the speed of light, so that relativistic effects are negligible. This implies that if l and t are typical length- and time-scales for a velocity v, then

$$l/t \sim v \ll c ,$$

and from equating the order of magnitude of the terms of

Equation (1.2.3),

$$\mathbf{E} \sim v\mathbf{B}.$$

But now

$$\frac{1}{c^2}\frac{\partial \mathbf{E}}{\partial t} \sim \left(\frac{v}{c}\right)^2 \nabla \times \mathbf{B} \ll \nabla \times \mathbf{B},$$

and so the second term on the left-hand side of Equation (1.2.4) can be neglected, reducing it to

$$\nabla \times \mathbf{B} = \mu \mathbf{j}. \qquad (1.2.5)$$

Ohm's law is

$$\mathbf{j} = \sigma (\mathbf{E} + \mathbf{v} \times \mathbf{B}), \qquad (1.2.6)$$

where σ is the electrical conductivity, assumed constant, which is easily valid for typical coronal parameters.

Since the electric field is effectively secondary to the magnetic induction it is usual to form a single equation for $\mathbf{B}$ from Equations (1.2.3),(1.2.5) and (1.2.6), namely the induction equation. This takes the form

$$\frac{\partial \mathbf{B}}{\partial t} = \nabla \times (\mathbf{v} \times \mathbf{B}) + \eta \nabla^2 \mathbf{B}, \qquad (1.2.7)$$

where $\eta = (\mu\sigma)^{-1}$ is the magnetic diffusivity. Equations (1.2.2) and (1.2.7) can now give $\mathbf{B}$ if $\mathbf{v}$ is known. The current can then be found from Equation (1.2.5) and the electric field from (1.2.6) if desired.

Equation (1.2.7) is coupled with plasma equations for

mass, momentum, state and energy. A one fluid model is assumed to be adequate. This is reasonable provided the density is high enough for there to be many collisions in time between the different particles. These equations can either be written in terms of the density, ρ, or the electron (or total) number density, N (or N_T). For convenience the electron number density is used, and it is related to the density ρ by

$$\rho = \tilde{\mu} m_p \left(\frac{N_T}{N}\right) N,$$

where $\tilde{\mu}$ is the mean molecular mass, the average mass per particle in units of m_p, where $m_p = 1.67 \times 10^{-27}$ kg is the mass of a proton. For a fully ionised hydrogen plasma $\tilde{\mu} = 0.5$ and $N_T/N = 2$, but the presence of heavier elements (about 1/5 helium some 1/20 all others by mass) makes $\tilde{\mu}$ about 0.6 and N_T/N about 1.9. Thus for the Sun

$$\rho \approx 1.1 m_p N. \qquad (1.2.8)$$

Using Equation (1.2.8) the equation for mass continuity is

$$\frac{\partial N}{\partial t} + \nabla.(N\mathbf{v}) = 0 \qquad (1.2.9)$$

or, equivalently,

$$\frac{DN}{Dt} + N\nabla.\mathbf{v} = 0, \qquad (1.2.10)$$

where the material derivative for time variations following the motion

$$\frac{D}{Dt} \equiv \frac{\partial}{\partial t} + \mathbf{v}.\nabla \ .$$

The momentum equation is given by

$$1.1\, m_p N \frac{D\mathbf{v}}{Dt} = -\nabla p + \mathbf{j}\times\mathbf{B} + 1.1\, m_p N \mathbf{g} + \mathbf{F} \ , \qquad (1.2.11)$$

where p is the pressure, $\mathbf{j}\times\mathbf{B}$ is the Lorentz force, $\mathbf{g}$ is the local attraction due to gravity, and $\mathbf{F}$ represents any additional forces such as that due to viscosity, which is usually assumed negligible in the solar atmosphere.

The equation of state can be written as

$$p = N_T k T = 1.9\, N k T \ , \qquad (1.2.12)$$

where $k = 1.38 \times 10^{-23}$ J deg^{-1} is Boltzmann's constant, and the 1.9 would read 2 for a fully ionised hydrogen plasma.

The energy equation can be written in the form

$$\frac{N^{\gamma}}{\gamma - 1} \frac{D}{Dt}\left(\frac{p}{N^{\gamma}}\right) = -\mathcal{L} \ , \qquad (1.2.13)$$

where γ ($= c_p/c_v$) is the ratio of specific heat at constant pressure to that at constant volume. $\mathcal{L}$ represents any forms of heat loss, taken here as

$$\mathcal{L} = -\nabla.(\chi \nabla T) + R - H \ , \qquad (1.2.14)$$

where the terms correspond to conduction, radiation and heating respectively, and κ is the coefficient of thermal conduction. In the adiabatic limit $\mathcal{L} = 0$.

The thermal conduction is best treated in terms of its components parallel and perpendicular to the magnetic field. That along the field, for a fully ionised hydrogen plasma, from Spitzer (1962), is

$$\kappa_{\parallel} = 1.8 \times 10^{-10} \frac{T^{5/2}}{\ln\Lambda} \quad \frac{\text{watt}}{\text{m deg}} \quad , \qquad (1.2.15)$$

where the Coulomb logarithm $\ln\Lambda$, tabulated by Spitzer, lies typically between 10 and 20. In a strong magnetic field (so that the ion cyclotron frequency x ion collision time $\gg$ 1) the transverse component $\kappa_{\perp}$ is reduced by an amount

$$\frac{\kappa_{\perp}}{\kappa_{\parallel}} = 5.5 \times 10^{-33} \frac{(\ln\Lambda)^2 N^2}{B^2 T^3} \quad . \qquad (1.2.16)$$

With a field of 10 gauss (10^{-3} tesla), this gives a ratio of about 10^{-5} at the base of the transition region and 10^{-14} in the corona. If L and l are typical length scales parallel and perpendicular to the field, then provided

$$l^2/L^2 \gg \kappa_{\perp} / \kappa_{\parallel}$$

the transverse component may be neglected. A good approximation for the parallel component throughout

the transition region and corona is then $10^{-11} T^{5/2}$ (denoted as $\kappa_0 T^{5/2}$).

Radiation can be assumed to be optically thin in and above the transition region, and so the radiation term R in Equation (1.2.14) can be assumed to be of the form

$$N N_H P(T) , \qquad (1.2.17)$$

where N_H is the hydrogen number density and $P(T)$ is the radiative loss function. This depends greatly on the abundance of elements relative to hydrogen, and since these abundances are not accurately known, $P(T)$ can only be taken to be accurate to within a factor of 2. Several authors have estimated $P(T)$, such as Pottash (1965); Cox and Tucker (1969); Tucker and Koren (1971); McWhirter, et al. (1975); Raymond (1978), as shown in Figure 1.1.

A convenient mathematical fit for this is a piecewise continuous approximation of the form

$$P(T) = \chi T^{\alpha} \qquad (1.2.18)$$

for a range of χ and α. One such approximation has been fitted to Raymond's curve by Rosner, et al. (1978) and is set out in Table 1. This approximation is used in this thesis for numerical calculations, although a single power law, usually $\alpha = -\frac{1}{2}$ has often been taken by many authors, and is sometimes useful analytically.

Table 1

The constants for the temperature dependence of the radiation term $\chi T^{\alpha} N^2$ according to the analytic approximation of Rosner, et al. (1978) in M.K.S. units.

Temperature Range	α	χ
$10^{4.3} < T < 10^{4.6}$	0	$10^{-34.85}$
$10^{4.6} < T < 10^{4.9}$	2	$10^{-44.0}$
$10^{4.9} < T < 10^{5.4}$	0	$10^{-34.2}$
$10^{5.4} < T < 10^{5.75}$	-2	$10^{-23.4}$
$10^{5.75} < T < 10^{6.3}$	0	$10^{-34.94}$
$10^{6.3} < T < 10^{7.0}$	-⅔	$10^{-30.73}$

The main feature of the radiative loss function, expression (1.2.18), is the maximum around $T = 10^5$ K, although for a given loop, since pressure is roughly constant throughout the transition region, the maximum in the radiation, $NN_H P(T)$, occurs at about $T = 1.15 \times 10^4$ K. Almost without exception the radiation will decrease with temperature above 10^5 K due to the fall off in density, although the curve for $P(T)$ in Figure 1.1 increases slightly if $T > 10^7$ K. For a fully ionised hydrogen plasma, $N_H = N$, but for the abundances in the solar atmosphere $NN_H \approx N^2/1.2$ in expression (1.2.17).

The remaining term H in Equation (1.2.14) represents

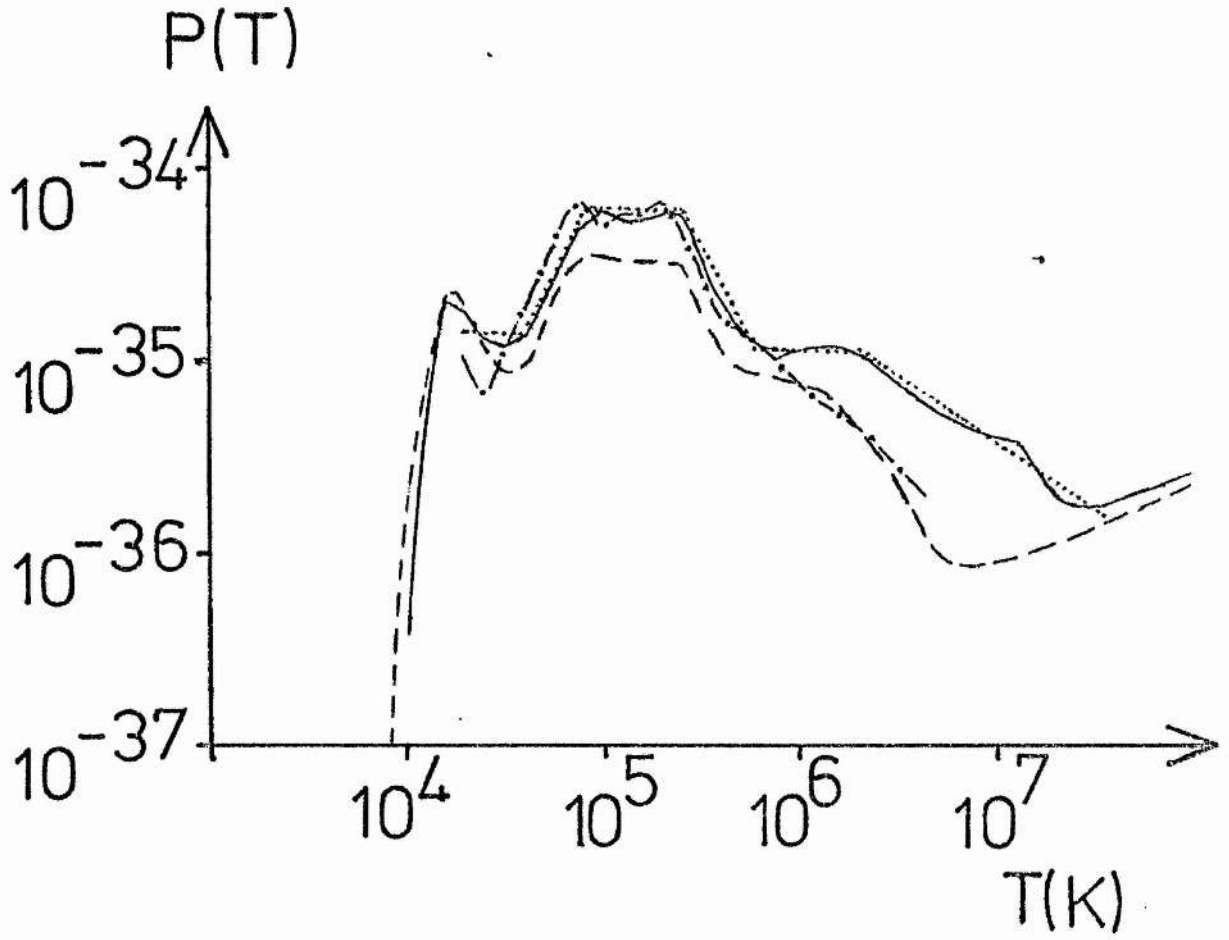

Figure 1.1 The radiative powerloss function P(T) as a function of temperature as estimated by Pottash (1965) .—.—.—.—; McWhirter, et al. (1975) – – – – ; Raymond (1978) ———— ; and the analytic approximation ····· to Raymond's curve used in this thesis, set out in Table 1.1 in the form $\propto T^{\alpha}$.

some unspecified form of heating. Observationally, heating would seem to be present since loops exist in a hot static state for times much greater than their radiative cooling time. Also, temperature gradients have been observed in apparently static loops.

At present the physical means of heating the corona is not certain. The mechanism could be provided by dissipation of acoustic or hydromagnetic waves, or possibly magnetic energy, either through current dissipation (suggested by Rosner, et al., 1978) or magnetic field annihilation. Waves from the chromosphere may dissipate low in the corona, due to short damping lengths, or interact at the top of closed loops after propagating up the field lines from both footpoints. Wentzel (1974, 1976) suggested Alfvén waves behave in this manner, and this would cause greater heating where there are larger photospheric field strengths. This could explain why the brightest loops seen are those with both footpoints located in areas of high magnetic field strength; loops reaching outwards from an active region are typically cooler (Sheeley, et al., 1975; Švestka, et al., 1977a). Waves may also dissipate due to the curvature of the field lines (Hollweg and Lillequist, 1978).

Athay and White (1978) saw difficulties with sound waves getting above the chromosphere, and also Alfvén waves where field is weak. Bruner (1978) agreed, though he stated that acoustic waves appear to have been detected in the transition region, and Hollweg (1978) suggested Alfvén

waves ought to be present because they are observed in the solar wind at 1 A.U. Observations have not clearly resolved this dilemma yet. Neupert, et al.'s (1975) observations warranted heating roughly uniform in volume, while Jordan (1976) and Withbroe and Noyes (1977) suggested heating of the lower transition region, but not necessarily the region between 10^5 K and 10^6 K. Yet for static loops some heating must occur around the summit since temperature maxima are observed there. Rosner, et al. (1978) calculated how some heating models may depend on loop parameters.

In the absence of a reliable form for the heating, two simple forms only have been considered here, namely heating proportional to volume,

$$H = E_H \quad \text{(a constant)},$$

and proportional to density (or mass),

$$H = hN \quad \text{(for } h \text{ a constant)}.$$

An alternative possibilty would be to treat the heating as unknown and use the energy equation only to deduce it (see Jordan, 1976; and Section 2.1.1).

It was found convenient to measure the heating relative to the radiation. For this typical coronal values for temperature and density were chosen, namely $T = 10^6$ K and $N = 5 \times 10^{14}$ m^{-3}, to give a typical coronal radiation, in units of which the heating is measured. In this non-dimensional form the heating is denoted by $\bar{E}_H$ or

$\bar{h}$. Thus heating would exactly balance radiation when this is equal to unity and the temperature and density are as above. The advantage of non-dimensionalising in this way, rather than in terms of base values (T_o and N_o), is that T_o or N_o can then be varied independently of the heating.

A quantity frequently referred to is the sound speed c_s , where

$$c_s^2 = \frac{\gamma p}{\rho} = \frac{\gamma k T}{\tilde{\mu} m_p} .$$

It is about $200 kms^{-1}$ in the corona. The (gravitational) scale height is given by

$$\frac{kT}{\tilde{\mu} m_p g}$$

where g is the local attraction due to gravity, taken as $274\ ms^{-1}$ at $1\ R_\odot$ (the solar surface). This is roughly 50 Mm for a coronal temperature of 10^6 K. β , defined as

$$\beta = \frac{p}{B^2/2\mu}$$

is the ratio of the plasma pressure to that of the magnetic field. Since the corona is so rare, $\beta \ll 1$, and the coronal structure can be considered to be implied by the coronal magnetic field, which in turn is probably controlled by the changes down in the photospheric field (Krieger, et al., 1976). Therefore, for this thesis, a given magnetic field configuration has been assumed and the consequences of the plasma equations on the plasma structure are derived.

Only the coronal and transition regions above a

temperature of 2×10^4 K are modelled. Here the conduction across the field is totally insignificant, and is neglected. Since the field lines channel energy carried by conduction in this way, and also guide the flow of material, it is sufficient to solve the equations of mass continuity (1.2.9), momentum (1.2.11), state (1.2.12) and an energy equation (1.2.13) in just one dimension, namely along any particular field line. Also, since only the range $T \geq 2 \times 10^4$ K is considered, the radiation has been assumed optically thin, and the hydrogen fully ionised. If s denotes the one-dimensional distance along a field line, the conduction term (Equation 1.2.14) reduces to

$$\frac{d}{ds}\left(K_{\parallel} \frac{dT}{ds} \right) - \frac{K_{\parallel}}{B} \frac{dB}{ds} \frac{dT}{ds}, \qquad (1.2.19)$$

where the second term is due to any splaying out of the field lines. If A (s) is the cross-sectional area of a flux tube, then since

$$\frac{d}{ds}(BA) = 0,$$

expression (1.2.19) can be rewritten as

$$\frac{1}{A} \frac{d}{ds}\left(K_{\parallel} \frac{dT}{ds} A \right), \qquad (1.2.20)$$

where $K_{\parallel} = 1 \times 10^{-11} \; T^{5/2}$ W deg^{-1} m^{-1}.

Given these assumptions, there results the following equations which form the basis of the following chapters:-

mass continuity $$\frac{\partial N}{\partial t} + \frac{\partial}{\partial s}(Nv) = 0 , \qquad (1.2.21)$$

momentum $$1.1 m_p N \frac{\partial v}{\partial t} + 1.1 m_p N v \frac{\partial v}{\partial s} = - \frac{\partial p}{\partial s} - 1.1 m_p N g_{\parallel} , \qquad (1.2.22)$$

state $$p = 1.9 NkT , \qquad (1.2.23)$$

energy $$- \frac{N^{\gamma}}{\gamma - 1} \left[v \frac{\partial}{\partial s} \left(\frac{p}{N^{\gamma}} \right) + \frac{\partial}{\partial t} \left(\frac{p}{N^{\gamma}} \right) \right] + \frac{1}{A} \frac{\partial}{\partial s} \left(\kappa_0 T^{5/2} A \frac{\partial T}{\partial s} \right)$$

$$= \frac{1}{1.2} N^2 \chi T^{\alpha} - H . \qquad (1.2.24)$$

$g_{\parallel}$ is the component of gravity (taken positive) parallel to the field. For notational ease, the factors 1.1 ($= \tilde{\mu} N_T/N$), 1.9 (N_T/N) and 1.2 (N/N_H) will be omitted from the text (with 1.9 replaced by 2). Many authors ignore them entirely by assuming a hydrogen plasma. This would seem quite acceptable since even the worst of these, 1.2, multiplies the radiative loss term which itself is uncertain to a factor of 2 because of uncertainties in the abundances of heavier elements.

1.3 OVERVIEW OF THESIS

The structure and energy balance of both open regions (Chapter 2) and closed regions in the form of loops (Chapters 3 and 4) are dealt with, assuming static or steady flow conditions. The aim is to show the effects and relative importance of different mechanisms for the range of observed parameters. An explanation of the

extraordinarily long lifetimes of loops is also considered (Chapter 5) by looking at their stability.

McWhirter, et al. (1975) presented a standard model for the transition region and inner corona that matches with the Harvard Smithsonian Reference Atmosphere. An open field-line configuration was assumed and the equations of energy and hydrostatic equilibrium were solved numerically. However, McWhirter, et al. neglected several features which may well be important, such as the presence of flows and of a more marked area divergence than spherically symmetric. The purpose of the next chapter is to generalise their model for the temperature and density as functions of height in several ways. In particular the effect on the temperature maximum and its location are determined when the following characteristics of the model are varied:

(i) boundary conditions on temperatures and density;

(ii) magnitude of the heating;

(iii) form of the heating term;

(iv) divergence of the field lines;

(v) presence of subsonic flows, either upward or downward.

It is found that if the heating is localised at great altitudes, it tends to produce a narrower and larger temperature maximum at a greater altitude than a uniform heating (and even more so than a heating proportional to density). For fixed base conditions, an increase in heatingor field-line divergence or downflow decreases the

coronal temperature and reduces the height of the temperature maximum, while a steady upflow has the opposite effects. A maximum possible upflow was found, beyond which a catastrophe occurs so that no steady hot solution exists.

Chapter 3 develops the case when the field lines are closed at the top, so that additional upper boundary conditions are required to match the two sides of the "loop". In particular, a symmetric loop has a vanishing heat flux at its summit. The temperature and density structure is computed for a comprehensive set of coronal loops that are in hydrostatic and thermal equilibrium. One of the main interests is the effect of gravity, which has not been comprehensively dealt with elsewhere. It produces significant deviations from the usual uniform-pressure scaling law ($T \sim (pL)^{1/3}$) when the loops are taller than a scale height.

For <u>thermally isolated loops</u> the heat flux vanishes at each footpoint and gravity lowers the pressure throughout the loop. This in turn lowers the density significantly and the temperature slightly, while modifying the above scaling law considerably. For more general loops, where the base conductive flux does not vanish, gravity lowers the summit pressure and so makes the radiation decrease by more than the heating. This in turn raises the temperature above its uniform pressure value for loops of moderate length but lowers it for longer loops. A divergence in loop cross-section increases the summit temperature by typically a factor of 2, and decreases the

density, while an increase in loop height (for constant loop length) changes the temperature very little but can halve the density.

One feature of the results is a lack of equilibrium when the loop pressure becomes too large. This may explain the presence of cool cores in loops which originally had temperatures below 2×10^6 K. Loops hotter than 2×10^6 K are not expected to develop cool cores because the pressure necessary to produce non-equilibrium is larger that values typically observed.

Chapter 4 takes up in more detail the special case of a thermally isolated loop, which has attracted a lot of interest, since coronal loops are often considered to be approximately of this type. Two aspects of the solutions for such loops are considered. The effect of gravity on the uniform-pressure scaling law is investigated by solving the equations of energy balance and hydrostatic equilibrium numerically. Also, solutions for loops with a given fixed mass are found to be non-unique over only a small parameter range.

Chapter 5 then moves on to consider the question of the thermal stability of loops. Observations have shown loops existing many hours or (in some cases) days, which would initally suggest that they are stable. Yet recently several authors have concluded that all thermally isolated loops of uniform pressure are unstable. In this chapter it is shown that the inclusion of gravity in the analysis is vital since it has the effect of stabilising loops if they are sufficiently long.

2 THE OPEN SOLAR ATMOSPHERE

2.1 INTRODUCTION

Originally the solar corona was thought to be vertically stratified, and so many authors set about modelling such a situation. It is now known that much of the corona has a closed magnetic field structure which would impose further restraints on models. The remainder consists of open structures, principally coronal holes, which occupy typically 10% of the solar surface, including both polar caps.

McWhirter and Wilson (1976) have reviewed some early energy-balance models which included processes such as mechanical wave heating, solar wind outflow, conduction or radiation. The solar-wind flux is so small (by comparison to other terms) that it is negligible. When the value of the electron flux in the solar wind was used to model the transition region, the results gave flows of less than 100 times that of the observed downflows in the inner corona (Chiuderi and Riani, 1974). The temperature is so insensitive that different models gave only slight differences in temperature even in the corona, although a consistent discrepancy with observations has been that the models do not reach coronal temperatures (10^6 K) at a low enough height. Models give this at around 15Mm as compared with only 5Mm from observations (Gabriel, 1976 a,b). In other words, according to observations,

conduction deposits more energy into the transition region than can be radiated away - a dilemma that has been apparent for some time. Mathematically, if the energy equation is solved for heating it is found to be negative in this region.

This difficulty may be resolved by including several extra terms in the energy-balance equation, such as a divergent cross-sectional flux-tube area, or flows. The temperature and density structures are systematically recalculated in the present chapter, to find the effects and relative importance of different boundary conditions, heating values, heating functions, flux tube divergences and flow velocities. Thus it is proposed that there is not just one unique model atmosphere, but a whole range which depend on the values of the above mentioned parameters. The equations and boundary conditions are described in Section 2.2, then the effect of each of these models is assessed in Section 2.3 before the numerical results are presented (Section 2.4).

Observations suggest a divergent field with a cross-sectional area which increases with height greater than that of a spherically symmetric one. In the transition region (e.g. at a temperature of 3×10^5 K) a "network" effect is observed, where most of the emission comes from localised regions. Presumably this is because at the base of the transition region (or lower) the field is squeezed into thin flux tubes between the supergranular cells. This effect is not seen at coronal temperatures

(e.g. 1.5 x 10^6 K) where the emission is more uniform (Tousey, et al., 1973; Reeves, et al., 1974; Mariska, et al., 1981).

Field lines must also diverge rapidly in the corona because at a height of a few solar radii most of the field lines are open, whereas they have originated from only about 10 % of the low corona.

The first of these aspects has been investigated by Gabriel (1976a,b). A two-dimensional magnetic field pattern showing this network characteristic was developed, and an energy-balance model was solved within it.

Boundary conditions were taken at the top of the model, with temperature and density fixed at 30 Mm from observations as 1.6 x 10^6 K and 2.8 x 10^{14} m^{-3}. Heating was assumed to be absent below this height. An integration was performed downwards, with the value of the initial conductive flux chosen to fit the observations best. Much better agreement with emission-measure observations than a spherically symmetric (or plane parallel) model was then claimed by Gabriel, at least for temperatures in excess of 2 x 10^5 K. One reason for this better coronal agreement, however, must be because coronal boundary conditions had been imposed. That this two-dimensional structure is indeed an improvement should be judged from the complete transition and coronal region taken together, which would seem to be the case from Figure 2 of Gabriel (1976b).

Gabriel's network model gave an erroneous emmision-measure curve below a temperature of 2×10^5 K, which was assumed to be due to the neglect of heating. This is, however, not the case, as heating only makes the situation worse. Because upper boundary conditions had been chosen, an increase in the amount of heat deposited would only narrow the transition region by increasing the conductive flux there. Since below 2×10^5 K the pressure is constant (to within ¼% (Gabriel)), the emission-measure intensity at any given temperature is proportional to the inverse of dT/dr and will thus decrease. To fit observations some method of transporting energy away must be sought instead.

Flows may be important in the low corona and transition region (e.g. Doschek, et al., 1976; November, et al., 1976). Doschek, et al. observed plasma in the transition region. They found that between temperatures of 7×10^4 K and 2×10^5 K there was greater emission produced by descending plasma than ascending plasma. This indicates that either there is more descending plasma at these temperatures, or that it is brighter. Various velocities were inferred, from no velocity, up to a maximum of 15 km s^{-1}.

Pneuman and Kopp (1977) pointed out that there are several observations which have indicated the presence of steady downflows of the order of a few kilometres per second in the transition region. This would appear reasonable because mass i known to be injected into the corona by spicules at a rate far in excess of that lost to

the solar wind. This mass must ultimately return to the surface by some means, and Pneuman and Kopp showed that the downflows are of the right order of magnitude to account for this. If indeed the downflows are included, Pneuman and Kopp showed that the enthalpy flux may well constitute the dominant energy source for the transition region.

A following paper by Pneuman and Kopp (1978) pursued this by solving an energy equation with just enthalpy flux and radiative loss, plus the assumption of hydrostatic equilibrium. After the temperature and density were imposed to be 5×10^5 K and 5×10^{14} m^{-3} at a (arbitrary) height of 4 Mm, a solution was specified by a suitable choice of the electron flux. It was found that an electron flux of 7×10^{18} m^{-2} s^{-1} gave an essentially identical model to Gabriel's (1976a) with conductive flux and no flow. Reasonable agreement with the observed emission measure can therefore be found for the upper transition region, provided the electron flux is chosen appropriately, but not for the lower transition region. A better fit is possible if the electron flux is assumed to decrease with height, which may be brought about if spicules deposit substantially more matter at lower heights than higher up.

McWhirter, et al. (1975) modelled the solar corona using an energy equation coupled with hydrostatic equilibrium. A stationary, spherically symmetric atmosphere was assumed. Heating was assumed to be due to the dissipation of sound waves from the chromosphere which

decay exponentially with height. A vanishing base flux was assumed at a height of 2 Mm where the temperature was set equal to 8000 K. It was also assumed that the total input of mechanical energy must balance the total energy lost by radiation. Mathematically this sets an upper boundary condition of zero temperature derivative at infinity.

The model was then uniquely determined by the prescription of the base density (or equivalently pressure) or the total heating. The main model which McWhirter, et al. computed had the base density set from the upper point of the Harvard Smithsonian Reference Atmosphere. Without this assumption for the pressure it was found that a greater amount of heating caused a larger pressure and an only slightly larger coronal temperature. The rise in pressure is because the atmosphere must radiate more in proportion to the increased heating.

These conclusions are, however, dependent upon their balancing the total heat input and the total radiation. This choice is convenient because it ensures the temperature does not increase without bound or reduce to zero, and measurements show it to be around 10^5 K at the Earth's orbit. However, it cannot be justified as it stands because the static equations will break down in the outer corona. There the expansion of the solar wind will have an increasingly dominant effect. The Sun may indeed impose some outer boundary condition but if so it is unlikely to be as straightforward as this.

2.1.1 Methods of Analysis

There are principally two methods that have been used to model the solar atmosphere, that of the emission-measure analysis and that using the energy-balance equation.

Physically, the differential emission measure, $Q(T)$, gives an indication of the amount of emitting material near any given temperature T. It is defined as

$$Q(T) = N^2 \, dV \, ,$$

where dV is the volume of plasma at temperature T. In one dimension this becomes

$$Q(T) = N^2 \, (dT/ds)^{-1} \, , \qquad (2.1.1)$$

where s represents the dimension in question. The emission-measure analysis seeks to generate empirically Equation (2.1.1) from the observed intensities of emission lines. In this case s is taken as the direction of the line of sight. With an assumption, such as hydrostatic equilibrium, the temperature and density structure can be calculated as functions of s. With further assumptions on flow and field-line divergence, an energy equation can then be used to deduce the heating deposited. The method has been used by Jordan (1975, 1976), where scaling laws relating the base conductive flux, the base pressure and the coronal temperature were deduced (see Chapter 3).

One advantage of this method when applied to the solar

atmosphere is that often a feature of interest (such as a coronal loop) dominates the emission in that vicinity. This allows the direction s in Equation (2.1.1) to be taken along the feature (along a field line in the case of a loop).

It has been suggested (Levine and Pye, 1980) that a certain amount of care is needed with this method. This is because only a small number of line intensities are used to produce the emission measure over a wide temperature range. This means that the empirically derived emission-measure curve does not predict a unique mathematical emission-measure curve derivable from a model, but a class of them. In other words, the empirically derived emission measure cannot predict the exact make-up of (e.g.) an active region composed of individual loops, although conversely, a (suggested) set of loops, or mathematical model, does produce a unique set of predicted line intensities and hence a predicted observed emission measure. In this manner the emission measure can show that certain models do not fit observations. This was done for the case of different heating functions which have been taken for various energy-balance models (Jordan, 1980).

Alternative to the emission-measure approach is that of solving the energy balance equation directly, coupled with other relations such as Equations (1.2.21) to (1.2.23), plus suitable boundary conditions. With initial assumptions on flow, area divergence and heating, this gives the temperature-density structure directly. This

method is more useful for predicting the effects of various situations (such as flows) and has been used in this and the following chapters.

2.2 EQUATIONS AND BOUNDARY CONDITIONS

2.2.1 Equations

Let r denote the distance from the centre of the Sun, and $T(r)$, $N(r)$ and $v(r)$ denote the temperature, (electron) density and (steady) plasma velocity respectively. The energy equation (1.2.24) can be transformed into the form

$$\frac{1}{A}\frac{d}{dr}\left[NvA\left(\tfrac{1}{2}m_p v^2 - 5kT + \frac{m_p g R_\odot^2}{r}\right) + K_0 T^{5/2} A \frac{dT}{dr}\right] = N^2 \chi T^{\alpha} - H, \qquad (2.2.1)$$

which is a physically useful form because the terms on the left-hand side can be seen to correspond to the fluxes of kinetic energy, enthalpy, gravitational energy and conduction.

The region of interest is the inner corona, which is modelled out to $2\ R_\odot$. In this region the flow speeds of interest are highly subsonic. For example, at 2×10^4 K the sound speed is 20 km s^{-1} and rises to 150 km s^{-1} at 10^6 K. By comparison the maximum base velocity that is considered here is 200 m s^{-1} and it gives a flow speed of about 20 km s^{-1} as the temperature approaches 10^6 K. Therefore, products of order velocity squared are assumed negligible by comparison with the sound speed

squared. This allows the term of gravitational energy flux in the energy equation (2.2.1), and in the momentum equation (1.2.22) to be dropped, the latter equation reducing to the equation for hydrostatic equilibrium, namely

$$-\frac{d}{dr}(NkT) = \frac{1}{2} g N m_p \frac{R_\odot^2}{r^2} . \qquad (2.2.2)$$

(Because gravity varies considerably over the height range considered, it is included in the equation as $gR_\odot^2/r^2$ rather than the constant value g.) It is noted as a reminder that these equations cannot be extrapolated out to give solar wind solutions because the speed of the solar wind increases and eventually becomes supersonic after a height of a few solar radii.

The particle flux has been assumed constant equal to its value at the base, which is taken as the place where the temperature is 2×10^4 K and is denoted by zero subscripts. Thus

$$N v A = N_o v_o A_o . \qquad (2.2.3)$$

This relation must eventually break down at some height (unless it applies to a siphon flow in a closed coronal loop (Cargill and Priest, 1980)) because it must ultimately reduce to the very much smaller value of the solar wind. Nonsteady mass injection by spicules was considered by Pneuman and Kopp (1978), but also effects like the diffusion of plasma across field lines (or reconnection of the field

lines) could play a role. It is assumed here that any effect of this sort occurs above a height of one solar radius so that Equation (2.2.3) is valid within the heights considered.

A simple form for the area profile $A(r)$ has been taken, namely

$$A = A_0(1 + a(r - R_\odot)/R_\odot)^2 , \qquad (2.2.4)$$

where a is a constant. The value $a = 0$ gives $A \equiv A_0$ and so represents a plane parallel atmosphere; $a = 1$ corresponds to the spherically symmetric case, while larger values of a make the field lines diverge more rapidly than in the spherically symmetric model.

2.2.2 Boundary Conditions

It was decided to follow McWhirter, et al. (1975) in integrating upwards from values of T, N and dT/dr derived from the Harvard Smithsonian Reference Atmosphere (Gingerich, et al., 1971) as

$$\begin{aligned} T &= T_0 = 2 \times 10^4 \text{ K}, \\ \frac{dT}{dr} &= 10.1 \text{ K m}^{-1}, \\ N &= N_0 = 2.12 \times 10^{16} \text{ m}^{-3}, \end{aligned} \qquad (2.2.5)$$

a at height of 2000 km. Above this the plasma can be considered fully ionised and the above Equations (2.2.1) to (2.2.4) become valid. In the majority of the present

chapter Equations (2.2.1) to (2.2.4) are therefore solved numerically subject to (2.2.5).

However, as a preparation, solutions are computed for other possible boundary conditions, showing how the results differ for various heating values. Rather than prescribe all the above quantities at the base and leave the upper boundary conditions free, it may be that in practice some upper boundary conditions are imposed, due to, for example, the solar wind on open field lines, or due to symmetry in closed structures. Two cases are considered, each time relaxing the condition that N_0 be fixed, and so allowing one upper boundary to be chosen. Also dT/dr is set equal to zero at the base rather than the value given in (2.2.5). (The base flux as prescribed in (2.2.5) is typically only one to two orders of magnitude less than that in the transition region, so reducing it to zero at the base is not a significant change.) In one case the temperature at 2 solar radii is imposed to be 1.5×10^6 K, and in the other case the temperature gradient is set equal to zero there. The results are presented in Section 2.4.

2.3 ANALYTIC AND ORDER OF MAGNITUDE APPROXIMATIONS

2.3.1 Magnitude of the Heating

Before embarking on a full numerical solution it is useful to approximate the full equations analytically and

so obtain a guide for what to expect.

Consider the effect of varying the magnitude of the heating. Since the radiation $(N^2 \chi T^{\alpha})$ is proportional to N^2 and falls off with temperature above 10^5 K, the heating term becomes more important relative to radiation as the height above the transition region increases. When the heating dominates over radiation the energy equation, in the absence of flows or area divergence, reduces to

$$\frac{d}{dr}\left(T^{5/2}\frac{dT}{dr}\right) = -H/\kappa_o, \qquad (2.3.1)$$

which implies that the conductive flux along a field line is decreasing at a rate proportional to the heating. In other words, heat supplied to an elementary volume of the plasma is being conducted away because more heat is flowing out of the bottom of the element than is flowing in through the top.

2.3.2 Boundary Conditions

Consider now the effect of varying the amount of heating on the solutions to Equation (2.3.1) when different boundary conditions are taken. Suppose first the temperature is fixed at a distance of $2R_\odot$. Then a larger heating causes the conductive flux to be smaller at $2R_\odot$ and so the temperature below $2R_\odot$ is hotter. In other words, an increase in heating will raise the temperature. If instead the temperature gradient is chosen to vanish at $2R_\odot$, then again a larger heating leads to a larger temperature. If H is a constant, this may be shown by integrating Equation

(2.3.1) to give

$$T^{7/2} = \frac{H}{\kappa_o}\left(-7s^2/4 + 7(2R_\odot - s_o)s/2\right) + T_*^{7/2},$$

where s is the height above s_o, and T_* is the temperature at s_o, the position where heating begins to dominate. The term multiplying H is positive, since $2R_\odot - s_o \geq s$, and so the result is proved. Now suppose that N and dT/dr are both fixed at the base. Since the conductive flux is fixed, a set amount of heat (in excess of radiation) is required to make the base flux fall to zero, and this point will correspond to the temperature maximum. Thus the greater the heating, the sooner (in height) this point will be reached and (unless the magnitude of the heating is very erratic in space) the lower the temperature T_{max} at that position (and any other position) will be. This can be seen by integrating Equation (2.3.1) to give

$$T^{7/2} = -7Hs^2/4\kappa_o + C_1 s + C_2,$$

where C_1 and C_2 are constants. The effect of increasing the heating, H, is to make the temperature decrease, provided C_1 and C_2 do not vary too much with H, which is especially true at large heights. The essential point for each of these types of boundary condition is that the greater the heating, the more concave are the profiles of conductive flux, and temperature. Furthermore, in each of these cases the equation for hydrostatic equilibrium gives, in order of

magnitude,

$$N = N_{s_o} T_{s_o} / (T + \bar{g} s), \qquad (2.3.2)$$

where $\bar{g} = \frac{1}{2} g m_p / k$

which suggests that the density increases as the temperature falls, and vice versa.

2.3.3 Field-Line Divergence

In investigating the effects of a widening flux-tube area and of flows, just the case when the boundary conditions are fixed at the base is considered. A widening flux-tube area effectively disperses the conductive flux, thus reducing its density per unit cross-sectional area. It is expected, therefore, that the widened part of the flux tube will be more isothermal compared to the narrower part, than would be the case of a uniform area.

For fixed base conditions, the transition-region divergence will tend to flatten out the coronal temperature profile sooner, and so lower the maximum temperature. However, any field-line divergence in the corona itself, where the plasma is nearly isothermal, will have little or no effect.

The effect can be estimated from an order-of-magnitude approach as follows. If s is now defined to be the distance above the surface, the energy equation with no heating term of flows is

$$\frac{d}{ds}\left(T^{5/2}\frac{dT}{ds}\right) + \frac{dA}{ds}\frac{1}{A} T^{5/2}\frac{dT}{ds} = N^2 T^{\alpha}\frac{\chi}{\kappa_o} ,$$

which may be approximated by

$$\frac{T^{7/2}}{s^2} + \frac{2a}{R+as}\cdot\frac{T^{7/2}}{s} = N^2 T^{\alpha}\frac{\chi}{K_0} \,. \qquad (2.3.3)$$

According to the equation of hydrostatic equilibrium, the density can be approximated by

$$N = N_0 T_0/(T + Cs),$$

where $C = g\tilde{\mu}m_p/k \approx 0.015 K m^{-1}$, and so Equation (2.3.3) reduces to

$$T^{7/2}\left(1 + \frac{2as}{R+as}\right) = \frac{s^2 N_0^2 T_0^2 T^{\alpha}}{(T+Cs)^2}\,\frac{\chi}{K_0} \,.$$

In the transition region, s is so small that $as \ll 1$ and $Cs \ll T$. T is therefore given by

$$T^{11/2-\alpha} \sim s^2.$$

For heights so large that $Cs \gg T$, α may be set equal to $-\frac{1}{2}$, so that

$$T^4 = \frac{N_0^2 T_0^2 \chi}{C^2 K_0}\left(\frac{1+as}{1+3as}\right)$$

is obtained, where the factor in brackets decreases from 1 to a lower bound of $\frac{1}{3}$ as a increases from zero. Thus increasing the flux-tube area through a decreases the temperature but never by an amount greater than $3^{1/4} \approx 1.3$. From Equation (2.3.2) such a temperature fall in turn raises the density.

2.3.4 Subsonic Flows

Several authors have suggested that flows present in the corona are not negligible, to the extent that the enthalpy flux may well be the dominant term in the energy equation (Pneuman and Kopp, 1977). A flow deposits material into a vicinity from the neighbouring position. If temperature increases with height, as in the transition region, then a downflow brings hotter material from the corona to lower heights. In this case the downflow will deposit additional energy and should have the same effect as heating. Similarly, an upflow must produce the opposite effect, removing energy by the deposition of cooler material. Again, as in the case of a diverging field, an isothermal atmosphere will be insensitive to a flow.

Let a flow be modelled by studying the effect of the enthalpy flux in the energy equation. In the transition region the pressure is constant, α can be approximated by 2, and the heating can be neglected. The energy equation reduces to a balance between enthalpy, conduction and radiation. If A is unity and q and χ are rescaled according to $q' = kq/\kappa_0$, $\chi' = \chi/\kappa_0$ to absorb the constants k and κ_0, then

$$-q'\frac{dT}{ds} + \frac{d}{ds}\left(T^{5/2}\frac{dT}{ds}\right) = \chi',$$

where $q = N v A$. This may be integrated to give

$$-q'T + T^{5/2}\frac{dT}{ds} = \chi' s + T_0^{5/2}\frac{dT}{ds}\Big|_0 - q'T_0. \qquad (2.3.4)$$

Then an expansion of T for small distances in the form

$$T = T_o + T_1 s + T_2 s^2 + \ldots$$

can be substituted into Equation (2.3.4). It gives $T_1 = (dT/ds)\big|_o$ and

$$T_2 = \left(\chi' + q' \frac{dT}{ds}\Big|_o - \frac{5}{2}\left(\frac{dT}{ds}\Big|_o\right)^2 T_o^{3/2}\right)\frac{1}{2T_o^{5/2}}.$$

As the upflow speed $v(>0)$ increases, so q increases, which causes a temperature rise and a density fall. Alternatively, the effect of increasing a downflow $(v<0)$ is to cool the plasma and raise its density. This is to be expected since the enthalpy flux has a similar effect in the energy equation to an additional heating term.

Pneuman and Kopp (1977) suggested enthalpy flux is considerably more important than conductive flux. In this case the energy equation may be taken as

$$-\frac{dT}{ds} = \frac{\chi'}{q'} T^{\alpha-2},$$

so that for the case $\alpha = 2$,

$$T - T_o = -\chi' s/q'. \qquad (2.3.5)$$

This gives no meaningful result for q positive (upflow), and thus suggests that, for a more general energy balance, there is a maximum positive q for a solution to exist, namely when the enthalpy and conductive fluxes are the same order of magnitude. Equation (2.3.5) also confirms that increasing a downflow decreases the temperature.

2.4 NUMERICAL RESULTS

2.4.1 Boundary Conditions

Equations (2.2.1), (2.2.2) and (2.2.3) were solved numerically for $T(r)$, $N(r)$ and $v(r)$. Figures 2.1a and b show the results for temperature and density when the boundary conditions $T = 2 \times 10^4$ K and $dT/dr = 0$ at the base, and $T = 1.5 \times 10^6$ K at the top were taken. Figures 2.1c and d give the corresponding profiles when the upper boundary condition $dT/dr = 0$ is adopted instead. The heating $\bar{E}_H = H/(N_c^2 \chi_c T_c^{\alpha_c})$ has been taken uniform in space, and is measured relative to the radiation at a typical coronal temperature and density of $T_c = 10^6$ K and $N_c = 5 \times 10^{14} m^{-3}$. In both cases it is seen that the temperature increases with the amount of heating, which agrees with the order-of-magnitude estimates in Section 2.3. In Figure 2.1a the conductive flux is still positive at $2R_\odot$ when the heating is small or absent; for larger heating there is a temperature maximum below this height. For Figures 2.1c and d there is no solution when $\bar{E}_H = 0$ since the temperature rises monotonically and so cannot possess a vanishing gradient at any finite height.

2.4.2 Magnitude of the Heating

Figures 2.2a and b show the results of different uniform heating values when the base boundary conditions (2.2.5) are taken. (These conditions are used for the rest of the calculations in this chapter. It can be seen, as

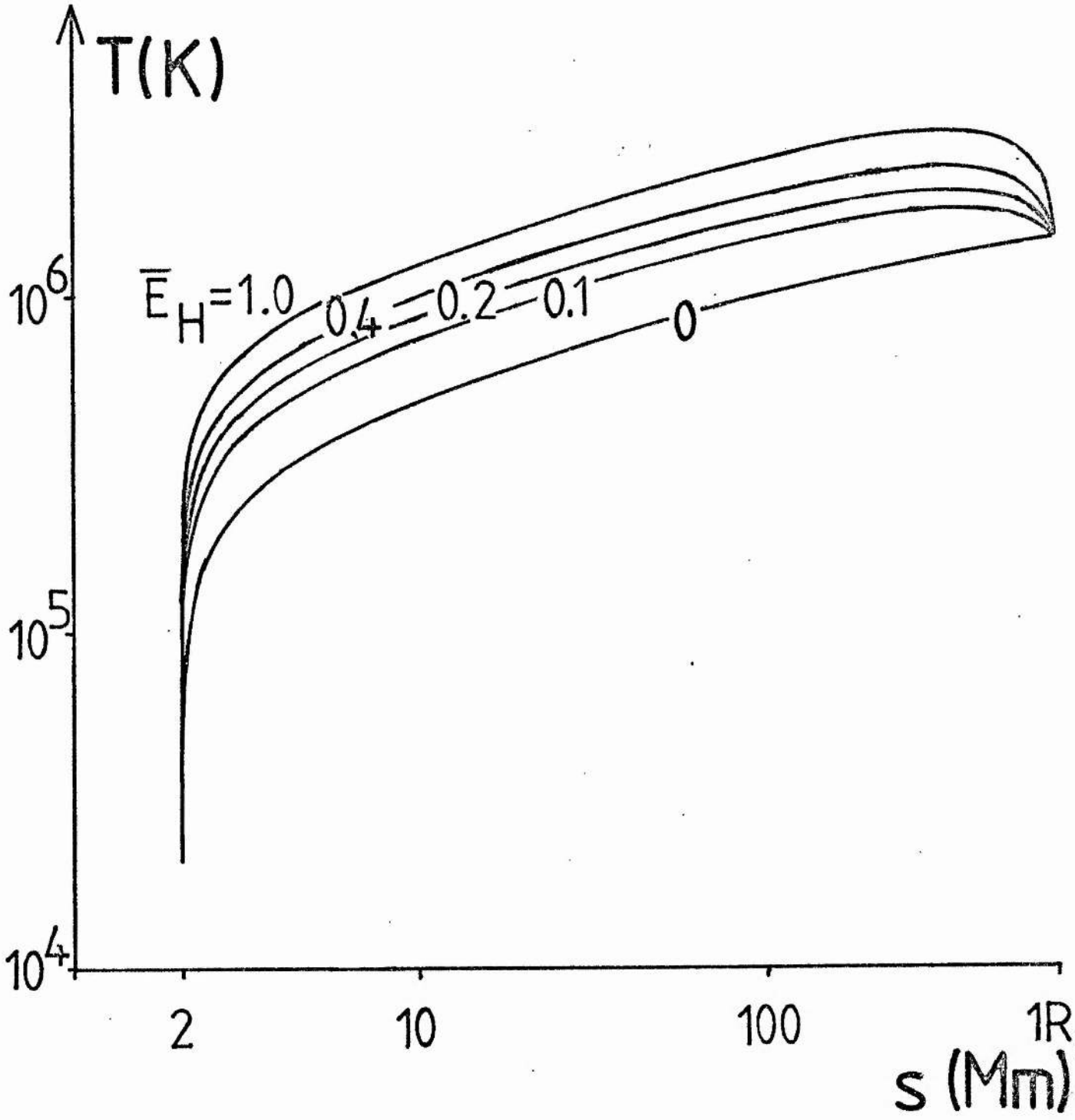

Figure 2.1a The effect of different boundary conditions on a static, spherically symmetric atmosphere with uniform heating $\bar{E}_H$. $T = 2 \times 10^4$ K and $dT/ds = 0$ are taken at the base, $s = 2$ Mm. The temperature is given as a function of distance s above the base when $T = 1.5 \times 10^6$ K at $2R_\odot$.

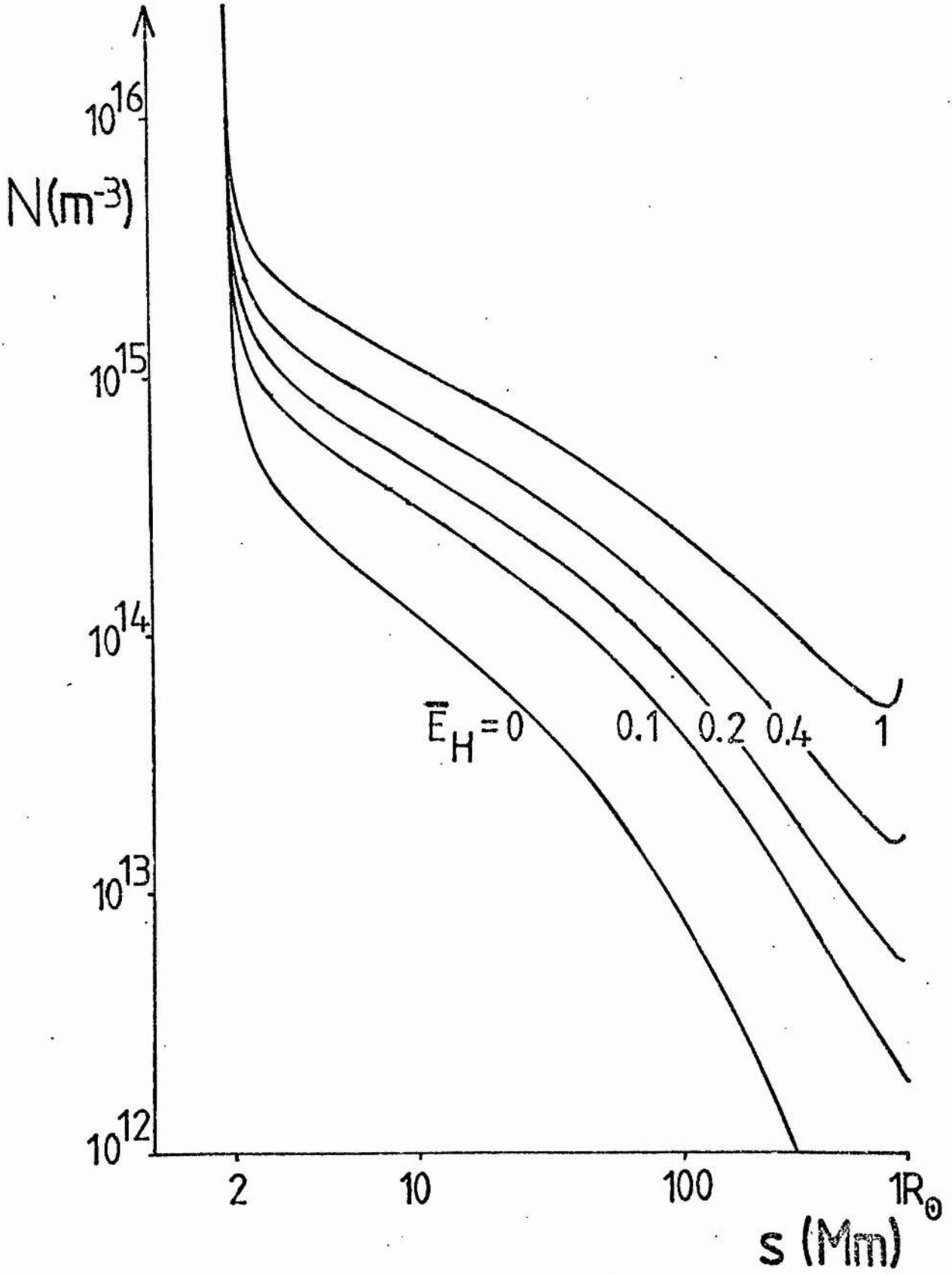

Figure 2.1b The corresponding density profile when $T = 1.5 \times 10^6$ K at $2R_\odot$

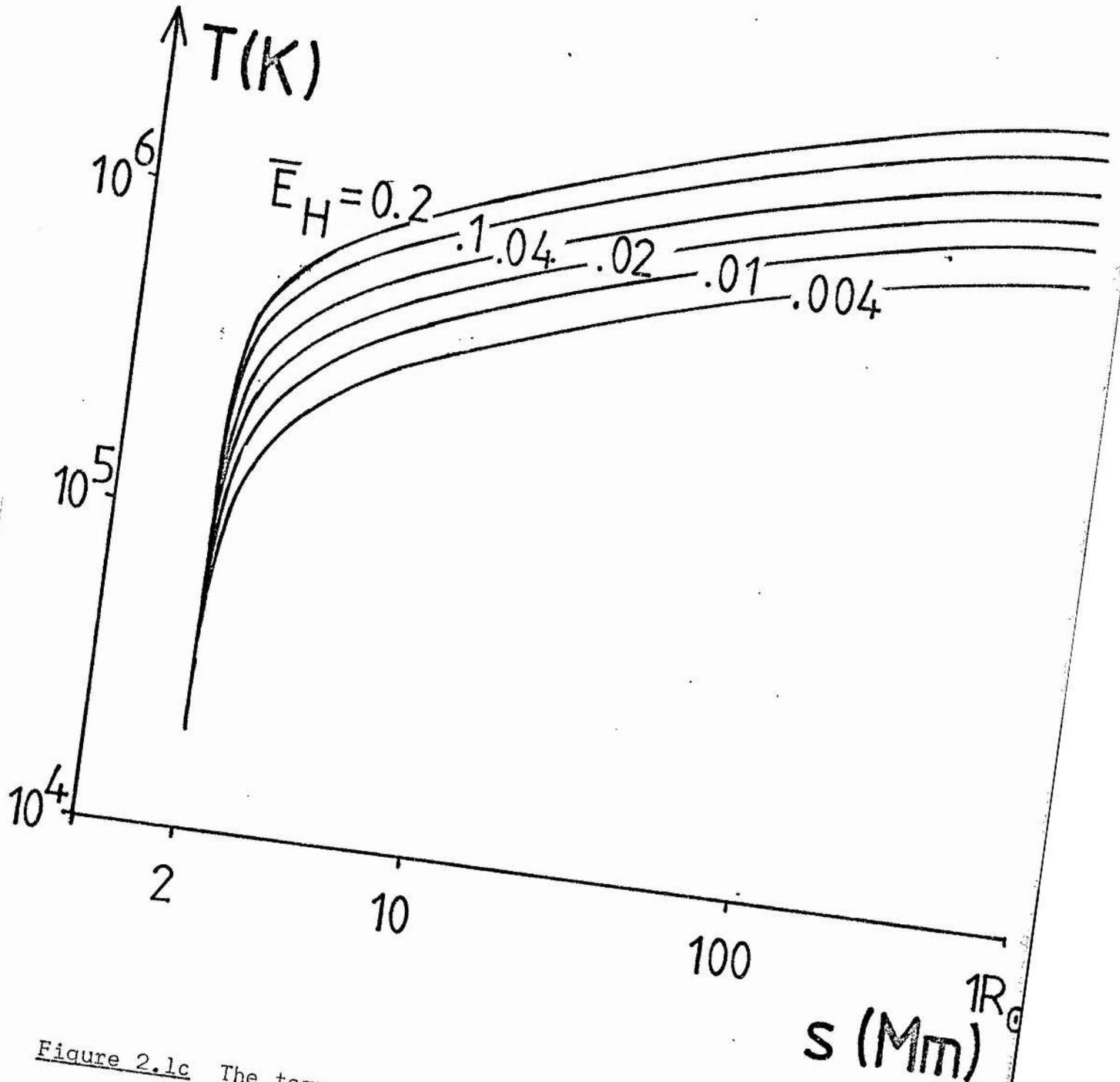

Figure 2.1c The temperature profile when $dT/ds = 0$ at $2R_\odot$.

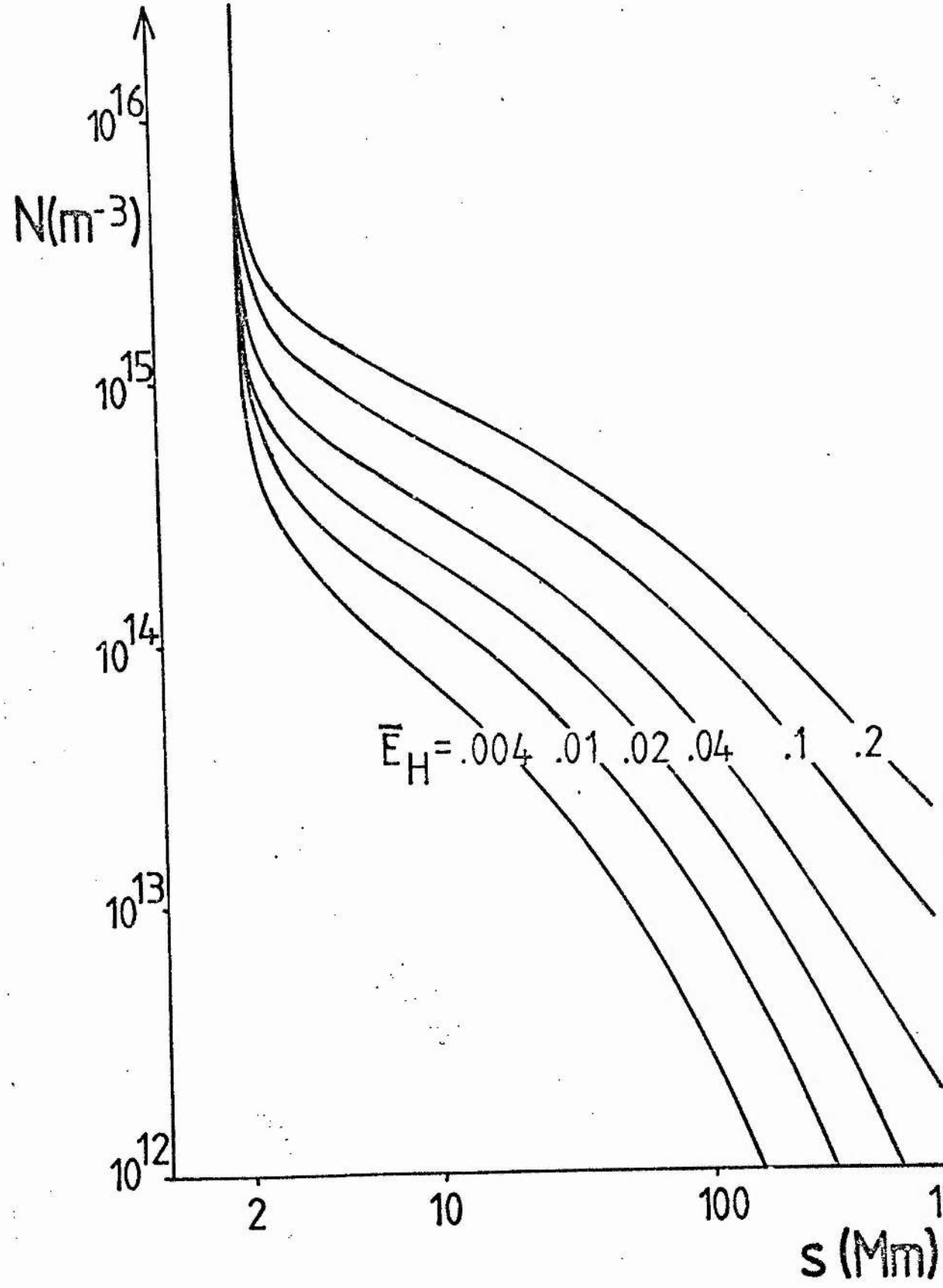

Figure 2.1d The density profile when dT/ds = 0 at $2R_o$.

predicted in Section 2.3, that increasing the heating decreases the temperature. This is because the difference between the heating and radiation gives the rate of decrease of conductive flux. Here there is a fixed flux at the base, and so increasing the heating causes a greater fall in the conductive flux and so a smaller rise in temperature. It is clear that the amount of heating hardly affects the transition-region profile at all, since the radiation dominates heating there. (Beyond the temperature maximum, the fall in temperature is deceptively abrupt simply because of the logarithmic scale.)

2.4.3 Form of the Heating

Figure 2.3 shows the effect of different forms of heating. Three forms are compared in Figures 2.3a and b. Curves A and B are for a heating proportional to volume or density respectively, while curve C is for the case when all the heating is localised uniformly in the height range $1.9R_\odot \leqslant r \leqslant 2R_\odot$. In Figure 2.3a the total amount of heating in the range $R_\odot \leqslant r \leqslant 2R_\odot$ is the same for the three curves. In case B most of the heating occurs lower in the corona where the density is greater and so the temperature rise is relatively small. In case C the heating occurs high up and this produces a hotter corona. In each case the temperature gradient at $2R_\odot$ is roughly the same. This feature was also observed (accidentally) by McWhirter, et al.(1975). The heating

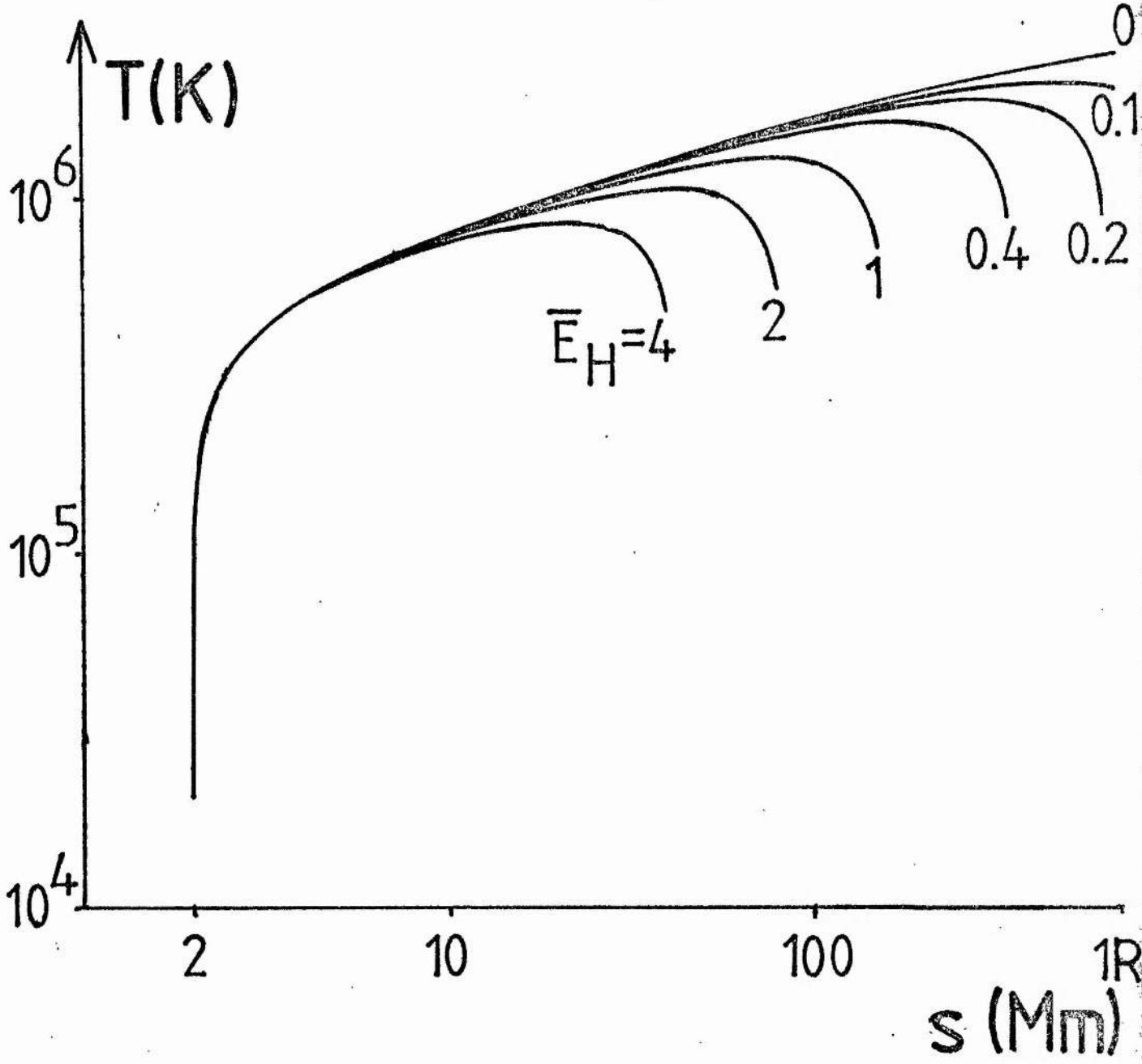

Figure 2.2a The temperature profile for base boundary conditions $T = 2 \times 10^4$ K, $dT/ds = 10.1$ K m^{-1}, $N = 2.12 \times 10^{16}$ m^{-3} and for a uniform heating $\bar{E}_H$.

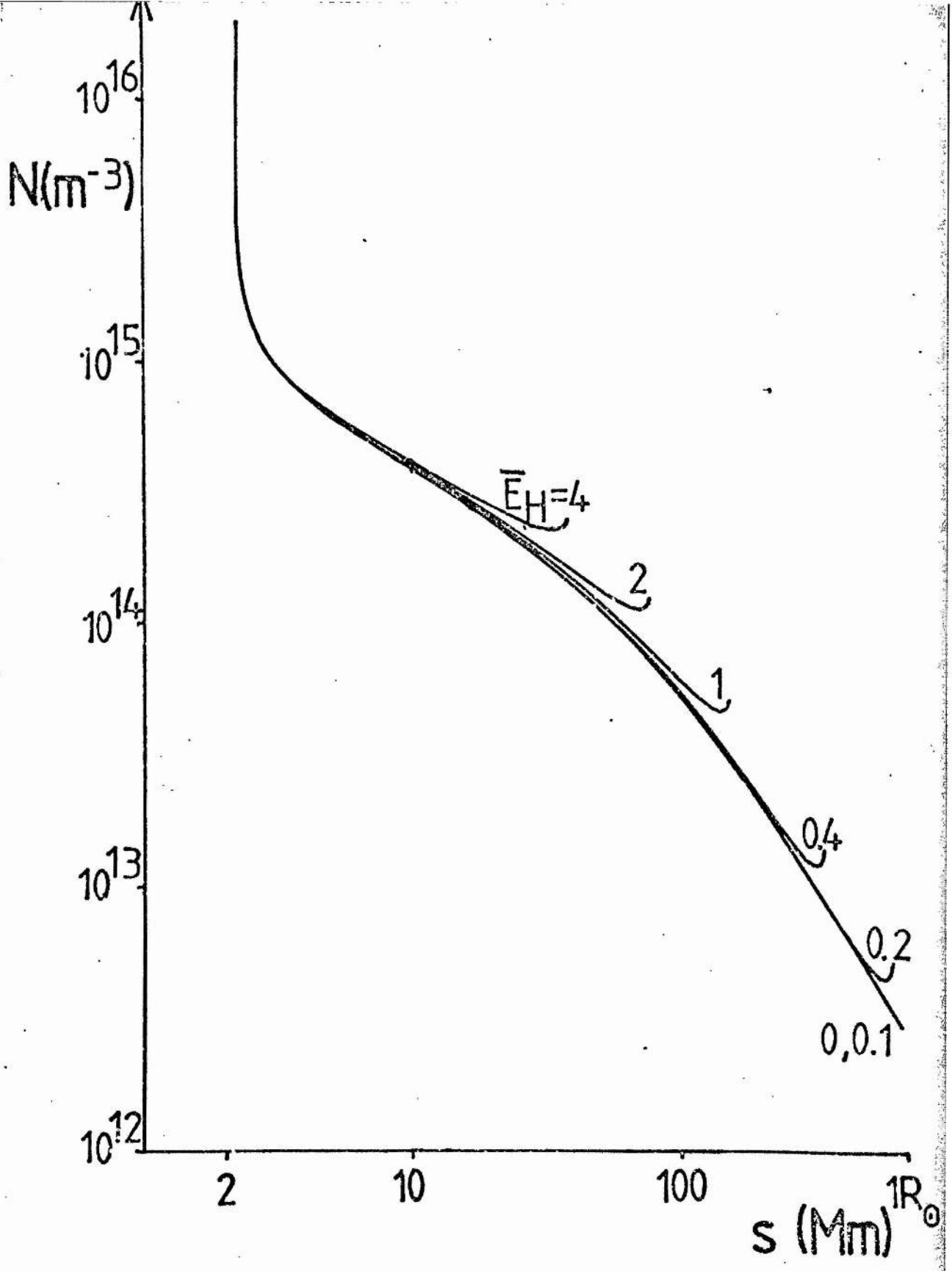

Figure 2.2b The corresponding density profile.

in the erratum is localised lower in the atmosphere compared with the original paper while the total magnitude is (virtually) the same in each case. The erratum gives T_{max} lower and at a lower height. In Figure 2.3b the three forms of heating are compared by imposing the same upper temperature, namely 10^6 K, in each case. The most heat is needed for curve C and the least for curve B. Again curve C gives the hottest corona and curve B the coolest.

Except for the case of no heating, where it rises indefinitely, the temperature has a maximum T_{max} at a certain height h_{max} which depends on the heating. It can be seen from Figure 2.3 that case B tends to produce the broadest and lowest temperature maximum (both in value and position), while case C gives the narrowest and highest maximum. Figure 2.4 shows how T_{max} and h_{max} vary with heating $\bar{H}$, which is measured at a typical coronal density of $5 \times 10^{14} m^{-3}$ in units of the radiation at the same density and a temperature of 10^6 K. Curves A and A^1 refer to uniform heating per unit volume, while B and B^1 are for heating proportional to density. Curves A^1 and B^1 are for a base density that is ten times as great as that of (2.2.5), namely $2.12 \times 10^{17} m^{-3}$. It can be seen that as the heating increases so both the maximum temperature T_{max}, and the height h_{max} at which this occurs, drop. This is more pronounced in the case of heating proportional to density than heating proportional to volume. Increasing the base density by a factor of 10 increases T_{max} by a

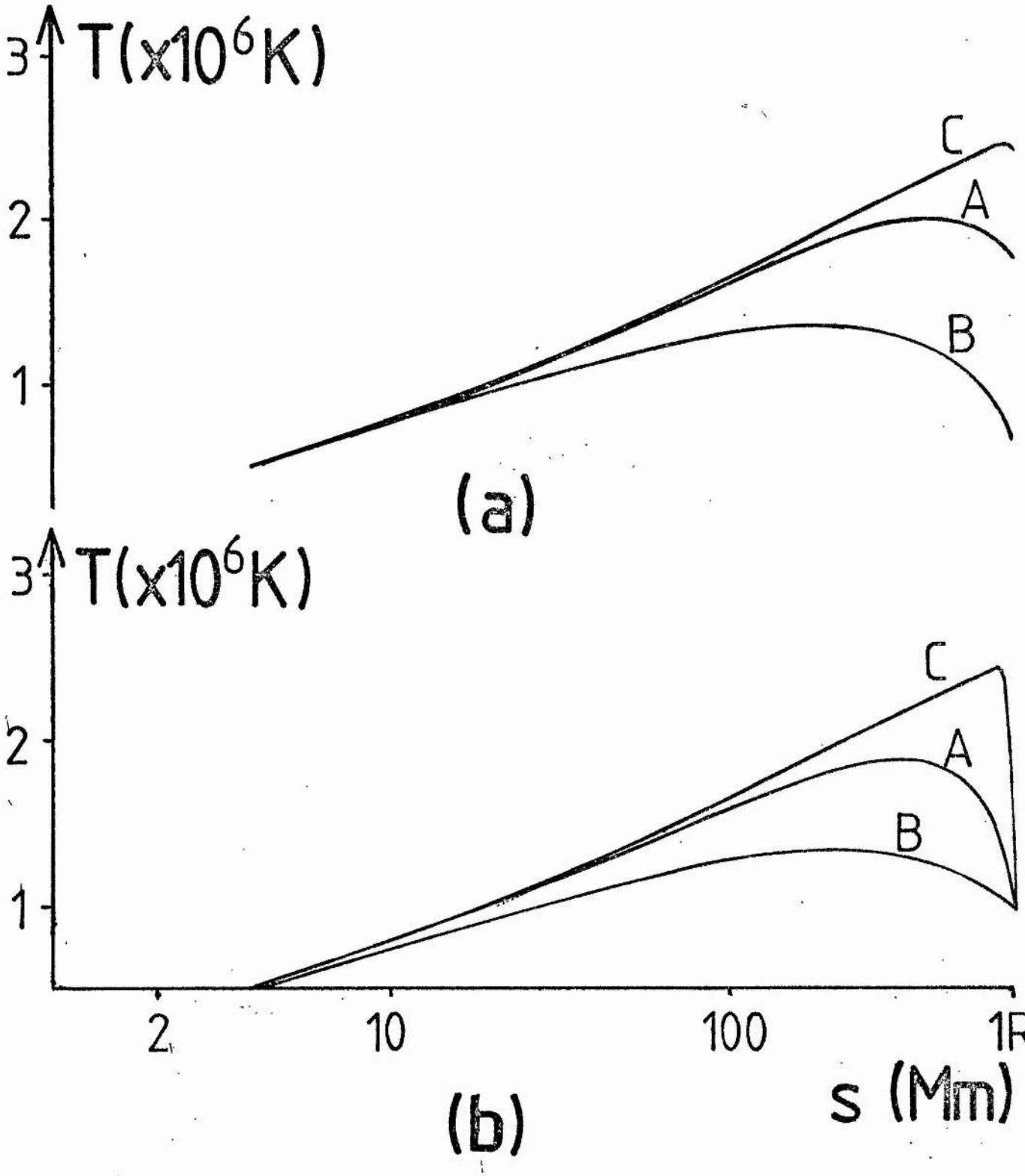

Figure 2.3 A comparison of different forms of heating:
(a) for a constant total amount of heating and
(b) for a given upper temperature, namely $T = 10^6$ K at $s = 1R_\odot$.
In each case curve A denotes uniform heating, B denotes heating proportional to density, and C is for heating localised between $0.9\ R_\odot \leq s \leq 1R_\odot$.

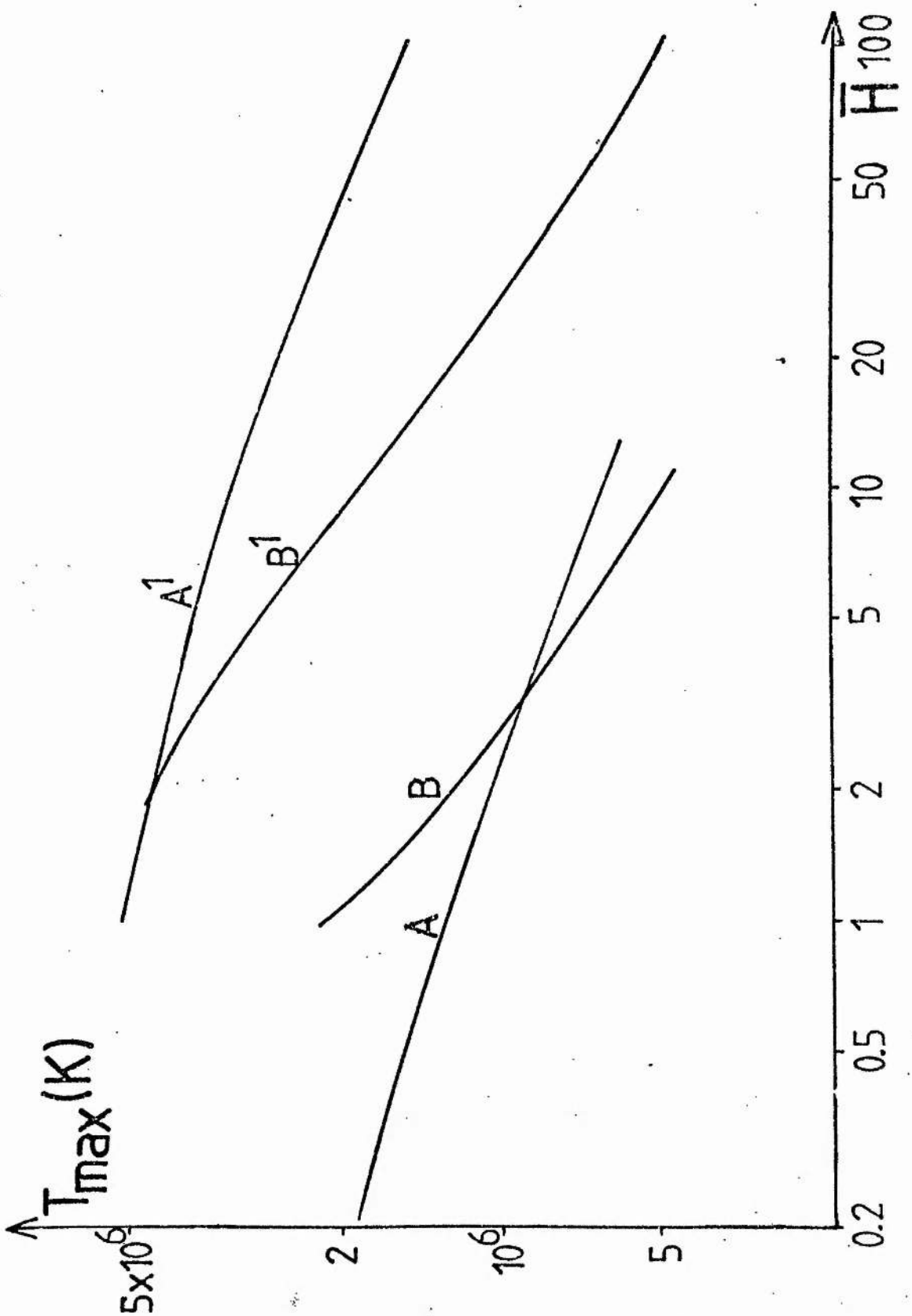

Figure 2.4a The temperature maximum T_{max} for different forms of heating as a function of the heating $\bar{H}$ at a density N_c. Curves A and A^1 are for uniform heating, and B and B^1 for heating proportional to density. The base density N_o is 2.12×10^{16} m^{-3} for A and B, and 2.12×10^{17} m^{-3} for A^1 and B^1.

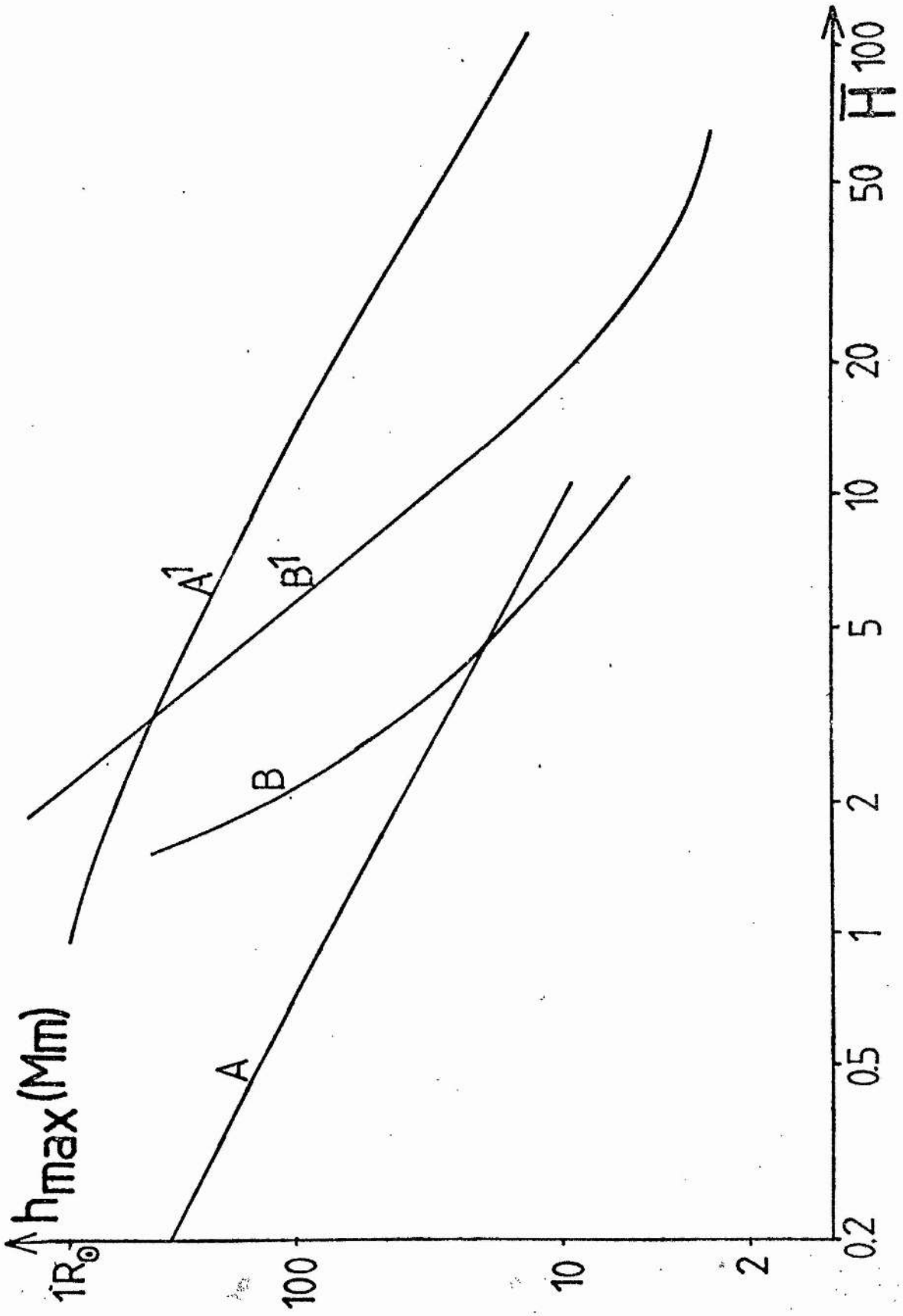

Figure 2.4b The height h_{max} at which T_{max} occurs for the forms of heating and base densities of Figure 2.4a.

factor of about 5 and the corresponding height by an order of magnitude.

2.4.4 Field-Line Divergence

Figure 2.5a shows the effect of a divergence of the field lines for the particular case $\bar{E}_H = 0.2$. It can be seen that the profiles begin to differ near the top of the transition region. As predicted in Section 2.3, the effect of increasing cross-sectional area is to decrease the temperature and to lower the height of the temperature maximum. Again this is dependent on the boundary conditions; imposing upper boundary conditions can make increasing A increase the temperature. With no heating present, the temperature always continues to increase with height, never reaching a maximum regardless of the area profile. A greater area divergence, however, still makes the temperature less because the rise in temperature with height is reduced, since the conductive flux per unit area decreases. If heating is present, an increase in the area divergence has the same effect; this is similar to an increase in the heating. This is expected since heating is proportional to volume and the volume is increasing.

Figure 2.5b gives a graph of T_{max} against heating for various values of A, the ratio of the loop area at the top to that at the base. Thus A = 1 corresponds to a plane parallel atmosphere, and A = 4 to a spherically symmetric one. It is seen that the temperature maximum is much more sensitive to changes in area divergence when

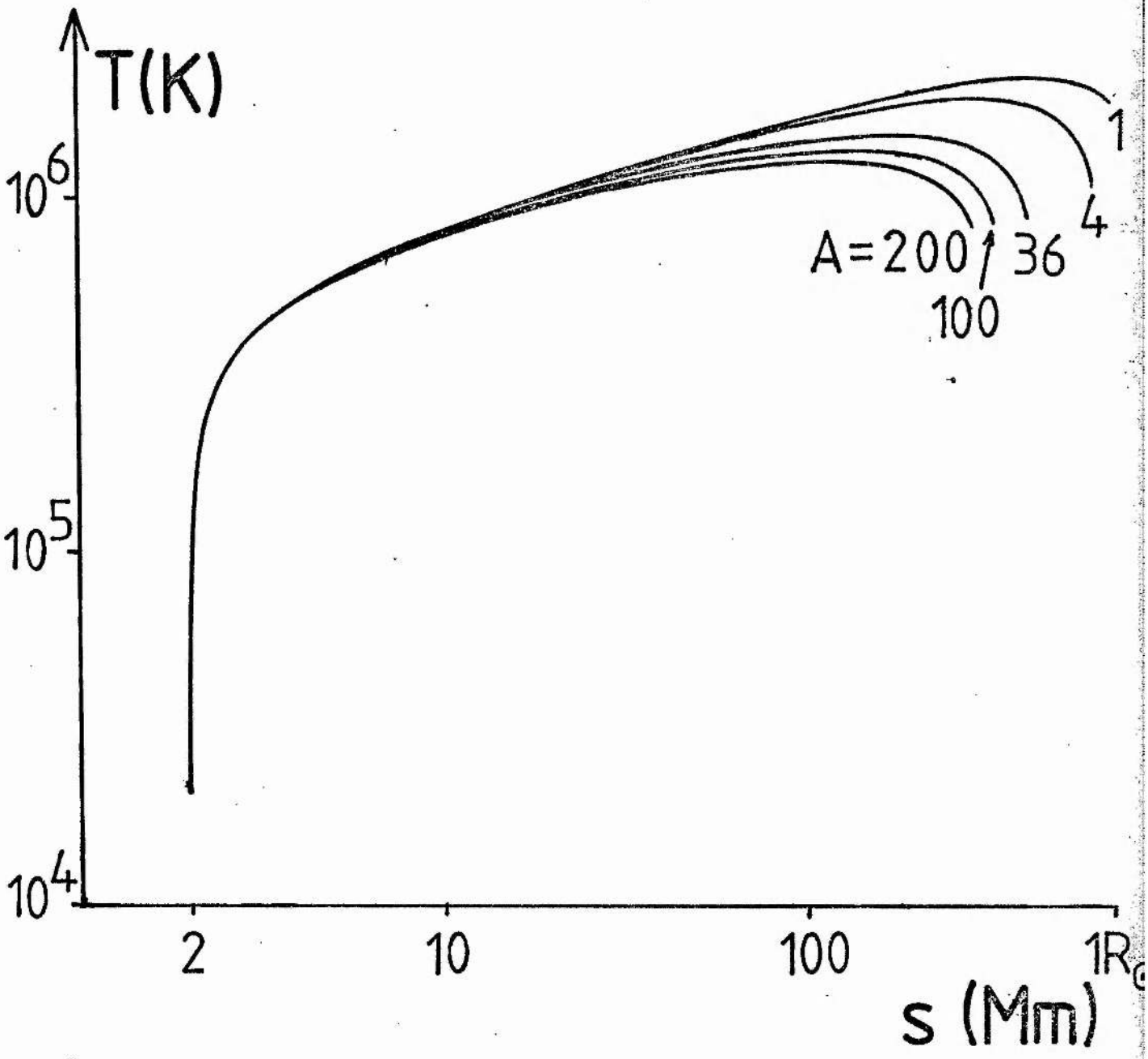

Figure 2.5a The effect of field-line divergence on the temperature profiles for a uniform heating $\bar{E}_H$ of 0.2. A is the ratio of the flux-tube area at the top to that at the base.

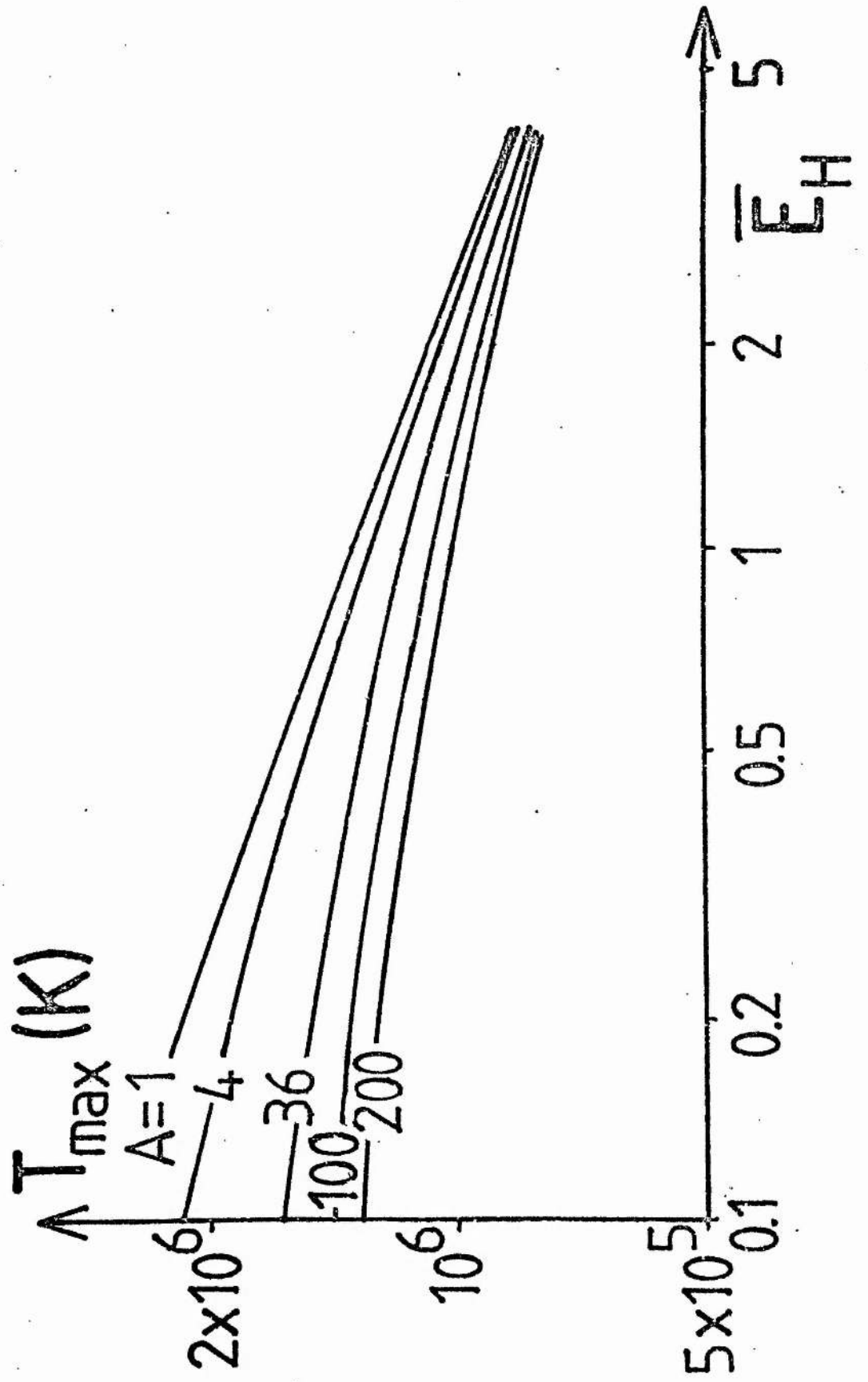

Figure 2.5b The temperature maximum T_{max} as a function of the heating $\bar{E}_H$ for various area divergences A.

the heating is small. Little change in density is observed.

2.4.5 Subsonic Flows

Figure 2.6 shows the effect of flows, both upward and downward when the area divergence and heating are fixed. For a uniform area Equation (2.2.3) implies that the velocity is proportional to the inverse of the density, which decreases by about 4 orders of magnitude between 1 and $2R_\odot$. Therefore, in order to obtain steady flows of a few tens of kilometres per second in the corona, a base velocity of only a few hundred metres per second is necessary. It can be seen in Figure 2.6a that an upflow increases the temperature and takes the temperature maximum further out. However, steady solutions cease to exist when the base upflow is in excess of 62 ms^{-1}. This critical speed depends on the other parametres; for example, when there is no heating in a plane parallel atmosphere, the critical speed is about 130 ms^{-1}. In Section 2.3 it was seen that for a hot steady upflow to exist, the flow must be sufficiently small for the conduction term to be important. A similar lack of steady flow, which may be called a catastrophe, has also been found in the siphon flow calculations of Cargill and Priest (1980) and represents a generalisation to include flows of the onset of thermal nonequilibrium (Hood and Priest, 1979; Chapter 3). At this maximum upflow velocity the hottest model corona was obtained, since the other effects considered (namely increasing heating, area divergence, or

downflow) all reduced the temperature.

A downflow has a similar effect to raising the heating; it decreases the temperature and reduces the height of the temperature maximum. However it is still the presence of heating which causes the temperature maximum; if there is no heating the temperature increases indefinitely with height. This is also evident in the work of Pneuman and Kopp (1978). For the base density which has been taken here, fast downflows never allow the temperature to reach 10^6 K, although higher base densities such as those found in active regions would allow higher temperatures.

The density, shown in Figure 2.6b, as expected increases with a fall in temperature, and vice versa, for heights up to 200 Mm above the surface. However, as can be seen on this graph, the lines of density cross over at 200 Mm; for heights above this the pressure has decreased so much that the density decreases with temperature. This is a general feature, not just confined to the case of flows, and will be seen again in Chapter 3. The reason is because in a situation where the temperature is consistantly lowered over a large height range, as in the case of a large downflow, the gravitational scale height is correspondingly reduced, and so the pressure decreases at a greater rate. This is the same effect as is assumed to occur in cool coronal loops.

In Figure 2.6d, T_{max} is plotted as a function of the heating, for different flows. As with the case of different area divergences, T_{max} is more sensitive to the

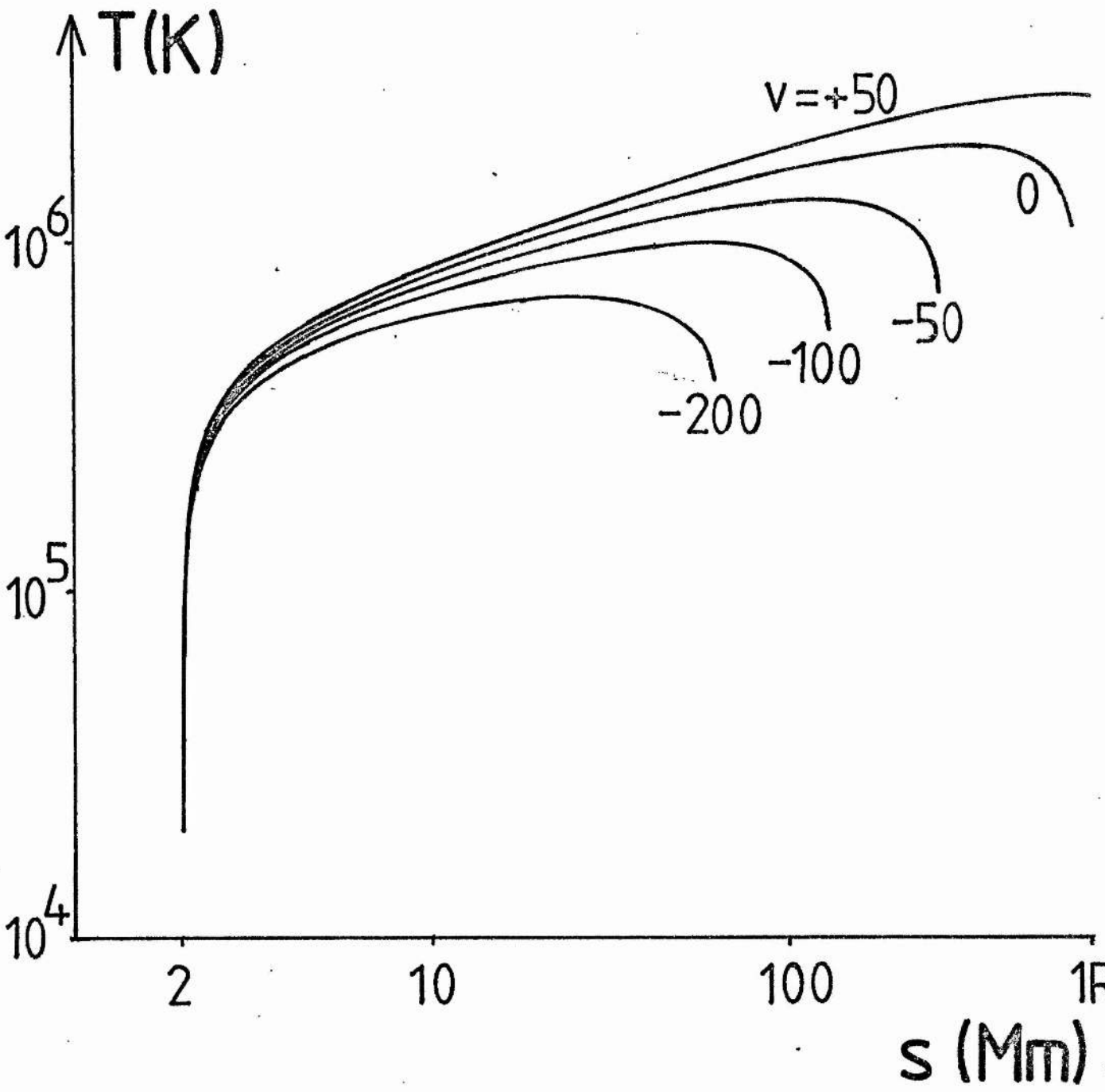

Figure 2.6a The effects of flow on a spherically symmetric model atmosphere with a uniform heating $\bar{E}_H$ of 0.2. The temperature profile for different base flow velocities in $m\,s^{-1}$.

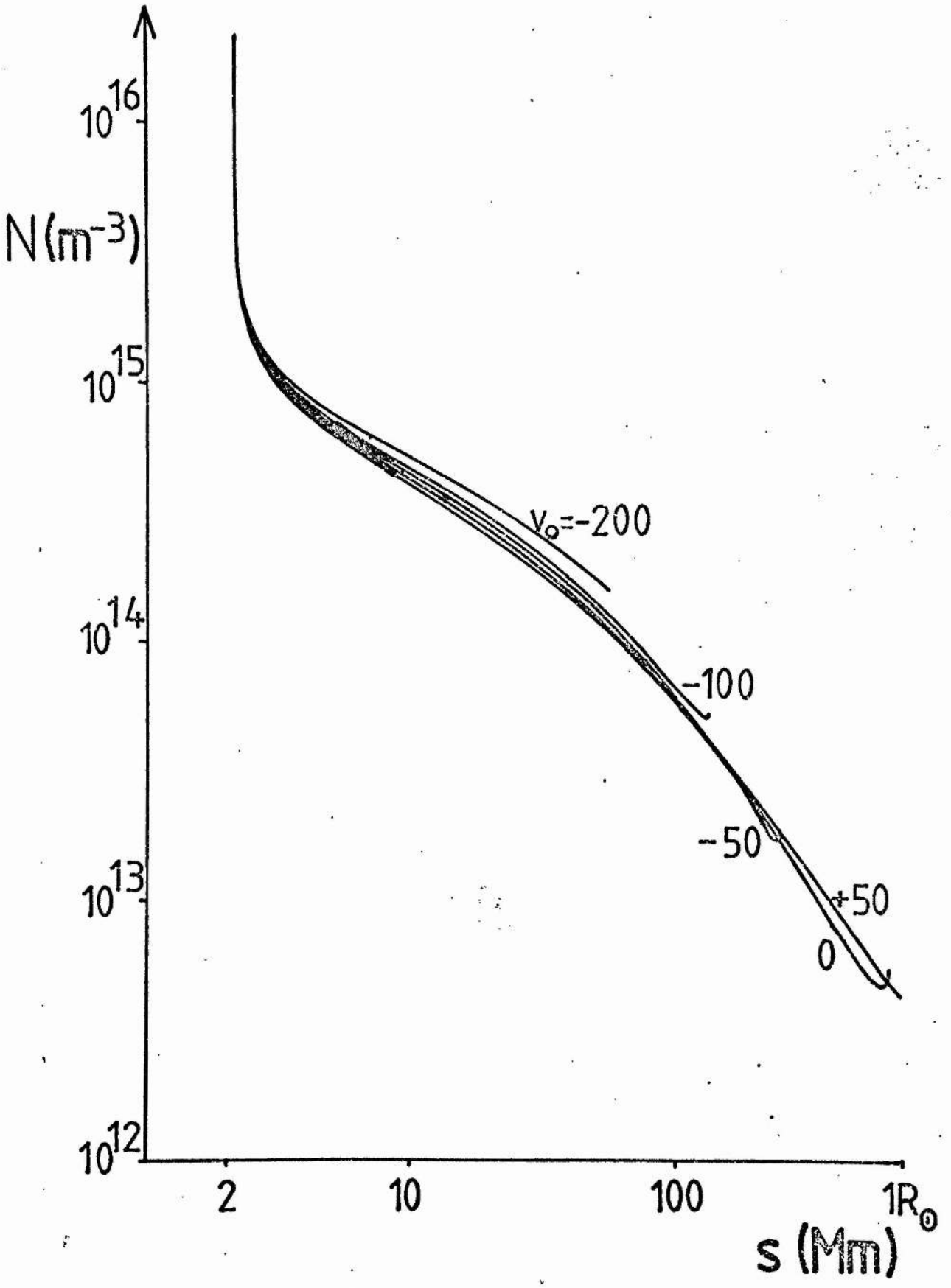

Figure 2.6b The effects of flow on the density profile.

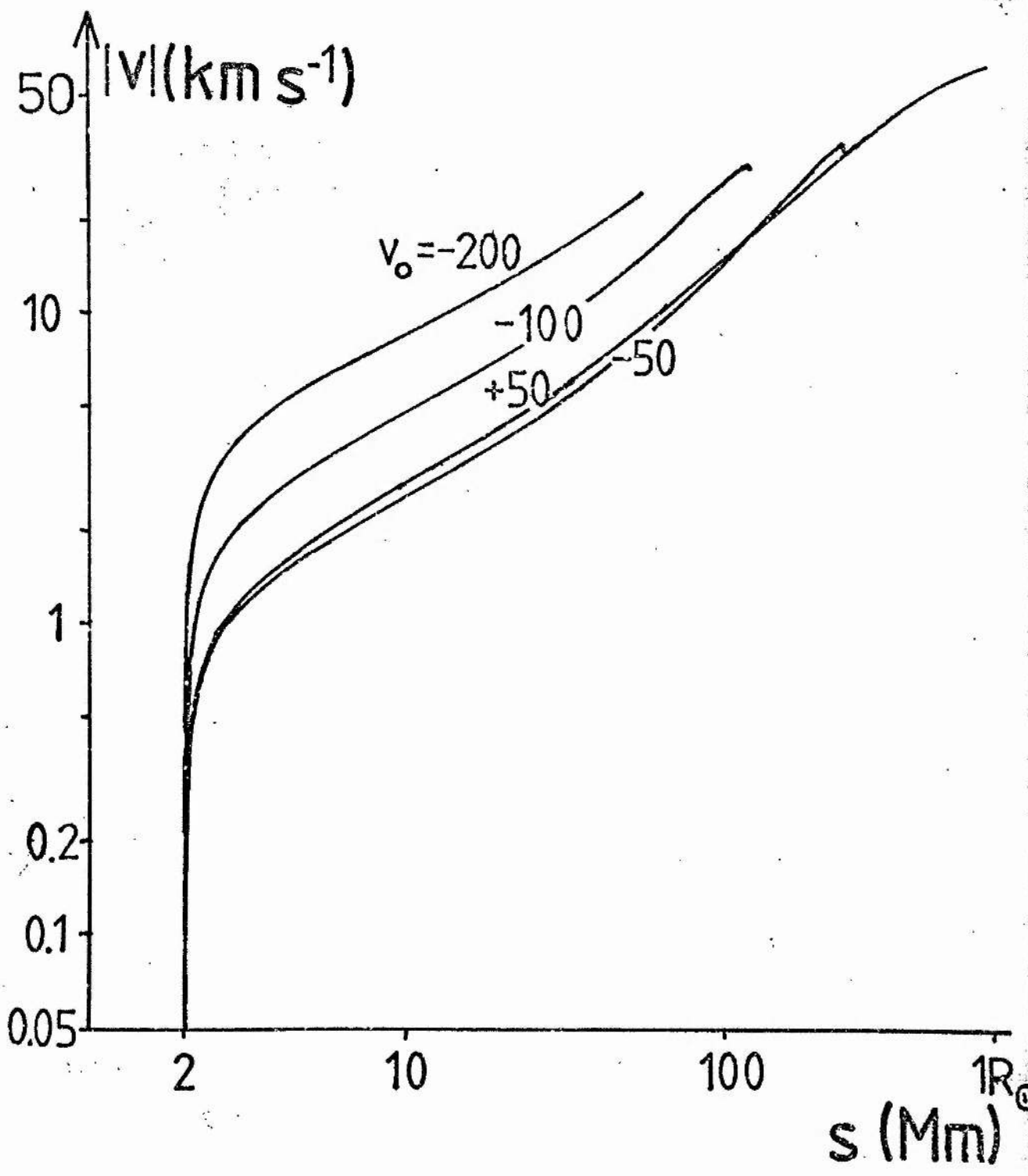

Figure 2.6c The effects of flow on the velocity profile.

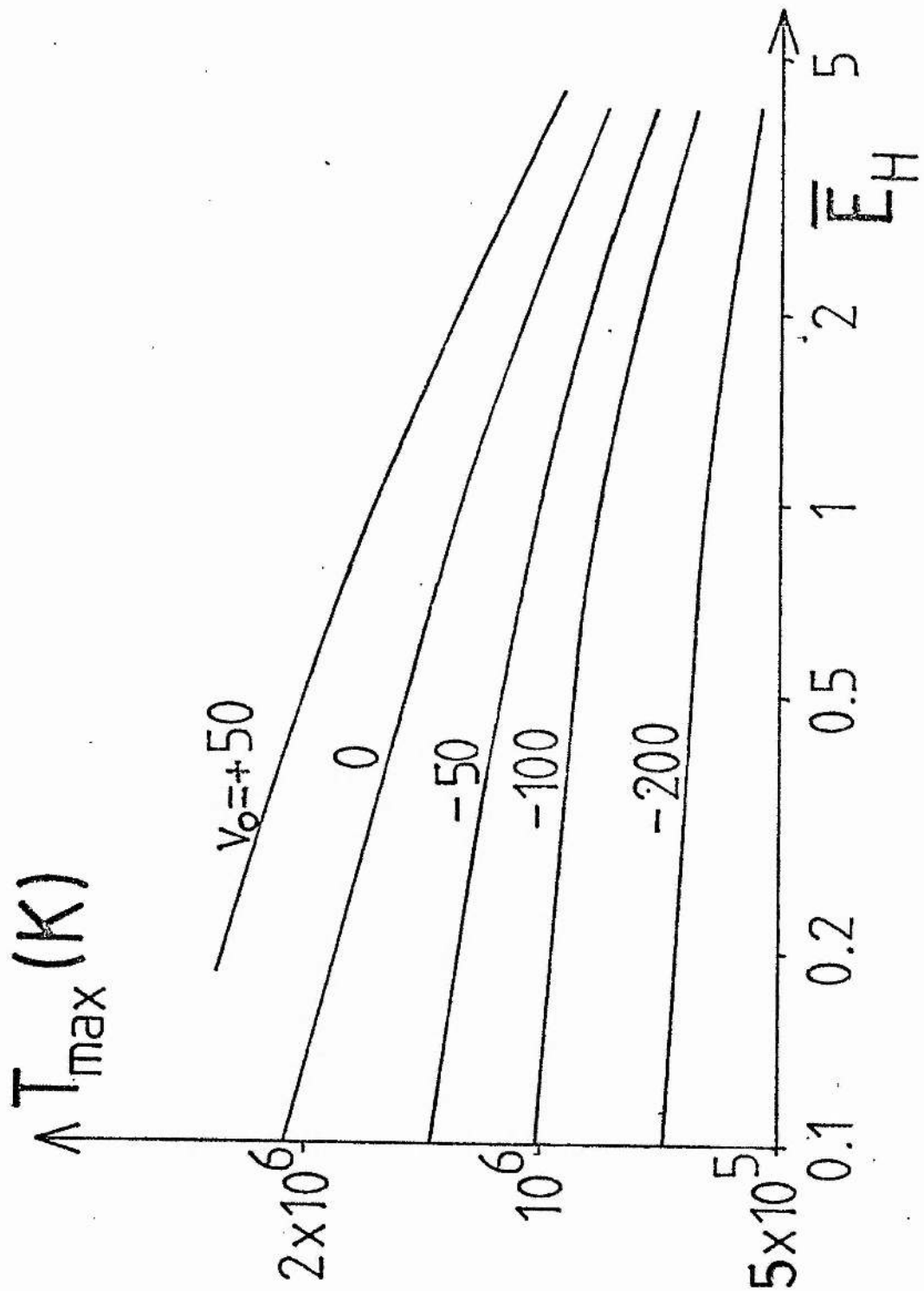

Figure 2.6d The temperature maximum as a function of the heating for various flow rates.

flow when the heating is small.

2.5 SUMMARY

The transition region and inner corona of an open field region such as a coronal hole have been modelled. Different boundary conditions have been compared, and a variety of values and forms of heating, rates of divergence of field lines, and up- or downflow velocities have been taken. The results may be summarised as follows:

(i) The boundary conditions chosen are important and alter the solutions appreciably. In particular, if a model atmosphere does not match with the Harvard Smithsonian Reference Atmosphere but rather some combination of temperature and temperature gradient is imposed at large distances, some of the conclusions below are altered. Generally an increase in the heating causes the temperature profile to be more concave, and thus decrease more rapidly at large heights.

(ii) If temperatures of order 10^6 K are to be obtained out at great distances from the Sun, then either the heating is very small or it must decrease rapidly with height (or the base pressure must be larger than taken here). A large uniform heating does not give realistic results because there is nothing to balance it at great heights. If the heating is localised at great altitudes, it tends to produce a narrower and larger temperature maximum at a greater altitude than a uniform heating and even more so

than a heating proportional to density.

(iii) Increasing the heating (for fixed base conditions) decreases the coronal temperature and reduces the height of the temperature maximum, but the transition region is unaffected. Heating is the only mechanism which can cause a temperature maximum; if it is assumed absent then the temperature will rise indefinitely with height, regardless of any other factors. This is because flows or area divergence merely redistribute energy along the loop rather than act as a source of heat.

(iv) A greater divergence of field lines acts to reduce the temperature. The difference between a plane parallel model and a spherically symmetric model is typically less than 10% below 200 Mm above the surface and only about 20% at two solar radii.

(v) An upflow increases the temperature and the height of the temperature maximum, while a downflow decreases them.

(vi) A maximum possible upflow was found, beyond which a catastrophe occurs so that no steady hot solution exists.

A clear result from Figures 2.2 to 2.6 is that for fixed base boundary conditions, the transition region appears virtually identical in each case; the height at which the temperature reaches 5×10^5 K or 10^6 K does not vary much with either different heating, area profiles or velocities. The difference in the height at which they reach 10^6 K between a plane parallel part of the

atmosphere and one which increases to 10 times its area at one solar radius above the surface is about 1 Mm. The effect of flow is a little more marked, but an upflow reaches 10^6 K at roughly the same height as the static case, while large downflows do not reach 10^6 K at all.

Varying the temperature gradient at 2×10^4 K has a negligible effect on the transition region, but varying the density there can cause important differences; for instance if the base density is increased by a factor of 5 the density at 10^6 K increases by an order of magnitude and the height at which it occurs decreases by 15 Mm.

All this suggests that it may be possible for the transition region and inner corona to be modelled as two separate problems. This is especially appealing in view of the difficulty of modelling the transition-region physics adequately. The temperature gradient in the transition region is so high that normal fluid pictures may be inadequate, and in any case a static profile may be thermally unstable (Antiochos, 1980; Hood and Priest, 1980; Chapter 5). Also the geometry of the transition region may be much more complex; see, for instance, Gabriel (1976a,b), where a two-dimensional structure is taken to model the configuration above a supergranular cell.

It is possible to deal with the corona separately from the transition region by fixing "base" parameters of T and N at the bottom of the corona at, say, 5×10^5 K or 10^6 K. This proceedure was adopted by Hood and Priest

(1979) and will be used in the following chapter. This allows a certain amount of flexibility for the conductive flux at the new base point chosen. It is assumed that this base flux must lie within a narrow region of values. This range will depend on the heating and the details of the transition region. Using a purely optically thin form for the radiation, there are, in any case, inaccuracies involved in starting as low as the plateau at 2×10^4 K, since the plateau is produced by an optically thick effect, namely the leakage of Lyman α photons. Furthermore, as indicated in the models of Basri, et al. (1979), the pressure at 2×10^4 K may vary from one feature to another and need not be the value that has been taken in the majority of cases here.

Above the transition region, the coronal magnetic field may be either open or closed. In some respects, the more interesting situation is the closed one. This will be modelled in the next chapter in the form of a coronal loop, starting with a base temperature of 10^6 K. Immediately this requires an upper boundary condition to match the two loop legs at the summit, the result of which gives interestingly complementary results to those thus far.

3. SOLAR CORONAL LOOPS

3.1 INTRODUCTION

As has been seen from observations, the corona is far from being vertically stratified, and most of it is a complex of loop structures dominated by the magnetic field. It is this feature which is modelled here as an extension to the theory developed in the preceeding chapter, which modelled open regions, mainly by fixing all boundary conditions at one point, namely the base.

Several static coronal-loop models have been put forward. Often a first assumption is to prescribe equal parameter values at both footpoints. In the absence of a flow this gives symmetry about the summit, so that only half of the loop need to be modelled. Loops are observed to endure for times between several hours and more than a day, while a loop's radiative cooling time is typically about one hour, which suggests the presence of some form of steady energy input. If the energy-balance equation is solved, a heating term is often assumed, due to some form of energy input, such as wave heating.

Rosner, et al. (1978) considered loops of constant pressure, symmetric about their summits with a zero temperature gradient there. They possessed a uniform heating (in volume), and a simple form for the radiation was adopted with $\alpha = 1.5$ or -0.5 in the temperature

range less than or greater than $10^{5.1}$ K, respectively. Also they assumed zero base conductive flux, and obtained an expression for the summit temperature T_1 in terms of the pressure p and loop length L,

$$T_1 \approx 1.4 \times 10^4 (pL)^{1/3}$$

in M.K.S. units, and heating

$$E_H \sim p^{7/6} L^{-5/6} .$$

They also suggested that static solutions with a temperature maximum away from the summit are thermally unstable. Serio, et al. (1981) have proceeded along similar lines and extended Rosner, et al.'s scaling laws to the case of tall loops where the pressure falls off in the isothermal part of the loop. Also they included a heat input which falls off exponentially with height at a given rate of damping.

Craig, et al.(1978) derived a "scaling law" of the form

$$T_1^{9/4} \sim N_1 L$$

under the same assumptions, except that they claimed theirs is independent of the form of the heating. They approximated α in the radiation term by -1.

In an unpublished paper, Emslie and Machado (1979) treated constant pressure, thermally isolated loops, allowing a heating function $H \sim N^{\delta}$. They found $\delta < 2$ is necessary for the existance of coronal temperatures unless T_o is much higher than 2×10^4 K. They obtained the same

scaling law as Rosner, et al. and found (for constant heating) that if T_o is increased, then T_l and N decreases.

Vesechy, et al.(1979) numerically modelled the effects of area divergence and gravity. They disagreed with Rosner, et al., saying that a maximum temperature away from the summit does not imply thermal instability. They found that raising the heating by a factor of 10 increases the temperature by a factor of only 2, and the density by 5. Varying the area divergence affects the density only slightly, and the temperature even less, with an increase in area divergence causing a density enhancement and a lower summit temperature. This is, however, very much dependent upon their chosen boundary conditions. Their factor Γ causes the height (for a fixed length) to change with the area divergence, since they modelled only a line dipole field. Consequently, a decrease in density may be due merely to a loop's height being taller and therefore having a correspondingly lower pressure and, at a given temperature, density. Also, they chose zero base conductive flux at 3×10^4 K, and so for constant length and heating rate, a change in area divergence must also affect the value of the base pressure. It was shown in the previous chapter that a divergent field has the same effect as heating, and so for Vesechy, et al.'s boundary conditions a greater field-line divergence with unaltered geometry should increase both the temperature and density.

Landini and Monsignori Fossi (1975, 1979) attempted

to model an active region as a collection of individual, vertical tubes of constant pressure, with a balance between conduction, radiation and heating. Temperature against height was evaluated and compared with observations. However, no upper boundary conditions were mentioned and their results would seem more applicable to an open region of the solar atmosphere.

Chiuderi, et al. (1981) derived a scaling law for a heating proportioned to T^{γ}. For vanishing base flux this gave, in M.K.S. units,

$$pL = 1.2 \times 10^{-14} T^{3.25} Z(\gamma),$$

where

$$Z(\gamma) \approx (\gamma + 6.8)^{-1.01}$$

is a useful numerical fit for $Z(\gamma)$. From this it was concluded that γ is so insensitive to changes in parameters of pressure, length and temperature, that even if these were observed to within an accuracy of 10%, the possible range of γ is enormous; for example if $Z(\gamma) = 0.14$, it can only be said that γ lies somewhere between -2.2 and $+6.7$.

Scaling laws relating the coronal temperature, and the transition-region pressure and conductive flux have been found by Jordan (1975, 1976) using the emission-measure technique introduced in Section 2.1.1. The differential emission measure from a feature of interest such as an active region can be calculated from EUV and

X-ray line intensities. Two examples have been shown in Figure 3.1. Figure 3.1a from Jordan (1976) shows the emission measure throughout the transition region. Here the "shape" of the curve in the upper transition region does not vary too much between different types of regions on the Sun; one reason is because (virtually) all features reach coronal temperatures of 10^6 K. Figure 3.1b from Levine and Pye (1980) gives one example of the differential emission measure throughout coronal temperatures. This part is seen to vary greatly from feature to feature. Only one emission line was used below 10^6 K in this graph and so the upper transition-region portion is not well represented.

In the upper transition region, 2×10^5 K $\lesssim T \lesssim 10^6$ K, the differential emission measure is well approximated by

$$\int_{\Delta T} N^2 \, ds = a T^b , \qquad (3.1.1)$$

where ΔT is the temperature range over which a given line is formed, and s represents height. a and b are found to be constants. For Figure 3.1a, the value of b is 2.7. However it is necessary to correct this value for the network effect caused by the splaying out of the field lines from the supergranular boundaries into the uniform corona (e.g. Mariska, et al., 1981). This brings the value of b down to 1.2, and 1.5 has often been used. The constant a depends on the total amount of emission and will vary from region to region. Assuming N and dT/ds are constant over ΔT, Equation 3.1.1 can be stated

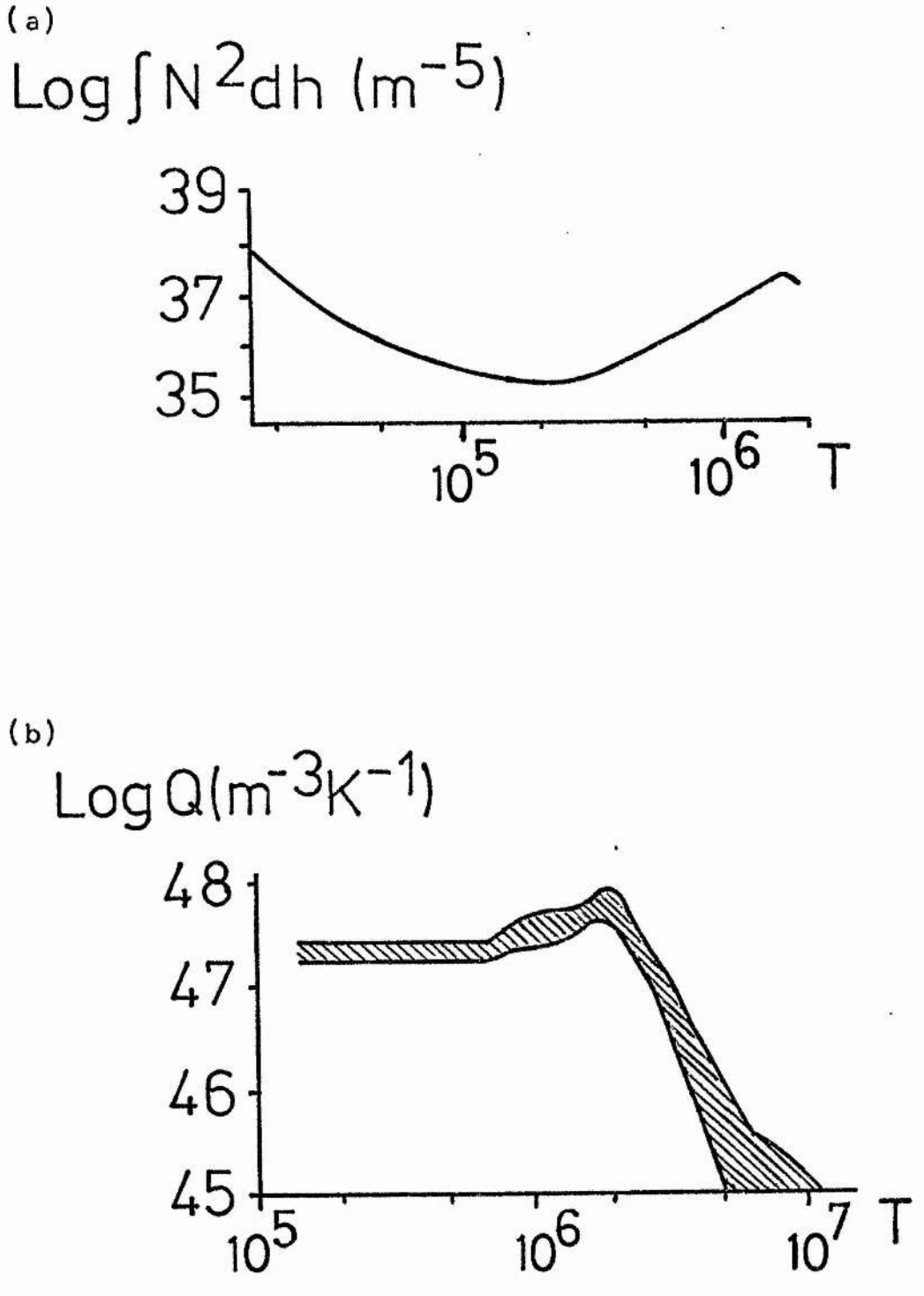

Figure 3.1 The empirically determined emission measure from (a) Jordan (1976) converted to represent the average flux from the whole of the solar disc, and
(b) Levine and Pye (1980) for active region McMath 12628 using helium-like X-ray lines.

in differential form as

$$\frac{dT}{ds} = \frac{N^2 T^{1-b}}{ab} \quad . \tag{3.1.2}$$

Also, the conductive flux F_c is

$$F_c = \frac{\kappa_o p^2 T^{3/2-b}}{4k^2 ab} \quad , \tag{3.1.3}$$

and it can be seen that under the assumption of constant pressure, $b = 3/2$ corresponds to constant conductive flux. Proceeding with Equation (3.1.2), using the equation of hydrostatic equilibrium, a first integral can be found to be

$$p_o^2 - p^2 = m_p abg\left(\frac{T^{b+1} - T_o^{b+1}}{b-1}\right) \quad , \tag{3.1.4}$$

where T_o is taken as 2×10^5 K and p_o is the pressure there. If it is now assumed that at the position of the coronal temperature maximum T_{max} the pressure becomes negligible and that this temperature is sufficiently high so that $T_{max} \gg T_o$, then Equation (3.1.4) reduces to

$$T_{max}^{b+1} = \left(\frac{b+1}{m_p abg}\right) p_o^2 \, .$$

If b is taken as $3/2$ then

$$T_{max}^{5/2} = \frac{5}{3 m_p ag} \, p_o^2 \, , \tag{3.1.5a}$$

and also from (3.1.3),

$$F_c(p_o) = \frac{\kappa_o p_o^2}{6k^2 a} \tag{3.1.5b}$$

so that

$$F_c(p_o) = \frac{\kappa_o m_p g}{10 k^2} \, T_{max}^{5/2} \, . \tag{3.1.5c}$$

These three relations (3.1.5) relate the coronal temperature with the pressure and conductive flux in the transition region. The pressure and the value of the constant a now completely define the structure.

It may be the case (Jordan, 1976) that the above analysis also holds for each of the individual loops which comprise an active region, each tube having its own value of p_o and T_{max}. Under this assumption a further paper (Jordan, 1980) compared several heating functions which have been taken for recent energy-balance models. She showed that in many cases they do not well reproduce the observed value of $b = 3/2$ in the upper transition region.

It was suggested by Priest (1978) that a possible cause for the astonishing cool cores observed in some active-region loops is a lack of static equilibrium at coronal temperatures. This was modelled in detail by Hood and Priest (1979) by solving the energy equation for a coronal loop. Constant pressure was assumed and based boundary conditions set for temperature and density. Values for the loop length and rate of heating were then chosen which specified a solution from which the base flux could be deduced. It was found that, because of the non-linearity of the energy equation, there are circumstance for which no equilibrium exists. It was suggested that a cool core may form when an originally hot loop evolves to such a state of non-equilibrium - usually by an increase in the loop's length or a twisting of its field lines.

One limitation of the work of Hood and Priest (1979)

is that their loops possessed uniform pressures, so their model was relevant only to loops with a height smaller than a coronal scale height. Their model is generalised in the present chapter to include the effect of gravity by assuming the plasma to be in hydrostatic equilibrium. In this case an extra, independent parameter exists, since the length, base pressure and heating rate cannot be combined into just two dimensionless parameters as was the case for Hood and Priest.

3.2 EQUATIONS

A loop is here represented by a magnetic field line in the shape of an arc of a circle, whose centre C may be above or below the photosphere. Figure 3.2 shows a typical loop, with distance s measured along the loop from $s = 0$ at a footpoint (where the temperature and density are T_0, N_0) to $s = L$ at the loop summit (where $T = T_1$ and $N = N_1$). The ratio of the diameter of the cross-section of the loop at $s = L$ to that at $s = 0$ is denoted by d, such that, when there is no flux-tube divergence, the value of d is unity. The length of the loop is assumed to be much greater than its cross-sectional diameter, so that the approximation by a single field line is reasonable. The height of the loop is taken to be rD and the distance between its footpoints 2D, so that $r = 1$ for a semi-circular loop. In the bulk of this chapter,

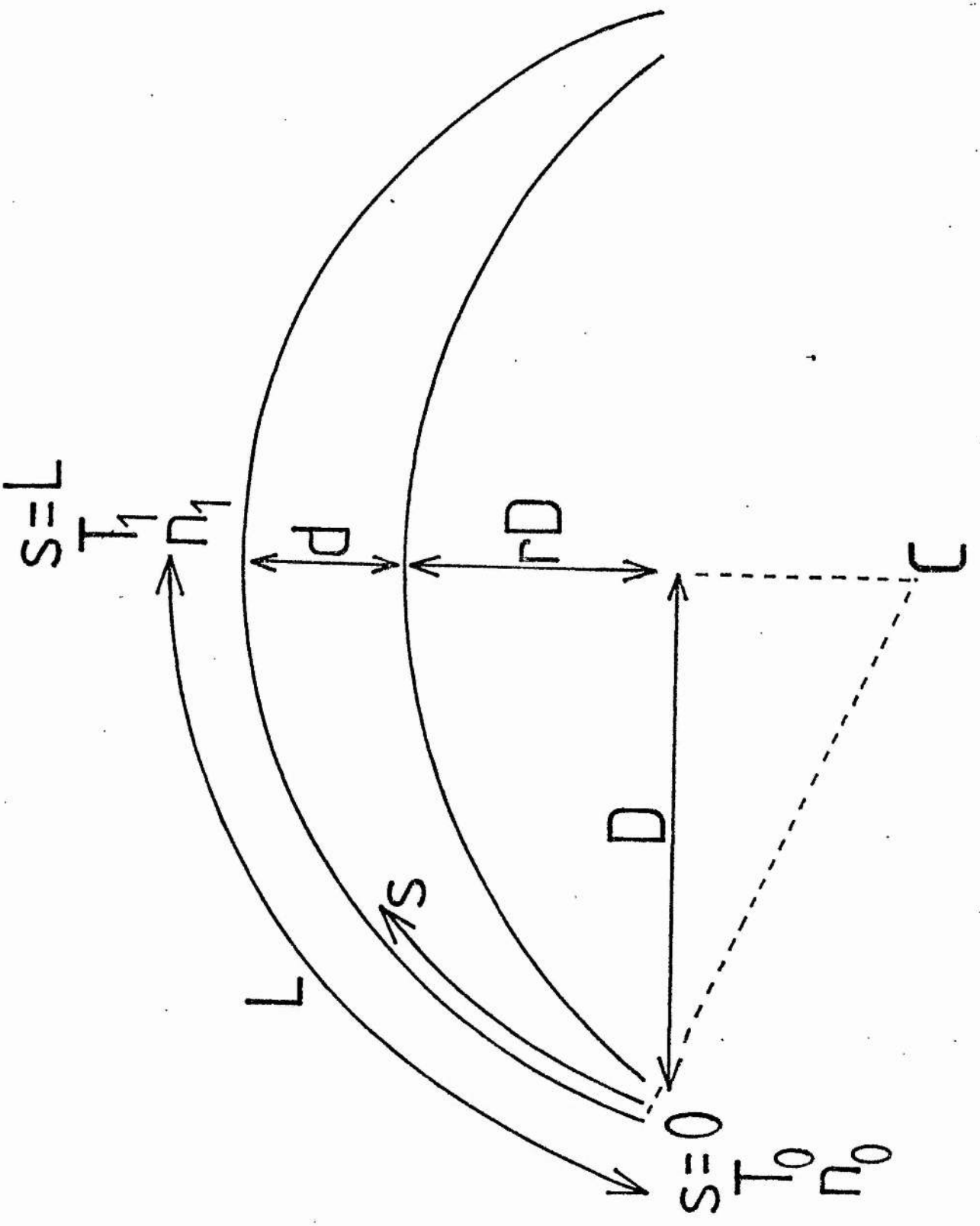

Figure 3.2 The notation for a loop of length 2L with temperature T_o and density N_o at the footpoints (s = O and 2L) and T_1 and N_1 at the summit (s = L). r is the ratio of the loop height, rD, to half the base length, D, and d is the ratio of the cross-section at the top to that at the footpoints.

both r and d are set equal to one, their departures from unity being studied in Section 3.7.

Although some loops are observed to have flows present, only the cases where the dynamical terms do not dominate are studied here. The occurrences where flows are important have been included in studies by Cargill and Priest (1980, 1981).

The energy equation (1.2.24) in the absence of flows reduces to

$$\frac{1}{A}\frac{d}{ds}\left(\kappa_0 T^{5/2} A \frac{dT}{ds}\right) = N^2 \chi T^{\alpha} - hN. \qquad (3.2.1)$$

The heating term, hN, where h is a constant, is assumed proportional to the density for simplicity. This is in line with Hood and Priest; though, in any case, the exact form taken for the heating is not crucial to the results (as agreed by Craig, et al. (1978); Emslie and Machado (1979)). This choice does not contradict the emission-measure observations in the way suggested by Jordan (1980) for some models because this chapter is only modelling the corona, where $T \geq 10^6$ K. In this region the heating may be even more complicated than in the transition region if, for instance, there is any significant heating from the non-linear interaction of waves near the summit.

The energy equation here expresses a balance between thermal conduction, radiation and heating. The momentum equation (1.2.22) reduces to the case of hydrostatic equilibrium when v = 0. After using the equation of state to relate p and N, it becomes

$$\frac{d}{ds}(NT)\Big/\cos\left[\frac{s}{L}\left(\frac{\pi}{2}-\sin^{-1}\left(\frac{1-r^2}{1+r^2}\right)\right)+\sin^{-1}\left(\frac{1-r^2}{1+r^2}\right)\right]$$

$$= -\frac{m_p g N}{2k} \quad . \qquad (3.2.2)$$

The cosine factor appears because of the inclination of the loop locally to the vertical (Figure 3.2).

The boundary conditions employed are

$$N = N_o \quad , \quad T = T_o \quad \text{at } s = 0$$

and (3.2.3)

$$dT/ds = 0 \qquad \text{at } s = L,$$

where $s = 0$ and L refer to the foot and summit of the loop, respectively, and the latter boundary condition is a result of assuming symmetry.

For the calculations in the order-of-magnitude (Section 3.3) and analytic work (Section 3.4), the Equations (3.1.1) and (3.1.2) are simplified by assuming the loop to be of constant cross-sectional area along its length ($d = 1$), so that in Equation (3.1.1) the A's vanish. Also the loop is assumed to be a semi-circle ($r = 1$), so that the cosine term in Equation (3.1.2) reduces to $\cos(\frac{1}{2}\pi s/L)$. These equations are then non-dimensionalised by introducing

$$\bar{s} = s/L, \quad \bar{T} = T/T_o, \quad \bar{N} = N/N_o,$$

$$\bar{L} = L\left(\chi_o N_c^2 T_o^{\alpha_o - 7/2}/K_o\right)^{1/2}, \quad N_I = N_o/N_c, \qquad (3.2.4)$$

$$\bar{\chi} = \chi T_o^{\alpha}/(\chi_o T_o^{\alpha_o}), \quad \bar{h} = h/(N_c \chi_o T_o^{\alpha_o}),$$

where it is convenient to define a standard density N_c of 5×10^{14} m^{-3}, so that the dimensionless length $\bar{L}$ does not contain the base density N_0, which can be varied independently of L. The dimensionless heating $\bar{h}$ has been defined (Section 1.2) such that a value of unity occurs when the heating and radiation terms balance at a standard density N_c and temperature T_0. The energy equation (3.1.1) then reduces to the dimensionless form

$$\frac{d}{d\bar{s}}\left(\bar{T}^{5/2}\frac{d\bar{T}}{d\bar{s}}\right) = N_L^2 \bar{L}^2 \left(\bar{N}^2 \bar{\chi} \bar{T}^{\alpha} - \bar{h}\bar{N}/N_L\right). \qquad (3.2.5)$$

Further, denote the ratio of the loop length to the base scale height by

$$\bar{g} = \tilde{\mu} m_p L g/(kT_0), \qquad (3.2.6)$$

so that the uniform pressure limit of Hood and Priest applies when the loop length is so small that

$$\bar{g} \ll 1.$$

The parameter $\bar{g}$ is just a dimensionless length and may be written in terms of the previously defined $\bar{L}$ as

$$\bar{g} = \frac{\tilde{\mu} m_p g}{k T_0}\left(\frac{K_0 T_0^{7/2}}{\chi_0 N_c^2 T_0^{\alpha_0}}\right)^{1/2} \bar{L},$$

or, for $T_0 = 10^6$ K,

$$\bar{g} = 0.58\ \bar{L}.$$

In terms of $\bar{g}$, Equation (3.2.2) with $r = 1$ reduces to

$$\frac{1}{\cos\left(\frac{1}{2}\pi\bar{s}\right)} \frac{d}{d\bar{s}}\left(\bar{N}\bar{T}\right) = -\bar{g}\bar{N} . \qquad (3.2.7)$$

The dimensionless boundary conditions must then be

$$\bar{T} = 1 \quad , \quad \bar{N} = 1 \quad \text{at } \bar{s} = 0$$

and (3.2.8)

$$d\bar{T}/d\bar{s} = 0 \qquad \text{at } \bar{s} = 1.$$

These dimensionless equations are used in the following analytical sections 3.3 and 3.4. They are particularly useful for showing the relative density throughout the loop independent of the base density. They are also used for the computational work, but the results are presented in terms of the real variables (with the exception of the heating) for interpretational ease.

These Equations, (3.2.5) and (3.2.7), subject to (3.2.8), are solved in the following sections to find the temperature $\bar{T}(\bar{s})$ and density $\bar{N}(\bar{s})$ along the loop for a variety of values of the parameters, heating $\bar{h}$, length $\bar{L}$ and base density N_I. Section 3.3 describes an order-of-magnitude approach, and Section 3.4 some analytic results. Section 3.5 gives the numerical results, while flare loops are discussed separately in Section 3.6. The effects of varying the additional parameters d, the flux-loop divergence, and r, the ratio of height to half the base length, are detailed in Section 3.7. It may be noted that for a typical coronal temperature of 2×10^6 K the scale height is about 100 Mm. Thus the presence of gravity

would be expected to affect significantly the temperature structure when their heights exceed 100 Mm.

3.3 ORDER OF MAGNITUDE

3.3.1 Scaling Laws

In this and the next two sections the loop is assumed to be a semi-circle ($r = 1$) and of constant cross-sectional area along its length ($d = 1$). Here a Taylor series expansion for the pressure, $\bar{p}$ ($\equiv \bar{N}\bar{T}$), is performed to second order about the summit, in the form

$$\bar{p} = \bar{p}_1 + \bar{p}^{(2)}(1 - \bar{s})^2. \qquad (3.3.1)$$

The condition that the loop be symmetric about the summit (i.e. $d\bar{p}/d\bar{s} = 0$ at $\bar{s} = 1$) is automatically satisfied by this form. Substituting it into (3.2.7) and equating powers of $(1 - \bar{s})$ yields

$$\bar{p}^{(2)} = \bar{p}_1 \pi \bar{g}/(4\bar{T}_1).$$

Then the boundary condition that $\bar{p} = 1$ at $\bar{s} = 0$ determines, from Equation (3.3.1), the summit pressure and density as

$$\bar{p}_1 = \frac{\bar{T}_1}{\bar{T}_1 + \bar{g}\pi/4},$$

and

$$\bar{N}_1 = \frac{1}{\bar{T}_1 + \bar{g}\pi/4},$$

in terms of the summit temperature $\bar{T}_1$. These expressions can then be substituted into the energy equation and scaling laws for $\bar{T}_1$ derived.

3.3.1.1. Uniform Heating

First consider the case of uniform heating $\bar{E}_H$ per unit volume, for which the energy equation is

$$\frac{1}{\bar{L}^2}\frac{d}{d\bar{s}}\left(\bar{T}^{5/2}\frac{d\bar{T}}{d\bar{s}}\right) = N_I^2\bar{N}^2\bar{\chi}\,\bar{T}^{\alpha} - \bar{E}_H. \qquad (3.3.2)$$

To a first order approximation, with α approximated by $-\frac{1}{2}$, which is reasonable for $T \gtrsim 10^5$ K, it gives in order of magnitude

$$\frac{1}{\bar{L}^2}\bar{T}_1^{7/2} = \frac{N_I^2\bar{\chi}\,\bar{T}_1^{-1/2}}{(\bar{T}_1 + \bar{g}\pi/4)^2} - \bar{E}_H \qquad (3.3.3)$$

at the loop summit. Now if heating and radiation are of the same order of magnitude, at the summit the result is

$$\bar{E}_H \approx \frac{N_I^2\bar{\chi}\,\bar{T}_1^{-1/2}}{(\bar{T}_1 + \bar{g}\pi/4)^2}. \qquad (3.3.4)$$

If, further, the conduction balances the radiation,

$$\frac{\bar{T}_1^{7/2}}{\bar{L}^2} \approx \frac{N_I^2\bar{\chi}\,\bar{T}_1^{-1/2}}{(\bar{T}_1 + \bar{g}\pi/4)^2},$$

or

$$\bar{T}_1^{4}(\bar{T}_1 + \bar{g}\pi/4)^2 = \bar{L}^2 N_I^2\bar{\chi}. \qquad (3.3.5)$$

From this it is seen that for small loops ($L \lesssim 100$) the gravitational parameter $\bar{g}$ does not dominate, and the summit temperature $\bar{T}_1$ is approximately given by

$$\bar{T}_1 \sim (\bar{L}N_I)^{1/3},$$

or, in dimensional variables, and in terms of the pressure,

$$T_1 \approx 9 \times 10^3 \, (Lp_o)^{1/3} , \qquad (3.3.6)$$

with χ taken as $10^{-31.8}$. Equation (3.3.6) will be derived analytically in Chapter 4. It is less ambiguous to talk in terms of p_o rather than N_o at this stage, because N (and T) vary greatly near and in the transition region, while p is roughly constant (McWhirter, et al., 1975). Although in the majority of this chapter T_o is specifically taken as 10^6 K, for these scaling laws the choice of T_o is irrelevant, provided $T_o^{7/2} \ll T_1^{7/2}$. (This is easily true for $T_o = 10^6$ K if T_1 is around 2×10^6 K.) For longer loops ($L \gtrsim$ 100Mm) (3.3.5) gives

$$T_1 = 7 \times 10^6 p_o^{1/2} . \qquad (3.3.7)$$

The corresponding heating rates are, from (3.3.4),

$$\bar{E}_H \sim p_o^{7/6} \, L^{-5/6} \quad \text{for} \quad L \lesssim 100\text{Mm}$$

and

$$\bar{E}_H \sim p_o^{7/4} \, L^{-2} \quad \text{for} \quad L \gtrsim 100\text{Mm}.$$

For all reasonable values of p_o ($< 7 \times 10^{-18} \, L^2$), Equation (3.3.7) yields smaller values for T_1 than (3.3.6). Thus the effect of gravity is to lower the temperature and to make the temperature of long (thermally isolated) loops independent of their length. This may explain why long interconnecting loops are not significantly hotter than smaller loops.

3.3.1.2 Heating Proportional to Density

The case of uniform heating per unit mass, which is that considered in the numerical program, can be treated similarly. When heating is of the same order as both the radiation and conduction terms, the expressions for T_1 are again given by Equations (3.3.6) and (3.3.7), with the heating

$$\bar{h} \sim p_o^{1/6} L^{-5/6} \quad \text{for} \quad L \lesssim 100 \text{Mm}$$

and

$$\bar{h} \sim p_o^{3/4} L^{-2} \quad \text{for} \quad L \gtrsim 100 \text{Mm}.$$

Although heating and radiation may, on average, be of the same order in a loop, it is of interest to consider the case when heating dominates. This would be the case when the base conductive flux is large. Equating conduction and heating at the summit gives, for uniform heating per unit volume,

$$T_1 \sim \bar{E}_H^{2/7} L^{4/7} ; \qquad (3.3.8)$$

while for constant heating per unit mass, $\bar{h}$,

$$T_1 \sim \bar{h}^{2/9} L^{4/9} \quad \text{when} \quad L \lesssim 100 \text{Mm}$$

and

$$T_1 \sim (\bar{h}L)^{2/7} \quad \text{when} \quad L \gtrsim 100 \text{Mm}.$$

3.3.1.3 Long Loops

For very loop loops the pressure decreases greatly in small regions near the base, being consistently low throughout most of the loop's length. In this case the

approximation (3.3.1) breaks down, and a better approximation for the pressure is

$$\bar{p} = \exp\left(-\frac{2\bar{g}}{\pi}\int \frac{1}{\bar{T}}\, d\bar{s}\right). \qquad (3.3.9)$$

For this it is necessary to prescribe a temperature profile, which is taken as

$$\bar{T} = \bar{T}_1 + \bar{T}^{(2)}\,(1-\bar{s})^2. \qquad (3.3.10)$$

Then $\bar{p}$ is given by

$$\bar{p} = \exp\left[-\frac{2\bar{g}}{\pi}\frac{1}{\bar{T}_1}\left(\frac{\pi}{4} - \tan^{-1}(1-\bar{s})\right)\right]. \qquad (3.3.11)$$

After integrating and using the boundary conditions $\bar{T} = \bar{T}_1$ at $\bar{s} = 1$ (giving $\bar{T}^{(2)} = -\bar{T}_1$ if $\bar{T}_0 \ll \bar{T}_1$), and $\bar{p} = 1$ at $\bar{s} = 0$, the density becomes

$$\bar{N} = \frac{1}{\bar{T}}\exp\left[-\frac{2\bar{g}}{\pi}\frac{1}{\bar{T}_1}\left(\frac{\pi}{4} - \tan^{-1}(1-\bar{s})\right)\right],$$

and, in particular, at the summit it is

$$\bar{N}_1 = \frac{1}{\bar{T}_1}\exp\left(-\frac{\bar{g}}{2\bar{T}_1}\right).$$

Substituting this into Equation (3.3.2) gives, in order of magnitude,

$$\frac{1}{\bar{L}^2}\bar{T}_1^{7/2} = N_I\,\bar{\chi}\,\bar{T}^{-1/2}\exp\left(-\frac{\bar{g}}{\bar{T}_1}\right)\frac{1}{\bar{T}_1^2} + \bar{E}_H.$$

Finally, if the conduction and radiation terms are of the same order, then

$$\exp\left(\frac{\bar{g}}{2\bar{T}_1}\right)\bar{T}_1^{3} = N_I\,\bar{L}\,\bar{\chi}^{1/2}$$

or, in dimensional variables,

$$\exp\left(10^{-2}\frac{L}{T_1}\right) T_1^{\,3} = 6 \times 10^{11}\, p_o L. \qquad (3.3.12)$$

This scaling law has a similar form to Equation (3.3.6) and indeed reduces to it as $\bar{L}$ becomes small. The solution is influenced by the presence of gravity through the exponential term, which implies that the summit temperature T_1 is smaller than the uniform pressure value and that, as $\bar{L}$ becomes very large, T_1 must stop increasing and eventually decrease. Thus for intermediate L, T_1 is approximately constant, independent of L. This is the range when (3.3.7) is valid, and the maximum temperature occurs at

$$L_{max} = 10^2 T_1 \log_e (6 \times 10^{13} p_o / T_1^{\,2}).$$

Equation (3.3.6) is obtained from (3.3.12) when L is small because then the exponential term is approximately equal to unity. The form (3.3.7) may be obtained from (3.3.12) when L equals L_{max}. In other words, Equations (3.3.6) and (3.3.7) are approximations to Equation (3.3.12) when the loop has a length that is small or intermediate, respectively.

If heating dominates over radiation the temperature is again given by Equation (3.3.8) because the density only appears in the radiation term. However, for this case the density is given by

$$N = \frac{p_o}{2kT} \exp\left\{-4 \times 10^{-2} \frac{L}{T_1}\left[\frac{\pi}{4} - \tan^{-1}\left(1 - \frac{s}{L}\right)\right]\right\},$$

which is lower than the uniform pressure case.

3.3.1.4 Order of Magnitude

Now consider a better order-of-magnitude treatment, by expanding both the temperature and pressure in Taylor series,

$$\bar{T} = \bar{T}_1 + \bar{T}^{(2)} (1-\bar{s})^2 ,$$

$$\bar{p} = \bar{p}_1 + \bar{p}^{(2)} (1-\bar{s})^2 .$$

The boundary condition at $\bar{s} = 1$ is satisfied automatically, while those at $\bar{s} = 0$ give, according to (3.2.2),

$$\bar{T}^{(2)} = 1 - \bar{T}_1,$$

$$\bar{p}(2) = 1 - \bar{p}_1. \qquad (3.3.13)$$

Substituting these expansions into the basic Equations (3.2.5) and 3.2.7), and equating powers of $(1 - \bar{s})$ yields

$$\bar{T}^{(2)} = N_I^2 \bar{L}^2 (\bar{\varkappa} \bar{T}_1^{\alpha-2} \bar{p}_1^2 - \bar{h}\bar{p}_1/(N_I \bar{T}_1)) \qquad (3.3.14a)$$

and, as before,

$$\bar{p}^{(2)} = \bar{p}_1 \pi \bar{g}/(4\bar{T}_1). \qquad (3.3.14b)$$

Then an elimination of $\bar{T}^{(2)}$, $\bar{p}^{(2)}$, and $\bar{p}_1$ between Equations (3.3.13) and (3.3.14) yields

$$2\bar{T}_1^{5/2}(1-\bar{T}_1)(\bar{T}_1 + \bar{g}\pi/4)^2 = N_I^2 \bar{L}^2 (\bar{\varkappa} \bar{T}_1^{\alpha} - \bar{h}(\bar{T}_1 + \bar{g}\pi/4)/N_I) \qquad (3.3.15)$$

for $T_o = 10^6$ K. Equation (3.3.15) determines the summit temperature T_1 implicitly in terms of the parameter N_I, $\bar{L}$, and $\bar{h}$.

The general behaviour of the solution to (3.3.15) is similar to that discussed by Hood and Priest in the uniform-pressure limit when L is so small that $\bar{g} \ll 1$. In particular, it is seen that $\bar{T}_1$ increases with either $\bar{h}$ or N_I provided N_I is not too large. $\bar{T}_1$ increases also with $\bar{L}$ provided

$$(1 + \bar{g}\pi/4) > N_I/\bar{h},$$

so that the right-hand side of Equation (3.3.15) is negative. For $\bar{h} \gg 1$, the radiation term is negligible in (3.3.15) and if in addition $N_o^2\bar{L}^2\bar{h} \gg 1$, then $\bar{T}_1 \gg 1$ so that (3.3.15)reduces to

$$2\bar{T}_1^{7/2}(\bar{T}_1 + \bar{g}\pi/4) = N_I\bar{L}^2\bar{h}. \qquad (3.3.16)$$

It is now seen that the solution for $\bar{T}_1$ depends on only two parameters. If the loop length is small enough ($\bar{L} \lesssim 1.7$), there results the uniform-pressure scaling law

$$\bar{L} \approx (\tfrac{1}{2}N_I\bar{h})^{-\frac{1}{2}}\bar{T}_1^{9/4} \sim \bar{T}_1^{9/4}.$$

For longer loops ($\bar{L} \gtrsim 1.7$), Equation (3.3.16) implies that

$$\bar{L} \approx 0.58\ \bar{T}_1^{7/2}/(N_I\bar{h}) \qquad (3.3.17)$$

and the summit temperature becomes less sensitive to changes in $\bar{L}$. A limitation of the scaling law (3.3.17) is that, for very long loops, as pointed out earlier, the temperature increase occurs predominantly in boundary layers near the feet rather than along the whole length of the loop, as is assumed in the simple form for the

temperature profile assumed in this section.

3.3.2 Non-equilibrium.

An important feature of the order-of-magnitude solution (3.3.15) when $\bar{g} \ll 1$ was stressed by Hood and Priest (1979), namely that, if the base density N_I is increased up to a certain critical value N_{crit} (that depends on the other parameters), then $d\bar{T}_1/dN_I$ tends to minus infinity, as indicated schematically in Figure 3.3. Beyond this point there is no neighbouring thermal equilibrium solution. The loop must therefore undergo some drastic change, cooling down along the dotted line by more than an order of magnitude and developing flows, which may explain the observations of cool cores (e.g. Foukal, 1975). The same effect occurs (for small enough $\bar{h}$) if the length $\bar{L}$ is increased to $\bar{L}_{crit}$. Similar features are found here in the treatment from Equation (3.3.15). Consider first the dependence of the summit temperature $\bar{T}_1$ on N_I. As N_I increases from small values, so $\bar{T}_1$ increases to a maximum, $\bar{T}_{max}$, given by

$$\bar{L}^2\bar{h}^2/8 = \bar{T}_{max}^{5/2}(\bar{T}_{max}-1), \qquad (3.3.13)$$

when N_I is

$$N_I = (\bar{T}_{max}+g\pi/4)\bar{h}/2,$$

and then $\bar{T}_1$ decreases again to the point of thermal non-equilibrium at N_{crit}. A typical curve for $\bar{T}_1$ against N_o at constant $\bar{h}$ is shown dotted in Figure 3.7,

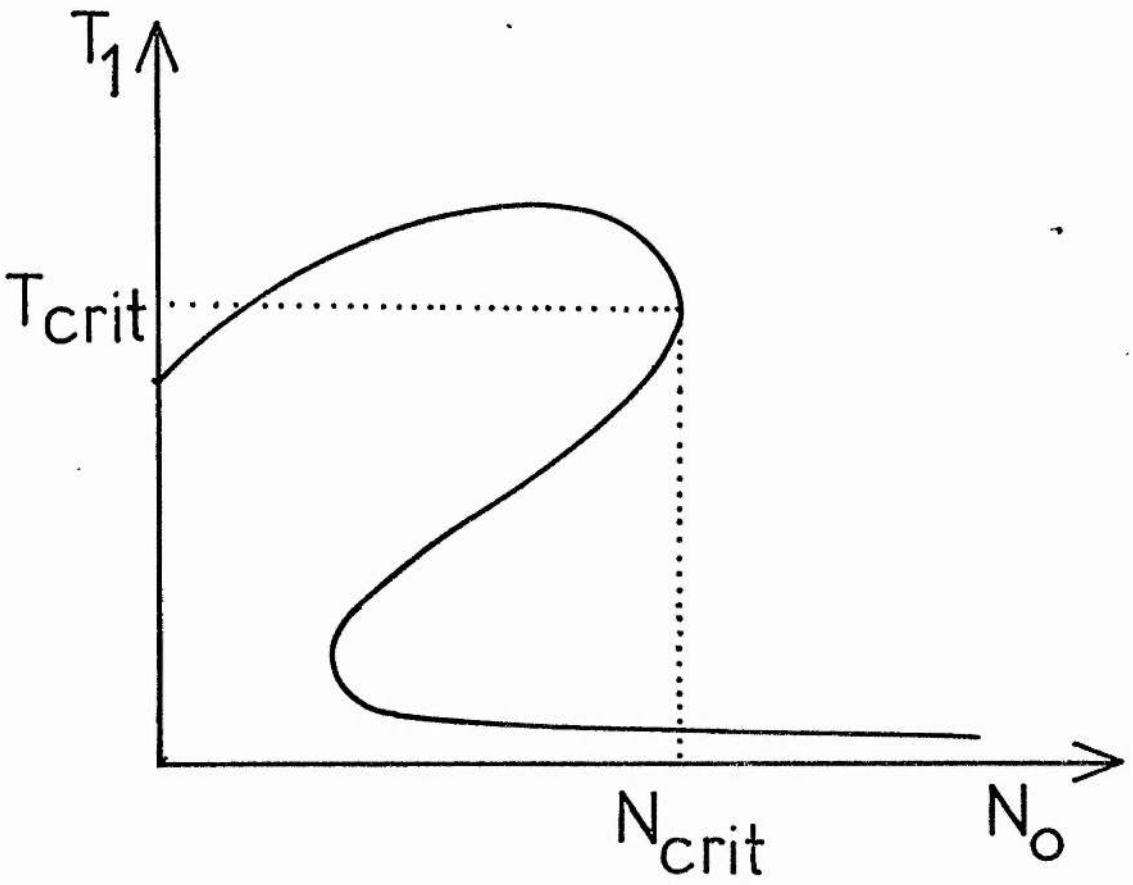

Figure 3.3 The equilibrium temperature T_1 at the summit of a coronal loop shown schematically as a function of the base density N_o. When the density N_{crit} is reached, the plasma cools down from T_{crit} along the dotted line seeking a new equilibrium well below the ambient coronal temperature.

in good agreement with the computed solution.

For long loops the effect of gravity is to increase N_{crit} over the uniform pressure values, generally by about 10%, while $\bar{T}_{max}$ is not appreciably altered. The values of N_{crit} and the corresponding temperature $\bar{T}_{crit}$ can be found by rearranging (3.3.15) into the form

$$N_I^2(\bar{L}^2\bar{\chi}\bar{T}_1^{\alpha}) + N_I(-\bar{L}^2\bar{h}(\bar{T}_1+\bar{g}\pi/4)) - 2\bar{T}_1^{5/2}(1-\bar{T}_1)(\bar{T}_1+\bar{g}\pi/4)^2 = 0. \quad (3.3.19)$$

Differentiating (3.3.19) and setting $dN_I/d\bar{T}_1$ equal to zero (with $\bar{T}_1 < 2$ so that $\bar{\chi}\bar{T}_1^{\alpha} = 1$) gives

$$N_{crit}\bar{L}^2\bar{h} = \bar{T}_1^{3/2}(\bar{T}_1+\bar{g}\pi/4)\left(-11\bar{T}_1^2 + (9-7\bar{g}\pi/4)\bar{T}_1 + 5\bar{g}\pi/4\right). \quad (3.3.20)$$

Equations (3.3.19) and (3.3.20) then determine $N_I = N_{crit}$ and the corresponding critical summit temperature $\bar{T}_1 = \bar{T}_{crit}$. For the particular case $\bar{h} = 0$,

$$\bar{T}_{crit} = \left((9-7\bar{g}\pi/4) + (49\bar{g}^2\pi^2/16 + 47\bar{g}\pi/2 + 81)^{1/2}\right)/22,$$

$$N_{crit} = \left(2\bar{T}_{crit}^{5/2}(1-\bar{T}_{crit})(\bar{T}_{crit}+\bar{g}\pi/4)^2/\bar{L}^2\right)^{1/2}.$$

Consider next the <u>effect on</u> $\bar{T}_1$ <u>of varying the length</u> $\bar{L}$. For this it is necessary to take the $\bar{L}$ dependence out of $\bar{g}$ by writing $\bar{g} = \bar{\bar{g}}\bar{L}$. Then Equation (3.3.15) may be rewritten as the following cubic in $\bar{L}$,

$$\left(N_I\bar{h}\bar{\bar{g}}\pi/4\right)\bar{L}^3 + \left(2\bar{T}_1^{5/2}\bar{\bar{g}}^2\pi^2(1-\bar{T}_1)/16 - \bar{\chi}\bar{T}_1^{\alpha}N_I^2 + N_I^2\bar{h}\bar{T}_1\right)\bar{L}^2 + \left(4\bar{T}_1^{7/2}(1-\bar{T}_1)\bar{\bar{g}}\pi/4\right)\bar{L} + 2\bar{T}_1^{9/2}(1-\bar{T}_1) = 0. \quad (3.3.21)$$

It was found by Hood and Priest (1979) that, for $\bar{h} > \bar{h}_c = N_I$, $\bar{T}_1$ increases monotonically with $\bar{L}$, but for

$\bar{h} < N_I$, non-equilibrium sets in at a critical length $\bar{L}_{crit}$ where $d\bar{T}_1/d\bar{L}$ becomes infinite. The same behaviour is present here but $\bar{h}_c$ is no longer equal to N_I. For N_I as large as about 10, $\bar{h}_c \approx N_I$, but as N_I becomes smaller, $\bar{h}_c$ becomes significantly less than N_I. For example, if $N_I = 4$ ($N_o = 2 \times 10^{15}$ m^{-3}), $\bar{h}_c$ is about 2, as can be estimated from the computed results of Figure 3.10.

Next consider directly the variation of loop temperature with $\bar{g}$ and compare with the case $\bar{g} = 0$ studied by Hood and Priest (1979). Equation (3.3.15) can be arranged into the form

$$\pi \bar{T}_1^{5/2}(1-\bar{T}_1)\bar{g}^2/8 + \pi\left(\bar{L}^2\bar{T}_1^{7/2}(1-\bar{T}_1) + N_I\bar{L}\,\bar{h}/4\right)\bar{g}$$

$$+ 2\bar{T}_1^{9/2}(1-\bar{T}_1) + N_I^2\bar{L}^2\bar{h}\,\bar{T}_1 - N_I^2\bar{L}^2\bar{\chi}\,\bar{T}_1^{\alpha} = 0 .$$

The solution of this shows that the presence of gravity acts as a stabilising factor. Near the critical point the temperature increases with gravity, opposing the decrease of T_1 as (for example) N_I is increased to N_{crit}. Thus higher densities (or lengths) can be achieved than those predicted in Hood and Priest (1979), before non-equilibrium sets in. Far from non-equilibrium (N_o sufficiently small), the introduction of gravity makes the loop more isothermal, thus decreasing the summit temperature. This is because the presence of gravity decreases the average density within the loop, and so lowers both the radiation and heating terms.

These observations can be seen from solving

Equation (3.3.21) for $\bar{\bar{g}}$. Figure 3.4 shows the result schematically. A given base density, length and heating gives a particular curve of similar shape, their magnitudes determining the position of the curve vertically on the graph (for example positions a or b). Solutions for a constant-pressure, horizontal loop ($\bar{\bar{g}} = 0$) or a semi-circular loop ($\bar{\bar{g}} = \bar{g}/\bar{L}$) occur at the intersections of a curve with the line $\bar{\bar{g}} = 0$ or $\bar{\bar{g}} = \bar{g}/\bar{L}$ respectively. Curve a depicts a case where a loop is far away from the critical condition. As $\bar{\bar{g}}$ increases, in particular from 0 to $\bar{g}/\bar{L}$, the loop becomes more isothermal by the curve asymptoting to the $T = T_0$ line. Near critical conditions (curve b) an increase in $\bar{\bar{g}}$ takes the solution further away from the critical point, at the same time raising the temperature. For any constant-pressure loop in static equilibrium, there is always a corresponding equilibrium for a semi-circular loop, while in some cases an equilibrium exists for only the semi-circular case.

3.4 ANALYTIC CONSIDERATIONS

Analytic solutions are sought to Equations (3.2.5) and (3.2.7), namely

$$\frac{d}{d\bar{s}}\left(\bar{T}^{5/2}\frac{d\bar{T}}{d\bar{s}}\right) = N_I^2\bar{L}^2\left(\bar{N}^2\chi\bar{T}^{\alpha} - \bar{h}\bar{N}/N_I\right) \qquad (3.4.1)$$

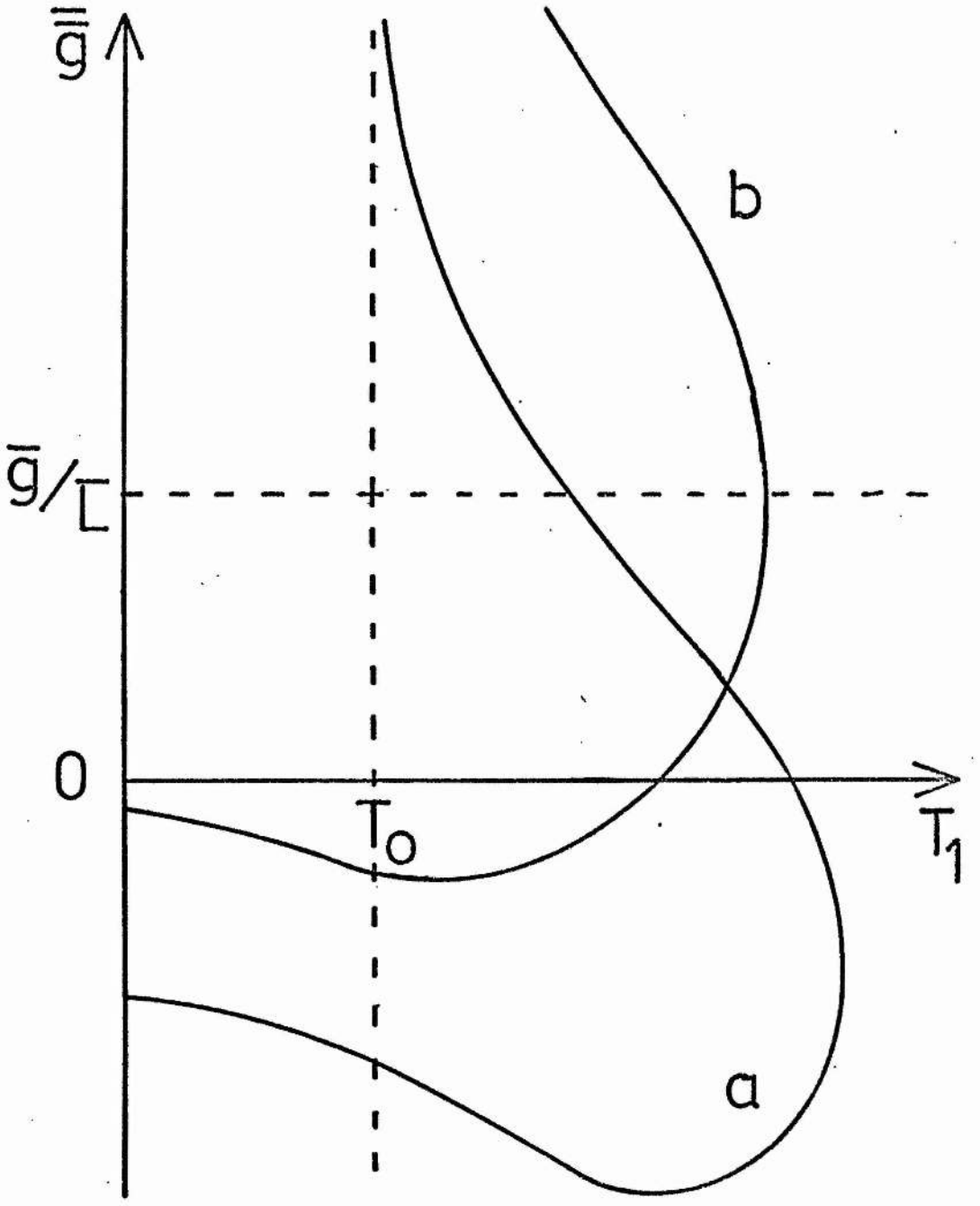

Figure 3.4 A schematic drawing showing the variation of the summit temperature T_1 subject to the presence of gravity.

and

$$\frac{1}{\cos(\frac{1}{2}\pi\bar{s})}\ \frac{d}{d\bar{s}}(\bar{N}\bar{T}) = -\bar{g}\bar{N}\,, \qquad (3.4.2)$$

subject to the boundary conditions

$$\begin{aligned} &\bar{T} = 1,\ \bar{N} = 1 \quad \text{at} \quad \bar{s} = 0, \\ &d\bar{T}/d\bar{s} = 0 \quad \text{at} \quad \bar{s} = 1. \end{aligned} \qquad (3.4.3)$$

As they stand these equations cannot be solved analytically, but some special cases are amenable to analytic treatment.

Consider first the case of a <u>short loop</u> for which $N_I\bar{L} \ll 1$ and <u>conduction dominates</u> so that the loop is nearly isothermal. Since the limit $\bar{L} = 0$ gives $\bar{T} \equiv \bar{N} \equiv 1$, the solutions are expanded

$$\begin{aligned} \bar{T} &= 1 + \bar{L}\bar{T}^{(1)} + \bar{L}^2\bar{T}^{(2)} + \ldots\,, \\ \bar{N} &= 1 + \bar{L}\bar{N}^{(1)} + \bar{L}^2\bar{N}^{(2)} + \ldots\,. \end{aligned}$$

Furthermore, the cosine terms in (3.4.2) is replaced by $2/\pi$, which means a curved leg of the loop is approximated by a straight field line of same length and reaching the same height. This is reasonable in view of the results of Section 3.7 which show that changing the loop geometry while keeping the height fixed does not appreciably alter the temperature structure. (A disadvantage, however, is that while it is still possible to enforce $d\bar{T}/d\bar{s} = 0$ at the summit, $d\bar{N}/d\bar{s}$ cannot simultaneously be zero.) To first order in $\bar{L}$, Equations (3.4.1) and (3.4.2) yield

$$d\bar{N}^{(1)}/d\bar{s} = -0.37 \quad \text{and} \quad \bar{T}^{(1)} \equiv 0.$$

To second order, the temperature equation is

$$d^2\bar{T}^{(2)}/d\bar{s}^2 = N_I^2 - \bar{h}N_I .$$

After solving these subject to the boundary conditions, the temperature and density are found to be

$$\begin{aligned} \bar{T}_1 &= 1 + \tfrac{1}{2}\bar{s}(\bar{h}N_I - N_I^2)\bar{L}^2 , \\ \bar{N}_1 &= 1 - 0.37\bar{s}\bar{L} + O(\bar{s}^2). \end{aligned} \qquad (3.4.4)$$

It is noticed that, to first order, the temperature is uniform while the density decreases linearly to a summit value $1 - 0.37\bar{L}$ independent of the heating. To second order, the temperature increases quadratically if the heating is large enough $(\bar{h} > N_I)$ to a summit value $1 + \tfrac{1}{2}\bar{L}^2 N_I(\bar{h} - N_I)$.

For loops whose height is <u>much smaller than a coronal scale-height</u> $(\bar{g} \ll 1)$, the <u>pressure is uniform</u>. The effect of gravity on taller loops is to make the plasma preasure fall off with altitude, which in turn influences the temperature and density. This can be estimated for loops lower than a scale-height by expanding in powers of $\bar{g}$. First consider the case $\bar{h} = N_I$, which makes the radiation and heating balance at the foot of the loop. When $\bar{g} = 0$ the loop is uniform with $\bar{T} \equiv 1$, $\bar{N} \equiv 1$, so nearby solutions to Equations (3.4.1) and (3.4.2) can be sought in the form

$$\begin{aligned} \bar{T} &= 1 + \bar{g}\bar{T}^{(1)} + \bar{g}^2\bar{T}^{(2)} + \cdots , \\ \bar{N} &= 1 + \bar{g}\bar{N}^{(1)} + \bar{g}^2\bar{N}^{(2)} + \cdots . \end{aligned} \qquad (3.4.5)$$

Equation (3.4.1) simplifies to

$$\frac{d}{d\bar{s}}\left(\bar{T}^{5/2}\frac{d\bar{T}}{d\bar{s}}\right) = N_I^{\,2}\bar{L}^2\bar{N}(\bar{N}-1),$$

since α remains equal to α_o when $\bar{T}$ is close to 1. Equating powers of $\bar{g}$ in (3.4.1) and (3.4.2) leads to equations

$$d^2\bar{T}^{(1)}/d\bar{s}^2 = N_I^{\,2}\bar{L}^2\bar{N}_1^{(1)},$$

$$d\bar{T}^{(1)}/d\bar{s} + d\bar{N}^{(1)}/d\bar{s} = -\cos(\pi\bar{s}/2),$$

from which

$$\bar{T} = 1 + \frac{8N_I^{\,2}\bar{L}^2\bar{g}}{\pi(\pi^2-4N_I^{\,2}\bar{L}^2)}\sin\frac{\pi\bar{s}}{2},$$

$$\bar{N} = 1 - \frac{32\pi}{(\pi^2-4N_I^{\,2}\bar{L}^2)}\sin\frac{\pi\bar{s}}{2}. \qquad (3.4.6)$$

The expansion (3.4.5) breaks down either when $\bar{g}$ is of order unity or, due to the singularity in $\bar{T}^{(1)}$, when $N_I^{\,2}\bar{L}^2$ increases to $\pi^2/4$. The latter condition is not attained by many loops in practice. When, for instance, the length 2L is taken equal to 200Mm and N_o is equal to $10^{15}m^{-3}$, $N_I^{\,2}\bar{L}^2$ is just less than 1. From Equations (3.4.6) it can be seen that the effect of gravity is to cause the temperature to be <u>higher</u> than with the uniform pressure loops ($\bar{g} = 0$). This agrees with both the order-of-magnitude results in Section 3.3 and the numerical results of Section 3.5. It is due essentially to the fact that the main effect of gravity is to make the density decrease with height, which in turn causes the radiation to

decrease more than the heating term; the resulting increased importance of heating then raises the plasma temperature. A greater increase in temperature occurs for greater base density N_o because the factor $N_I^2\bar{L}^2$ is then larger. This also agrees with the order-of-magnitude results.

When <u>heating dominates</u>, progress can be made most easily by assuming it to be proportional to the volume. Then the energy equation (3.4.1) becomes

$$\frac{d}{d\bar{s}}\left(\bar{T}^{5/2}\frac{d\bar{T}}{d\bar{s}}\right) = -\bar{L}^2\bar{E}_H ,$$

with solution

$$\bar{T}^{7/2} - 1 = -7\bar{L}^2\bar{E}_H(\bar{s}^2-2\bar{s})/4.$$

Thus the summit temperature $\bar{T}_1$ at $\bar{s} = 1$ is given by

$$\bar{T}_1^{7/2} = 1 + 7\bar{L}^2\bar{E}_H/4,$$

and so, for $\bar{T}_1^{7/2} \gg 1$, the summit temperature increases with loop length like $\bar{L}^{4/7}$ and with heating like $\bar{E}_H^{2/7}$.

The plasma density $\bar{N}$ then can be found from the Equation (3.4.2) of hydrostatic equilibrium. With $\cos(\frac{1}{2}\pi\bar{s})$ approximated by $4(1-\bar{s})/\pi$, the density is given by

$$\bar{N} = \left\{1 - \frac{7\bar{L}^2\bar{E}_H(\bar{s}^2-2\bar{s})}{4}\right\}^{-2/7} \exp\left\{\frac{8\bar{g}}{5\pi\bar{L}^2\bar{E}_H}\left[\left(1 - \frac{7\bar{L}^2\bar{E}_H(\bar{s}^2-2\bar{s})}{4}\right)^{5/7} - 1\right]\right\},$$

or, at the summit,

$$\bar{N}_1 = \left(\frac{4}{4+7\bar{L}^2\bar{E}_H}\right)^{2/7} \exp\left(\bar{g}\,\frac{2^{11/7}(4+7\bar{L}^2\bar{E}_H)^{5/7} - 8}{5\pi\bar{L}^2\bar{E}_H}\right).$$

So, for large heating ($\bar{L}^2 E_H \gg 1$),

$$\bar{N}_1 = \left(\frac{4}{7\bar{L}^2\bar{E}_H}\right)^{2/7} \exp\left(\frac{2^{11/7}\,7^{5/7}}{5\pi}\,\frac{\bar{g}}{(\bar{L}^2\bar{E}_H)^{2/7}}\right) ,$$

which implies that the density decreases with increasing heating or length.

3.5 NUMERICAL RESULTS

Equations (3.2.1) and (3.2.2) were solved numerically for T(s) and N(s) subject to boundary conditions (3.2.3). Because it is a two-point boundary-value problem, the value of dT/ds at the footpoint s = O was iterated until the required value, namely dT/ds = O, was obtained at the summit, s = L. The experience gained by Hood and Priest with the case $\bar{g}$ = O was utilised. For instance, the multiple solutions they obtained were disregarded and the critical points in the phase plane are absent when g ≠ O, since a third dimension is now present. In this section the results will be presented for the basic loop model when r = 1 and d = 1, leaving until Section 3.7 the effects of flux tube divergence and varying the loop height for a fixed footpoint separation.

As an initial digression, the program was run for thermally isolated loops with a low base temperature ($T_o = 2 \times 10^4$ K) in order to compare with the uniform pressure result of Rosner, et al.(1978). The dependence

of the summit temperature T_1 on L and N_o is graphed in Figure 3.5 (solid line). The scaling law derived in Equation (3.3.7), of the same type which Rosner, et al. obtained, is shown dashed, and Equation (3.3.7) (dotted) is the scaling law which should be used for longer lengths. Thus the full scaling law modified by gravity is the dashed line up to where this and the dotted line cross, and then the dotted line. It is clear that this behaviour agrees with the computed solutions. Thus Rosner, et al.'s law is seen to be a good approximation for small lengths or high densities, but not for long lengths or small densities. The fall in density from the base to the summit is much larger than in the uniform-pressure case, often by as much as an order of magnitude. This is a direct consequence of the effect of gravity in decreasing the pressure.

The restriction of zero base conductive flux is now relaxed and T_o is taken as 10^6 K. This makes the third parameter, namely the heating, $\bar{h}$, independent and allows the problems of the transition region to be bypassed. The solutions depend on the parameters L, $\bar{h}$, N_o, each being varied over a wide range. In Figures 3.6a and 3.6b the resulting summit temperature T_1 and density N_1 have been plotted as functions of the base density N_o for a range of values of $\bar{h}$. These figures apply to a loop of length $2L = 10$Mm and the corresponding results for loops of length 100Mm and 400Mm are shown in Figures 3.7 and 3.8.

It can be seen from Figures 3.6 to 3.8 that, up to a

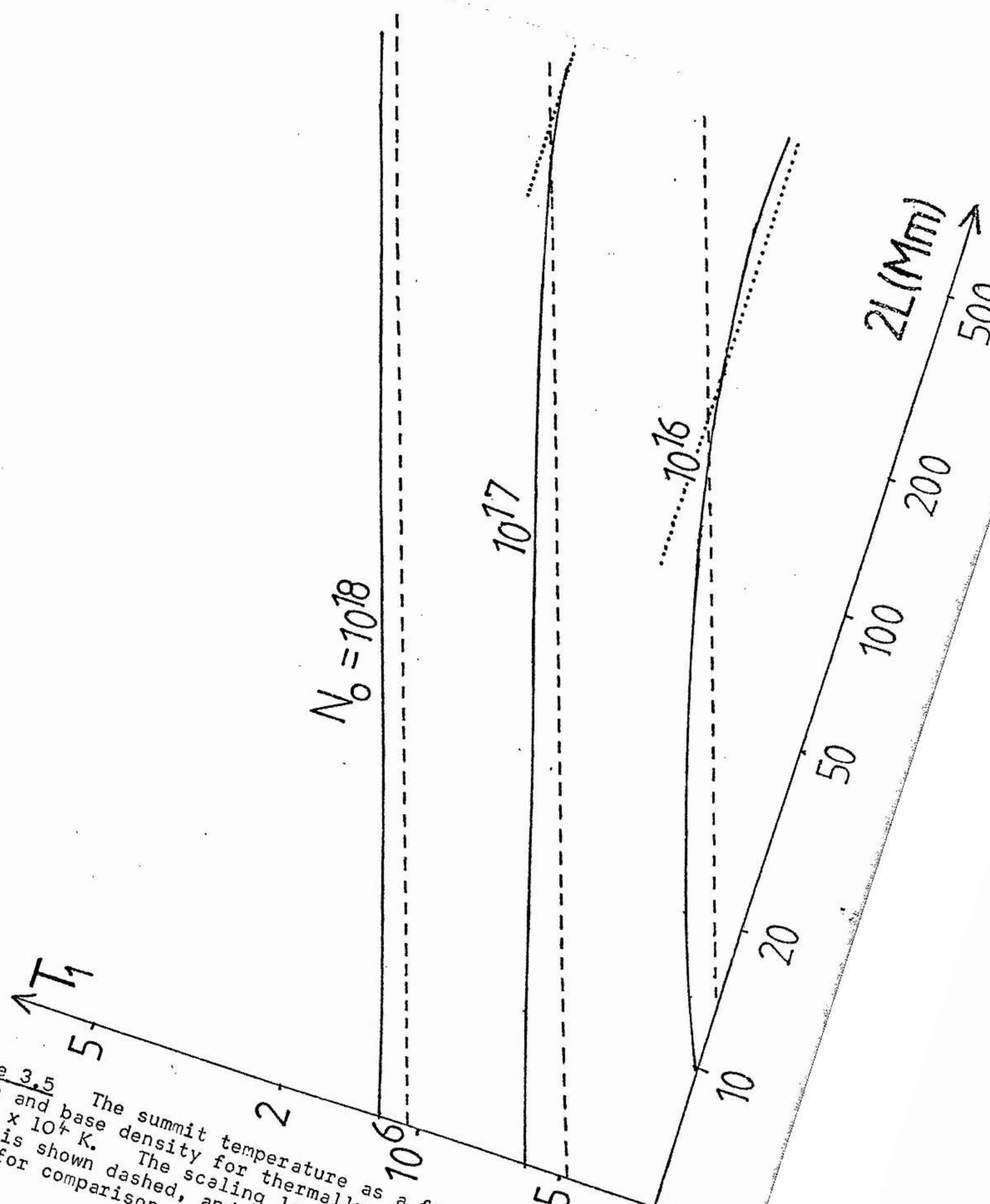

Figure 3.5 The summit temperature as a function of the loop length and base density for thermally isolated loops with $T_o = 2 \times 10^4$ K. The scaling law $T_1 \sim (p_o L)^{1/3}$ (for most loops) is shown dashed, and $T_1 \sim p_o^{1/2}$ (for longer loops) dotted for comparison.

certain maximum value of N_o, the summit temperature increases with both the base density N_o and the heating rate $\bar{h}$. Furthermore if the summit density N_1 is known, it is possible to deduce a relationship between the heating $\bar{h}$ and the loop length for any summit temperature. Figure 3.9 shows such curves in the particular case $N_1 = 10^{15}$ m^{-3}. This method can be used to determine the main unknown, namely $\bar{h}$, once the temperature, length and base density are known for a particular coronal loop. Another feature of the numerical solutions is that, as the base density N_o increases for a loop of a given length $2L$ and heating rate $\bar{h}$, so the summit temperature increases up to a maximum value T_{max}, (and then decreases to T_{crit}). The expression derived in the order-of-magnitude section, namely

$$T_{max}^{5/2}(T_{max}-1) = 12 \times 10^{-6} L^2 \bar{h}^{-2},$$

(where T_{max} is measured in units of 10^6, and L in Mm) holds remarkably well, provided T is not too large ($T_{max} \lesssim 2 \times 10^6$ K). For larger T_{max} the order-of-magnitude approximation does not take into consideration the change in α and $\varkappa$ (see Table 1) above 2×10^6 K, and is less accurate. Instead the simpler expression

$$T_{max} - 1 = L\bar{h}/500$$

is a good approximation.

An important feature of the solutions (Figures 3.6 to 3.8) is that, if the base density is increased to a critical

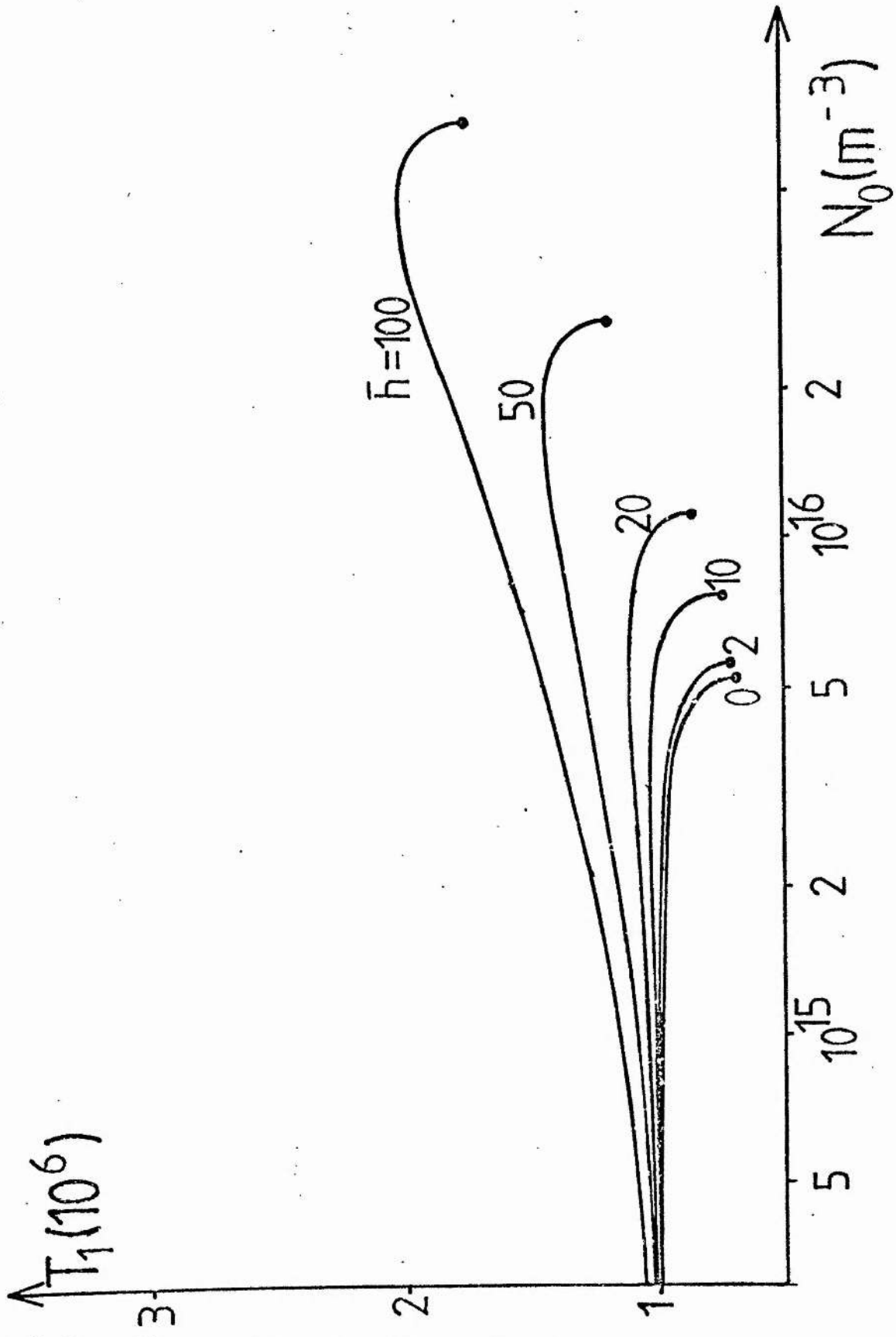

Figure 3.6a The summit temperature T_1 for a loop of length $2L = 10Mm$, as a function of the base density N_o for various values of the heating $\bar{h}$. Critical points beyond which the equilibria cease to exist are denoted by dots.

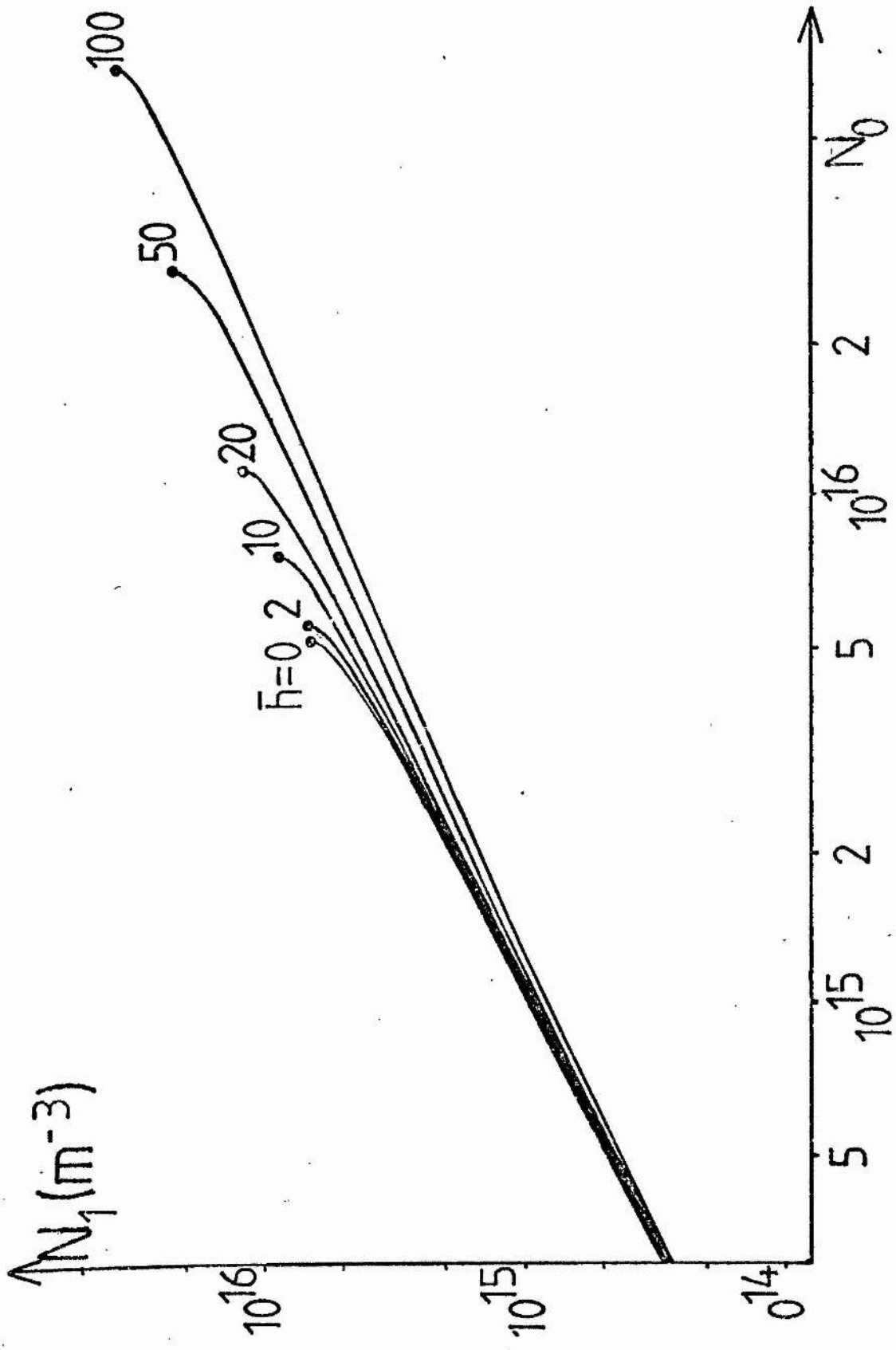

Figure 3.6b The summit density N_1 for a loop length 2L = 10 Mm.

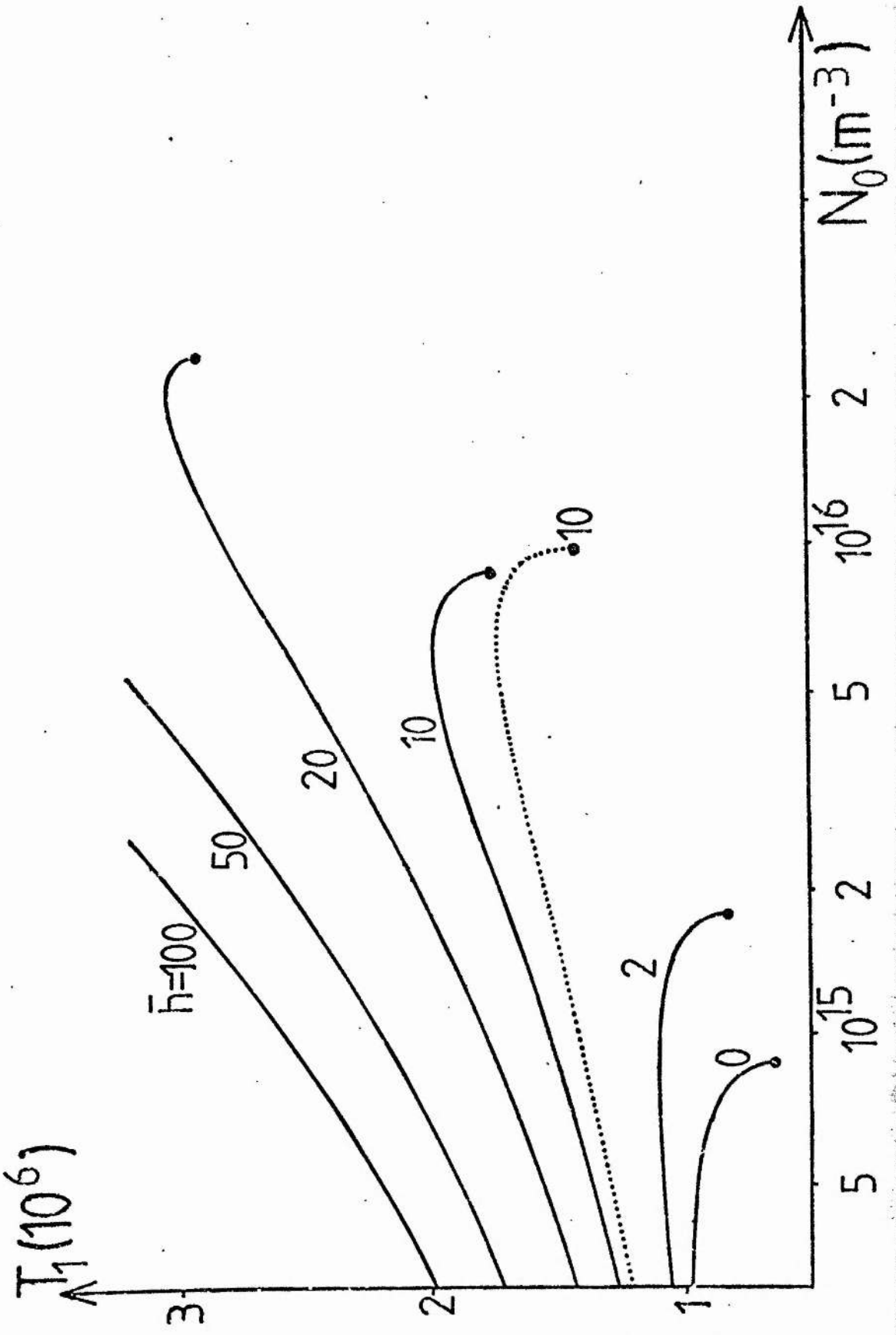

Figure 3.7a The summit temperature for a loop of length 2L = 100Mm. The dotted curve shows the order of magnitude result when $\bar{h}$ = 10 for comparison.

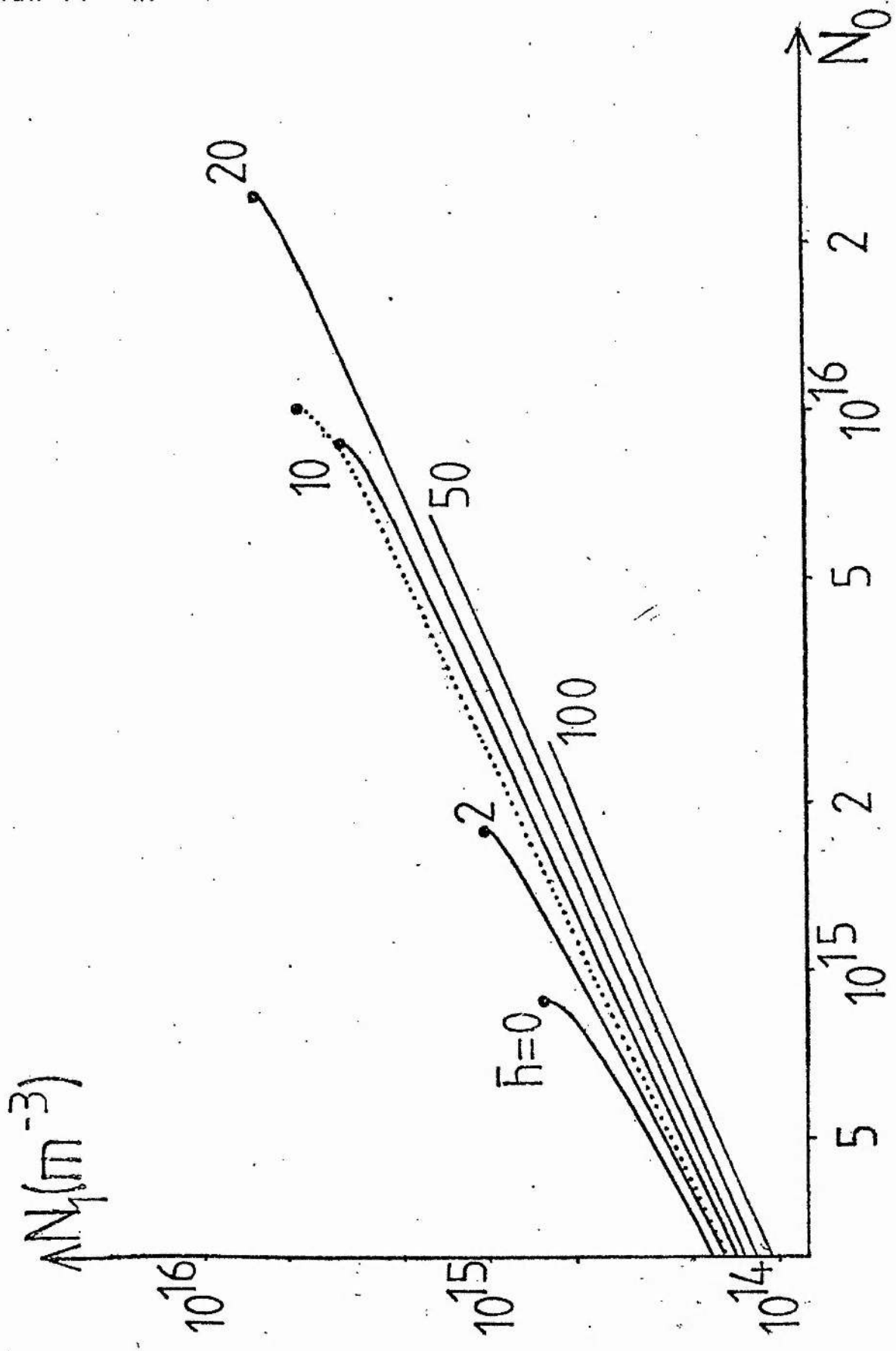

Figure 3.7b The summit density for a loop of length 2L = 100Mm. The dotted curve shows the order of magnitude result when $\bar{h}$ = 10 for comparison.

Figure 3.8a The summit temperature for a loop of length 2L = 400 Mm.

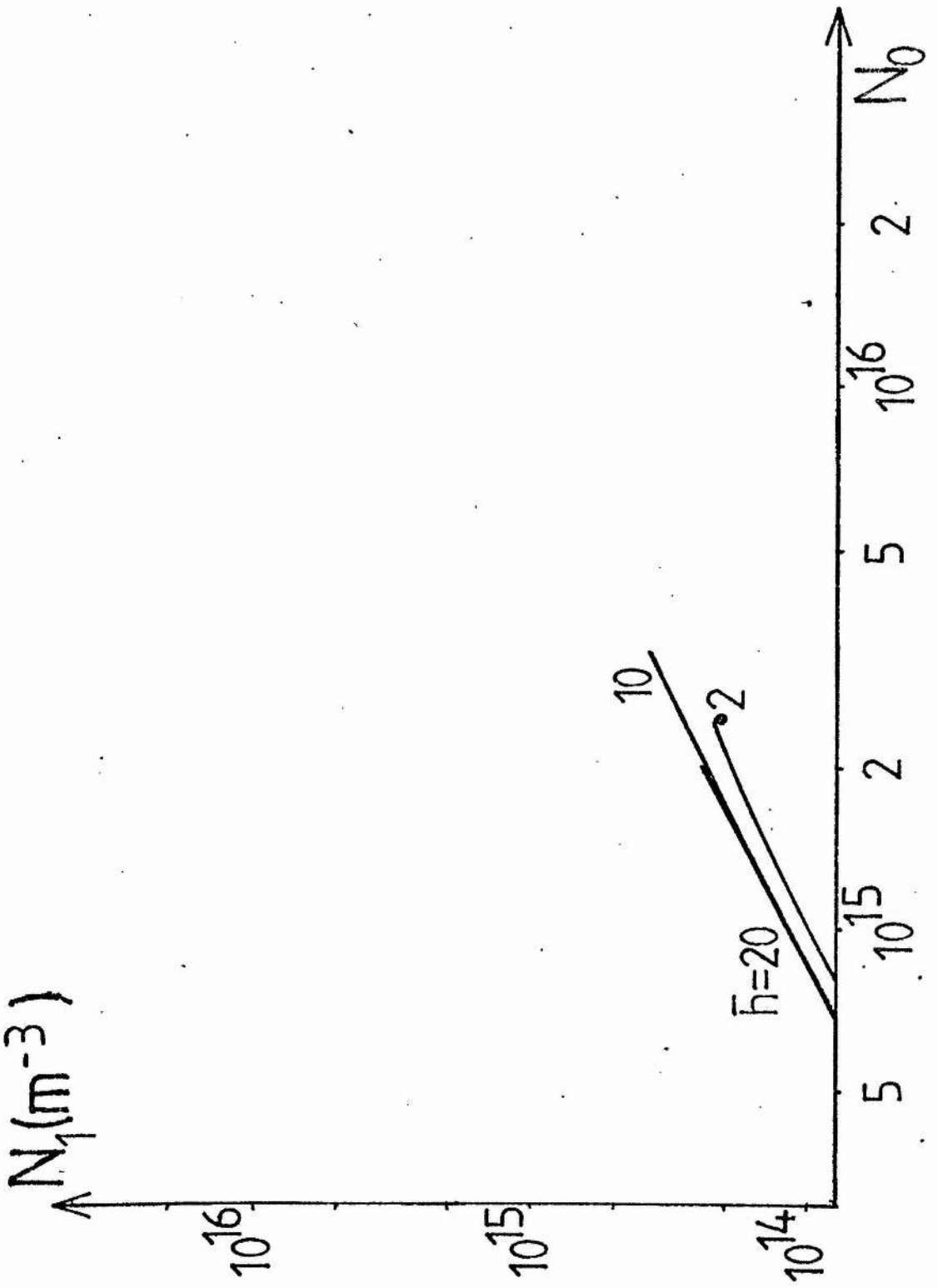

Figure 3.8b The summit density for a loop of length 2L = 400 Mm.

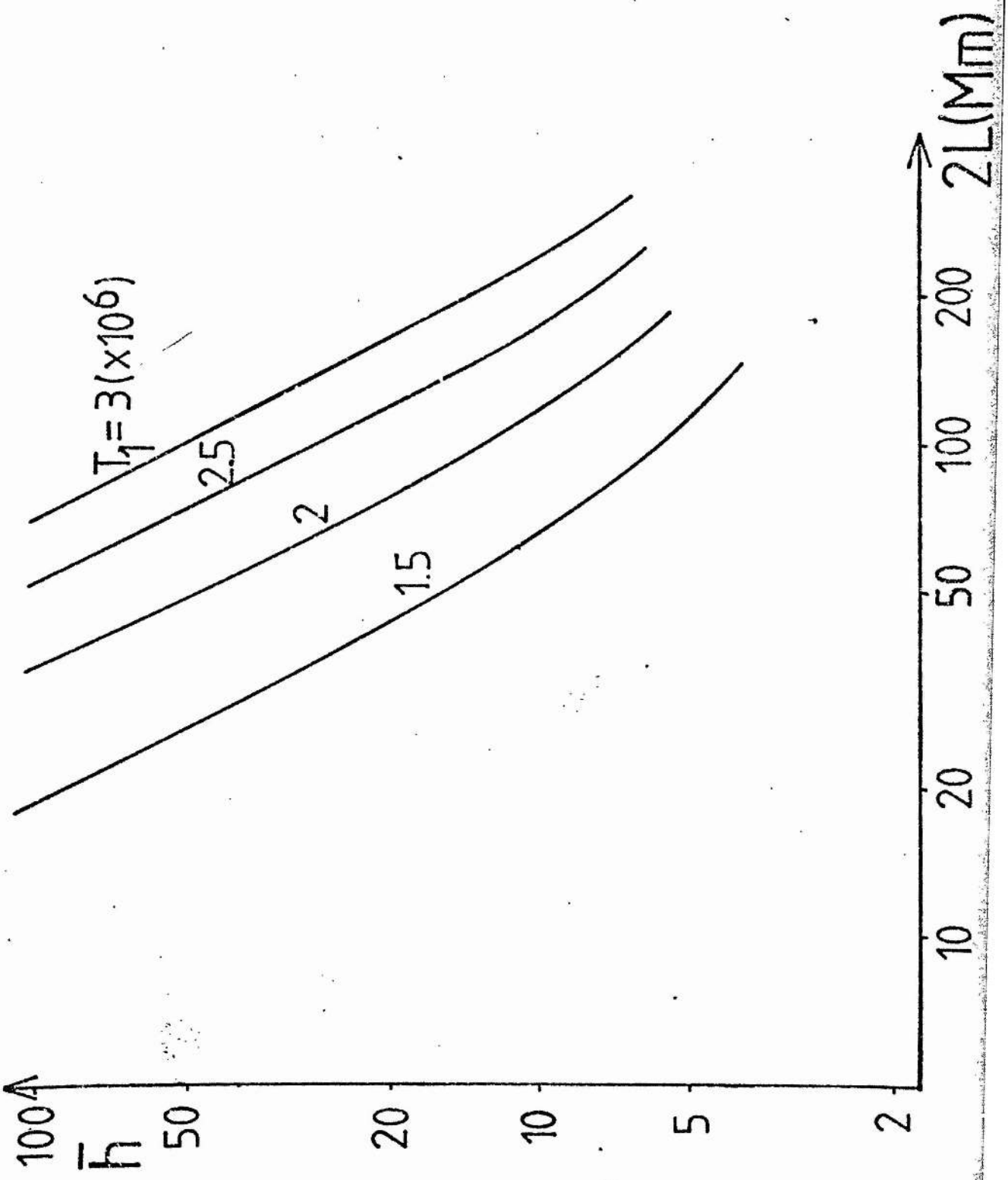

Figure 3.9 The dependence of heating $\bar{h}$ on length 2L for various values of the summit temperature T_1, given a summit density of $N_1 = 10^{15}\ m^{-3}$.

value N_{crit} the gradients dT_1/dN_o and dN_1/dN_o become infinite, as in the order-of-magnitude analysis. Beyond N_{crit} there is no neighbouring equilibrium solution and thermal non-equilibrium sets in. The dependence of the critical density N_{crit} on $\bar{h}$ and L is shown in Figure 3.10. For small loops N_{crit} can be seen to be rather insensitive to the size of the heating $\bar{h}$, but for large loops it is much more sensitive. Furthermore, Figures 3.6 to 3.8 show that for most lengths of interest, ($2L \lesssim 200$Mm) the critical conditions are reached by the curves for $N_1(N_o)$ bending upwards and dN_1/dN_o tending to plus infinity, as in the case $\bar{g} = 0$, whereas longer loops approach criticality by $N_1(N_o)$ bending downwards. Furthermore, for moderate length loops, a larger heating gives a smaller summit density, whereas if $2L \gtrsim 300$Mm, the larger heating results in a denser loop.

An example of the way the temperature profile T(s) along the loop varies as the base density is raised can be seen in Figure 3.11 for a loop of length $2L = 50$Mm and heating $\bar{h} = 20$. For this particular case, as N_o increases, so the summit temperature T_1 increases to a maximum value of 2×10^6 K when $N_o = 10^{16} m^{-3}$ and then decreases to 1.8×10^6 K at the critical density $1.5 \times 10^{16} m^{-3}$, beyond which there is no neighbouring equilibrium. It is interesting to notice that, as the critical density is reached, the temperature gradient at the base may reduce considerably. This is because, as pointed out by Hood and Priest (1979), the critical

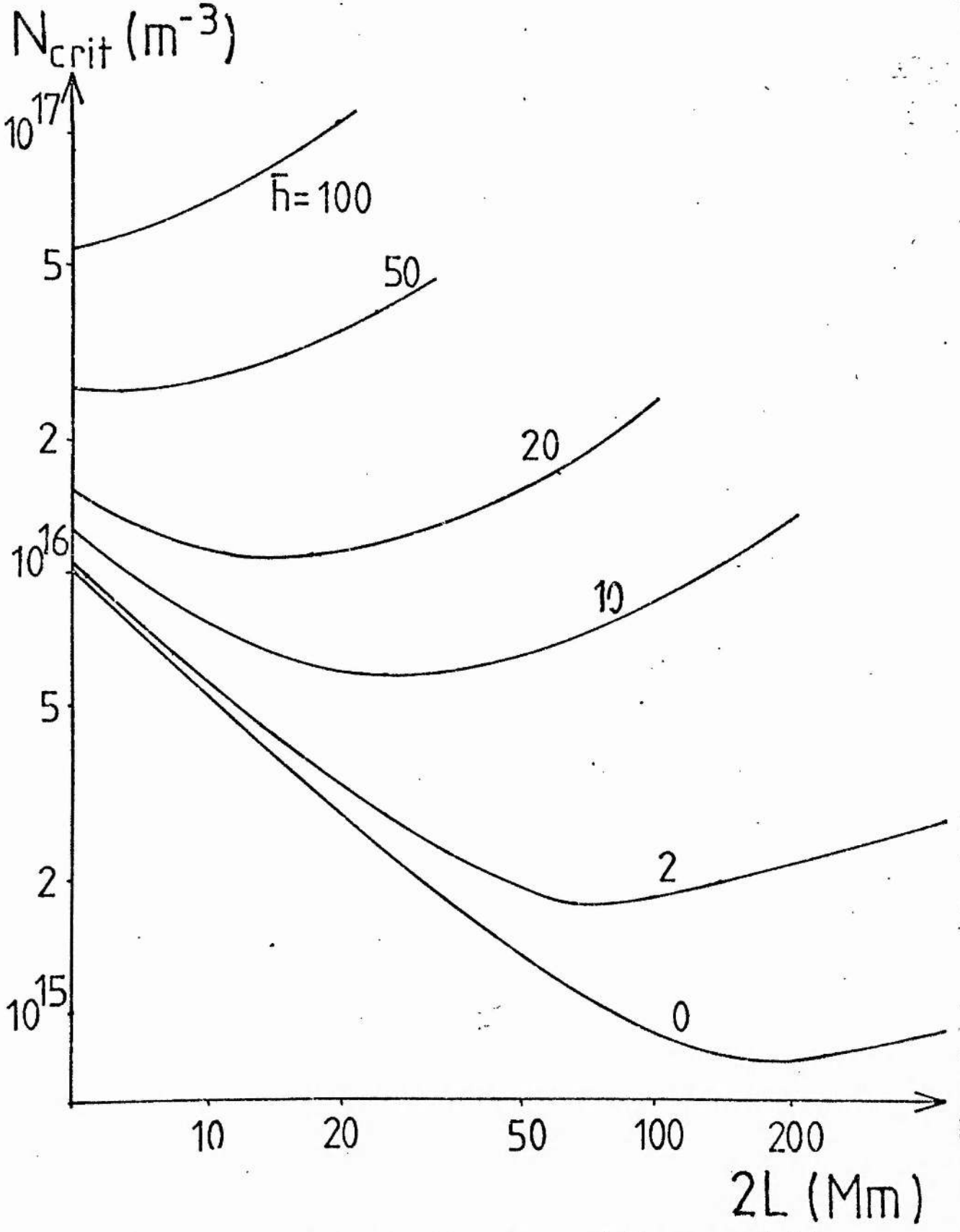

Figure 3.10 The critical value N_{crit} of the coronal base density $N_o(m^{-3})$ at which a lack of equilibrium sets in, as a function of the loop length 2L(Mm), for various values of $\bar{h}$. If instead the density N_o is regarded as being increased, the horizontal axis gives the critical length 2L for the onset of thermal instability.

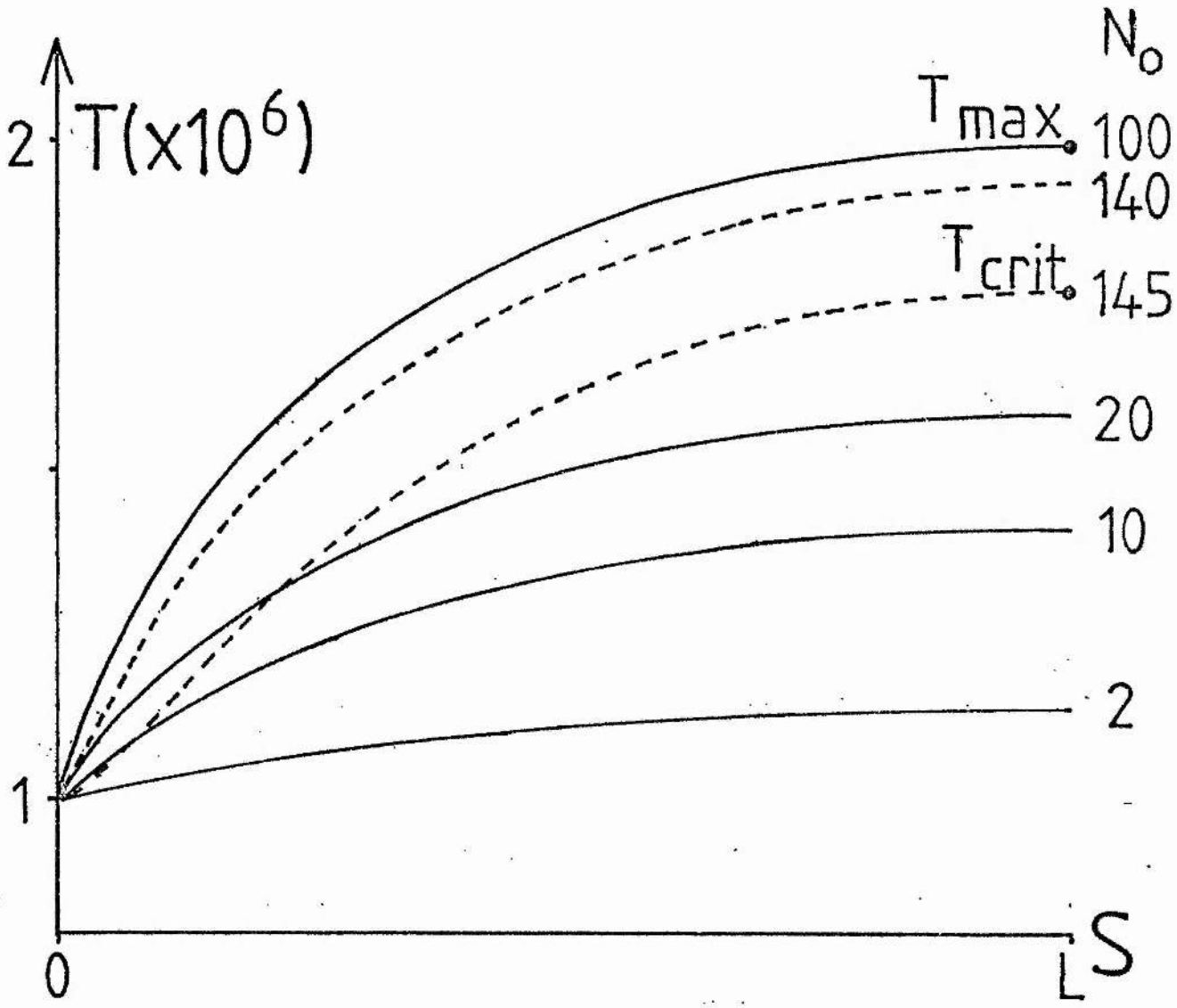

Figure 3.11 The profile of the temperature T(s) along a loop of length 2L = 50Mm, possessing a heating h = 20. It can be seen how the profile varies as the base density N_o (in units of $10^{14} m^{-3}$) is increased from $2 \times 10^{14} m^{-3}$ up to the critical value of approximately $1.5 \times 10^{16} m^{-3}$. The solid lines refer to values of N_o less than $10^{16} m^{-3}$ (which gives rise to the maximum summit temperature T_{max}) while the dashed lines refer to larger values of N_o.

condition arises when the radiation has become important compared to the conduction.

In some cases, particularly if the loop length is large or the density is not too great, the base conductive flux reduces to zero before criticality is reached. In this case the total radiation balances the total energy input and the loop is said to be "thermally isolated". This result cannot occur for a horizontal loop where the pressure is uniform. Figures 3.12 and 3.13 show the effect of stretching a loop on its summit temperature and density. It exhibits graphs of T_1 and N_1 as functions of the length 2L shown here for the cases when the base density N_o is 10^{15} m^{-3} and 2×10^{15} m^{-3}, respectively, with several values of the heating. One result is that for $\bar{h}$ smaller than a critical value $\bar{h}_c$ (N_o) (as in Section 3.3), dependent on the base density, there is a finite range of lengths that possess no equilibrium solutions. The effect of stretching such a loop from a small size is thus to make it pass through a series of equilibria until the critical length is reached, at which equilibrium fails. Further stretching finds equilibrium solutions again after a second critical point is passed. This is easily seen for the case $\bar{h} = 2$ in Figure 3.13, and also can be deduced from Figure 3.10. For many densities and heating values, these occur at lengths too large for physical relevance. For $\bar{h}$ larger than $\bar{h}_c$ an equilibrium solution always exists. The value of $\bar{h}_c$ for very dense loops is

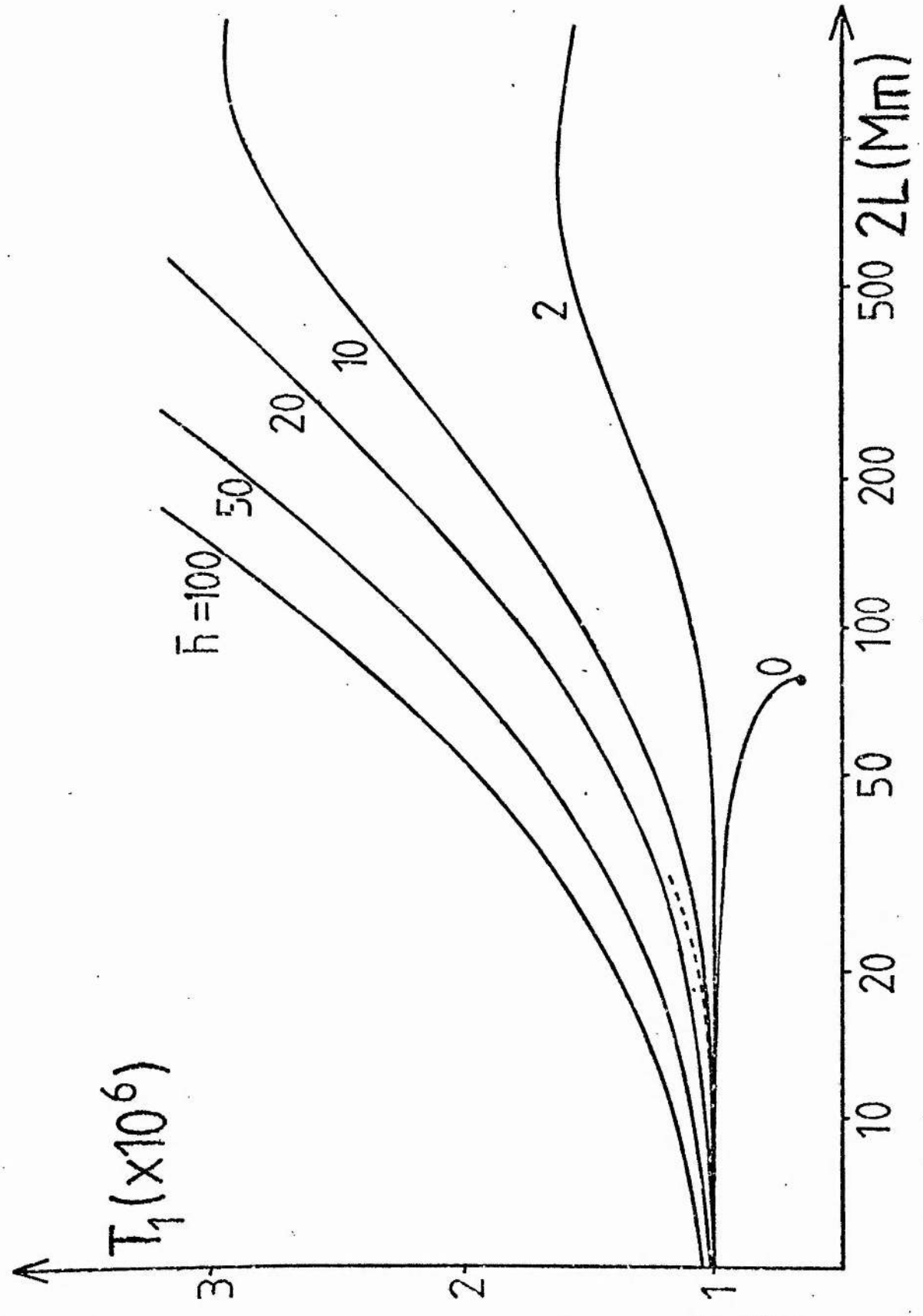

Figure 3.12a The summit temperature T_1 as a function of the length 2L, whose base density is 10^{15} m^{-3}, for various values of $\bar{h}$. The dashed lines give the analytic result obtained in Section 3.3, when $\bar{h} = 10$

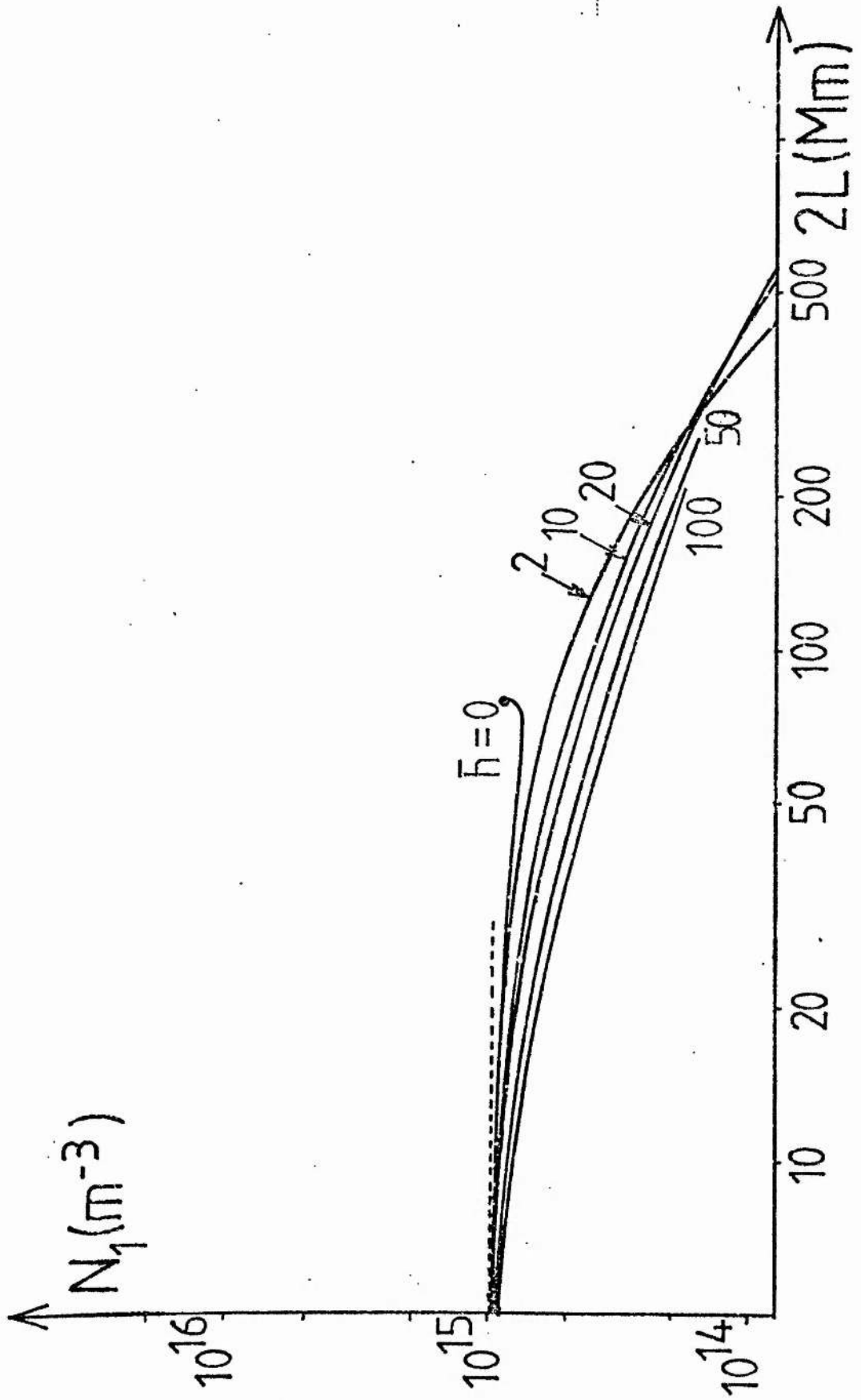

Figure 3.12b The summit density N_1 as a function of the length 2L, whose base density is 10^{15} m^{-3}, for various values of $\bar{h}$. The dashed lines give the analytic result obtained in Section 3.3, when $\bar{h} = 10$.

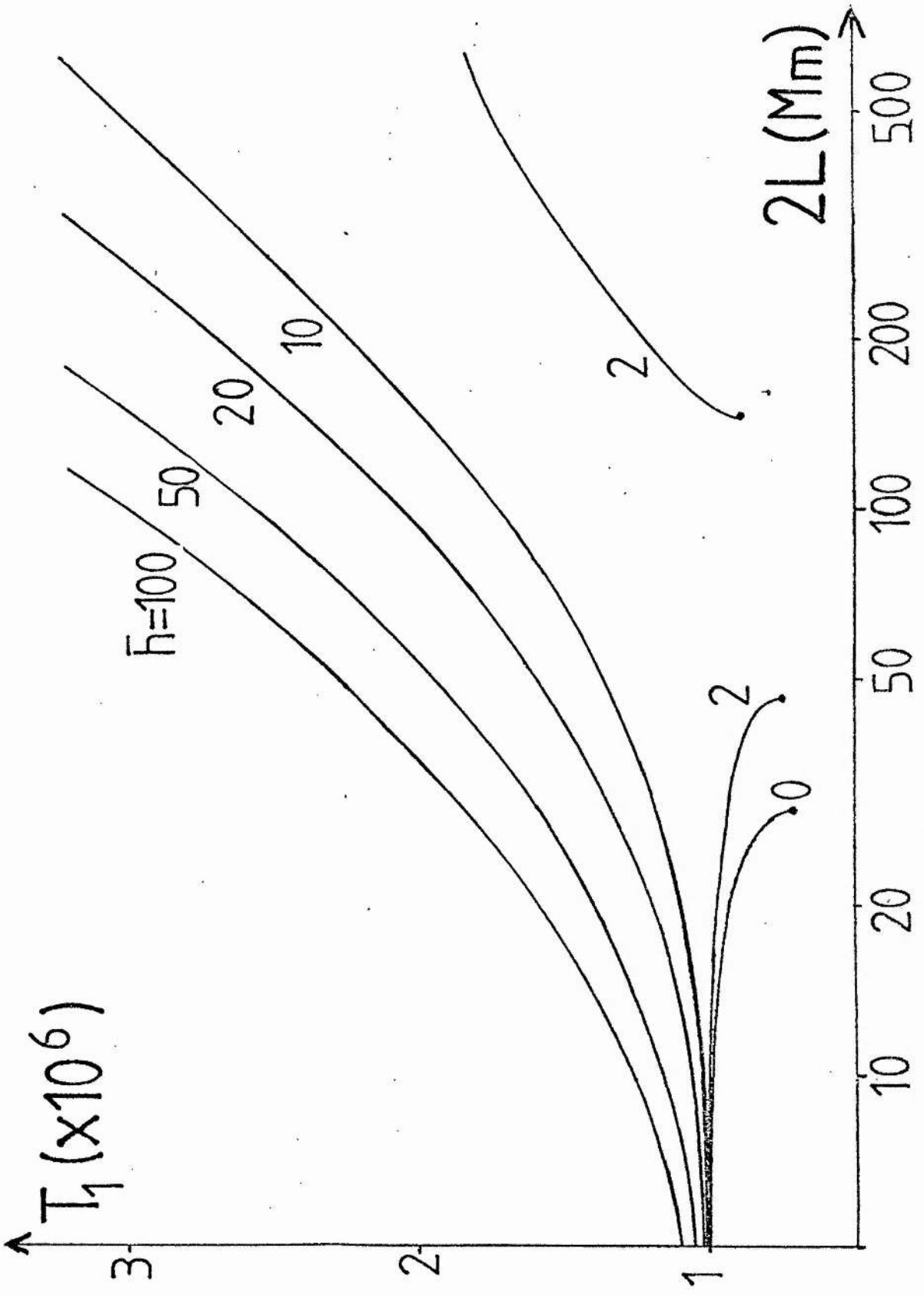

Figure 3.13a The summit temperature for a loop with a base density of $N_o = 2 \times 10^{15}$ m^{-3}.

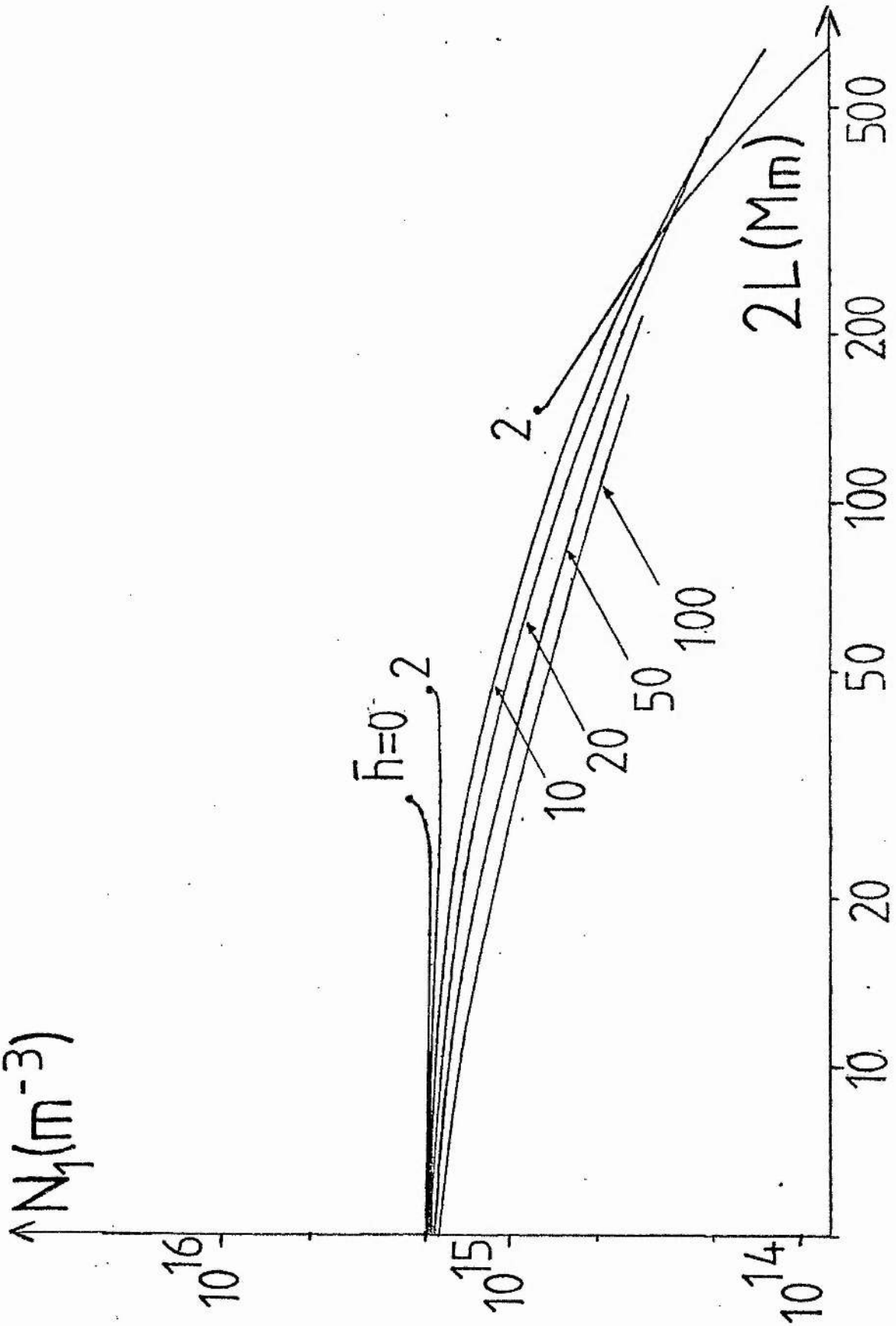

Figure 3.13b The summit density for a loop with a base density of $N_o = 2 \times 10^{15}$ m^{-3}.

$$\bar{h}_c \approx N_o/N_c,$$

while for low density loops

$$\bar{h}_c < N_o/N_c.$$

For various values of $\bar{h}$ Figure 3.10 gives the critical density N_{crit} as a function of the loop length 2L, or equivalently the critical loop length $2L_{crit}$ as a function of the base density N_o. One interesting point to notice is that there exists a particular minimum value of the base density $N_{crit} = N_{min}(\bar{h})$ below which an equilibrium solution always exists, regardless of the value of L. N_{min} is a monotonically increasing function of $\bar{h}$ and for $\bar{h} = 0$ it takes the absolute minimum value of $7.6 \times 10^{14} m^{-3}$. This feature was not present in the uniform pressure analysis of Hood and Priest, for which N_{crit} approaches zero as $\bar{h}$ decreases. The effect of gravity in the present treatment has therefore resolved a difficulty of the Hood and Priest work. It explains that very long hot loops, with temperatures in excess of 5×10^5 K and small heating values, can indeed exist in equilibrium, provided their densities are sufficiently small. The reason for this is as follows. Hood and Priest (1979) found that, with heating equal to zero, there does not exist a solution to the energy equation

$$\frac{d}{d\bar{s}}\left(\bar{T}^{5/2}\frac{d\bar{T}}{d\bar{s}}\right) = N^2\bar{L}^2\bar{\chi}\bar{T}^{\alpha}$$

when the right-hand side is large enough. At constant pressure $N^2\bar{L}^2$ increases monotonically with $\bar{L}$ and so

eventually non-equilibrium is reached. However, under hydrostatic equilibrium the pressure falls off with altitude, so that as $\bar{L}$ increases, the radiation term at first increases and then decreases. This decrease for long loops makes the equilibrium move further away from critical conditions.

It is easily seen on these graphs showing the summit density, how the curves cross over at $2L \approx 300$Mm, giving the initally surprising result that hotter loops are more dense than cooler loops of the same base pressure, seen in Figures 3.6 to 3.8. This is due to the fact noted in Chapter 2 that the cooler plasma has a smaller gravitational scale height which results in a greater depreciation of pressure.

The numerical results for small heating in conduction-dominated loops agree well with the analytic solution worked out in Equations (3.4.4), as can be seen in Figures 3.12, where the analytic solution is drawn dashed. Furthermore, a balance of heating and radiation at the foot ($\bar{h} = 2$) in the uniform pressure treatment makes the loop isothermal (Hood and Priest); however for $\bar{h} = 2$ Figure 3.12 shows that the summit temperature is in excess of 10^6 K and increases monotonically with L (for $2L \lesssim 500$ Mm). This is in agreement with the analytic expansion performed for small $\bar{g}$ in Section 3.4.

One final feature of the curves in Figure 3.12 is that, for given heating $\bar{h}$, very long loops ($2L \gtrsim 500$Mm) have summit temperatures that reach a maximum value, rather

than continuing to increase with L. For such long loops the temperature profiles exhibit most of their rise in a boundary layer near the footpoints where heating and radiation are comparable with conduction, and, along most of the loop, the temperature rises much more slowly due to conduction domination. This feature would not be expected if heating was to occur throughout the loop independent of the density. Thus a certain amount of caution is needed when applying scaling laws obtained from constant-pressure models to very long loops.

Probably one of the most restrictive assumptions for these results is that flows are regarded as unimportant. Flows have been studied by Cargill and Priest (1980) and one result was that a steady (siphon) flow through the loop reduces the temperature maximum and carries it away from the summit into the downflowing leg. It is quite easy to explain qualitatively this feature from the results of this and the previous chapter. An upflow to the summit has the same type of effect as reducing the heating, which for coronal-loop boundary conditions reduces the temperature. Similarly the structure past the summit experiences a downflow, similar to enhancing the heating, which will increase the temperature, and cause the shift in the position of the maximum.

3.6 FLARE LOOPS

Though flare loops are the result of the release of a great amount of energy, one particular observation (Petrasso, et al., 1979) showed that energy was still being added at the top of the loop in question more than 11 hours after the flare, and that throughout much of that time there was only a gradual decrease in temperature and density.

Under the assumption that flare loops are passing through a series of quasi-equilibria, the computer program was run again to model this state. The length 2L was varied between 5 and 100Mm (a typical range for flare loops). In order to obtain summit temperatures and densities comparable with observations the heating $\bar{h}$ was an order of magnitude or so higher than before. Since $\bar{h}$ is defined to be the ratio of heating to radiation at the standard density of 5×10^{14} m^{-3}, it should be noted that, for example, a value of 300 for $\bar{h}$ means that the heating at the foot is only twice the radiation (although higher up the loop the heating greatly dominates). The results are graphed in Figures 3.14 and 3.15. In flaring loops the increased heating leads to an increased base pressure according to the scaling laws of Section 3.3 and this in turn enhances the density throughout by a time-dependent process of evaporation; the results here illustrate the new quasi-steady states which are implied by enhanced heating rates.

Figures 3.14 and 3.15 give the summit temperature and density as functions of length for various values of heating with base densities of 2×10^{17} m^{-3} and 2×10^{18} m^{-3}, respectively. These graphs exhibit the same features as before, with temperature increasing with either L, N_o or $\bar{h}$. Whereas the higher heating values give solutions above the critical points, it can be seen that the lower heating values start at the critical points. These are actually the "second" critical points described in connection with Figure 3.13; the finite region of non-equilibrium has here moved from large lengths to small lengths. Thus the higher temperatures can be obtained at constant L only by an evolution of both N_o and $\bar{h}$ which avoids the critical points. For a given L and N_o, the summit temperature can be made as high as one likes by taking a suitable value of $\bar{h}$, but it cannot be made too small (e.g. as small as active-region temperatures) because of the presence of the critical points. For loops with temperatures around 10^7 K, the temperature gradient at 10^6 K becomes very large indeed, being as much as 10^3 times larger than loops with summit temperatures of only 2×10^6 K.

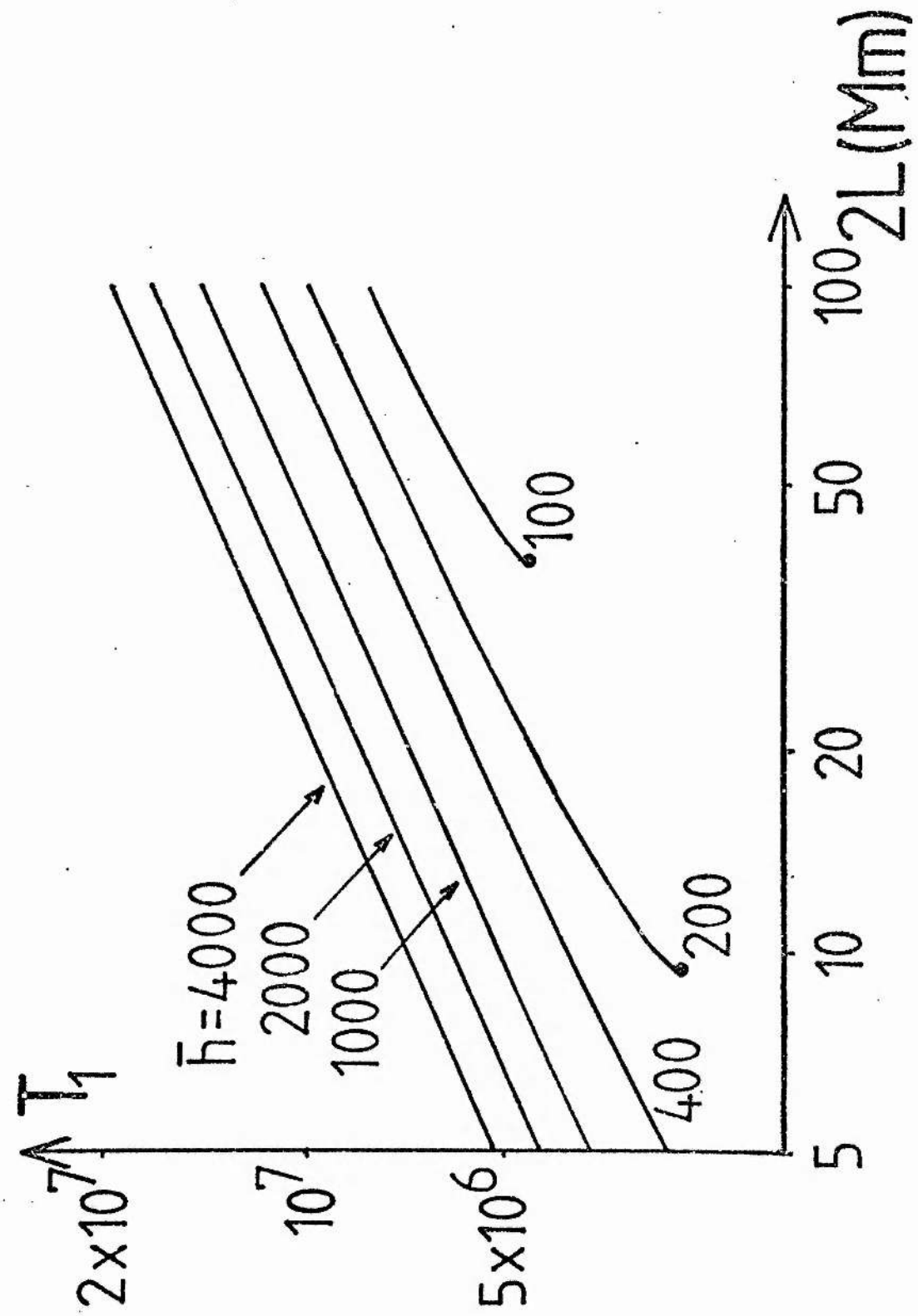

Figure 3.14a The summit temperature T_1 for quasi-static flare loops whose base density N_o is 2×10^{17} m^{-3} as a function of the length 2L, for various values of $\bar{h}$.

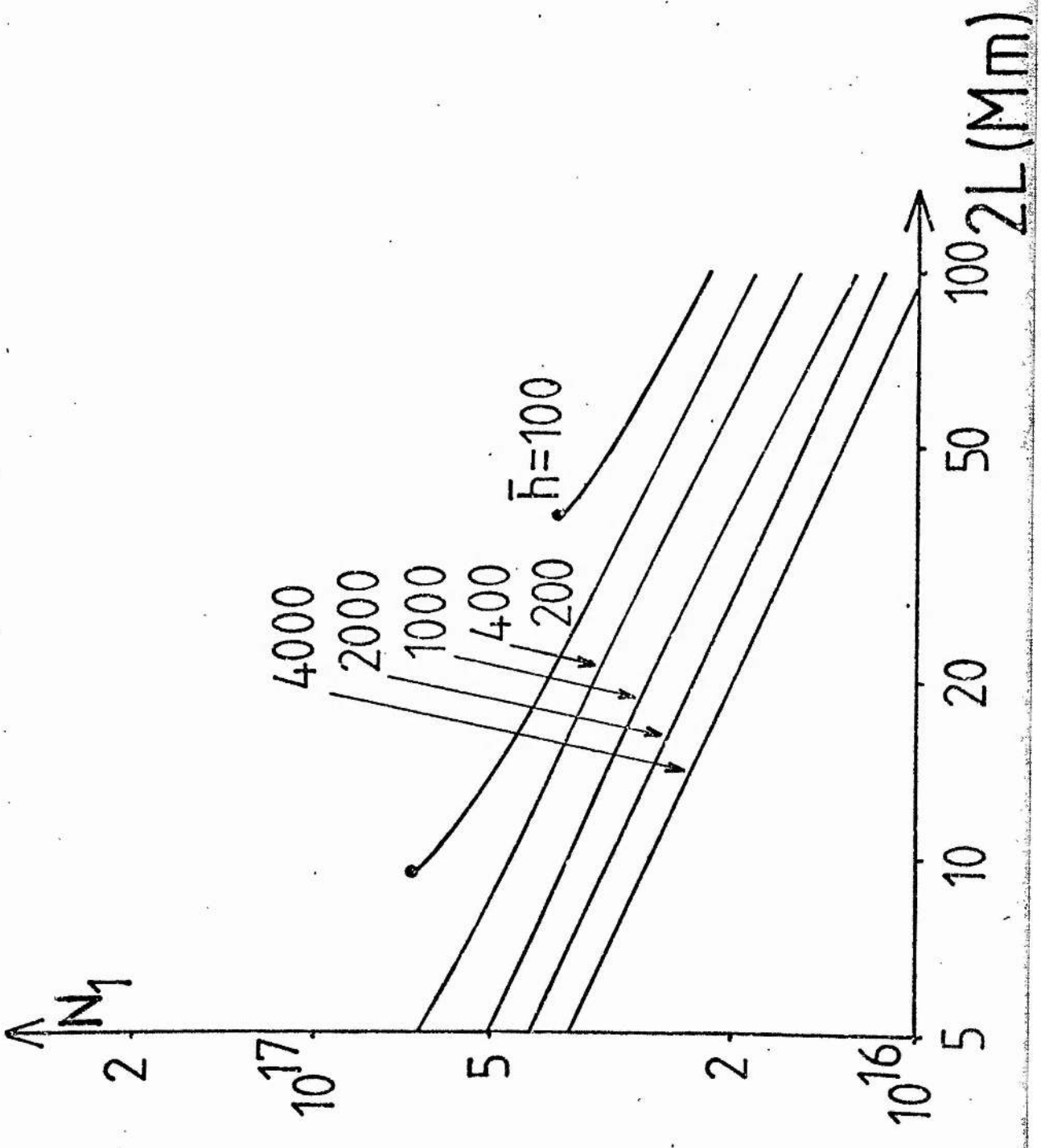

Figure 3.14b The summit density N_1 for flare loops whose base density N_o is 2×10^{17} m^{-3}.

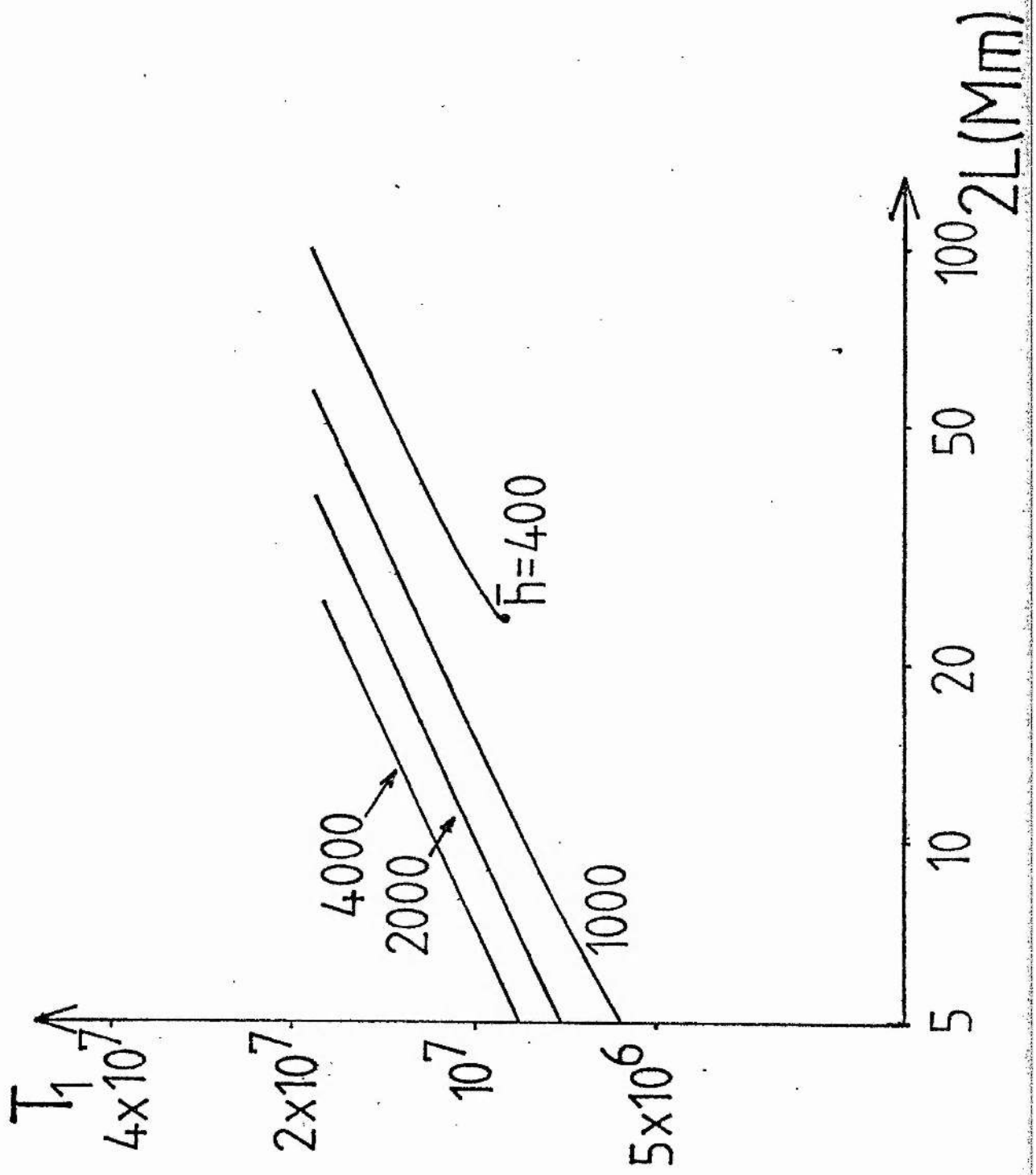

Figure 3.15a The summit temperature T_1 for flare loops of base density $N_o = 2 \times 10^{18}$ m^{-3}.

Figure 3.15b The summit density N_1 for flare loops of base density $N_o = 2 \times 10^{18}\ m^{-3}$.

3.7 EFFECTS OF THE FLUX-LOOP DIVERGENCE AND GEOMETRY

3.7.1 Flux-Loop Divergence

Consider first the flux-loop divergence, measured in terms of d, the ratio of the diameter of the loop at the summit to that at the base (Figure 3.2). This brings into play an extra term due to the factor

$$\frac{1}{A}\frac{dA}{ds}$$

not vanishing. For geometrical symmetry about the summit, the form used in Chapter 2 must be modified, and so

$$A = A_0(1 + (d^2 - 1)\sin(\tfrac{1}{2}\pi s/L)) \qquad (3.7.1)$$

has been taken, for a base area A_0. Here d then represents the diameter of the flux tube relative to the base. Thus area ratios from summit to base of 1, 4, 25 and 100 correspond to values d = 1, 2, 5, 10, respectively. It is not the network effect, which occurs far below 10^6 K, but rather the various coronal geometries which are sought to be modelled by this approach. For (3.7.1) the extra term in the energy equation becomes

$$K_0 T^{5/2}\frac{dT}{ds}\frac{(\frac{1}{2}\pi s/L)(d^2-1)\cos(\frac{1}{2}\pi s/L)}{1 + (d^2-1)\sin(\frac{1}{2}\pi s/L)} . \qquad (3.7.2)$$

The qualitative effect of loop divergence is independent of the choice of parameters L, N_0 and $\bar{h}$, and so Figure 3.16 gives the profiles of temperature and density for one typical active-region loop. It has length 80Mm, heating $\bar{h}$ = 20, and base density $6 \times 10^{15} m^{-3}$.

Increasing the summit area through increasing d causes the summit temperature to rise, and the density to fall slightly. This is because the extra term (3.7.2) is positive and so has the same effect as an extra heating source. Physically, an increase of area at a given location makes the temperature gradient smaller to preserve the same conductive flux, as seen in Figure 3.16. The greatest effect is near the footpoints, where all of the factors $1/A$, dA/ds and dT/ds have their largest values. The density is decreased much more near the footpoints than at the summit. Since, for a given N_o, the base pressure gradient is constant from (3.2.2), an increase in base temperature gradient must produce a corresponding decrease in base density gradient. The differential emission measure is shown in Figure 3.16c, plotted as that which would result from a whole loop (of length $2L$) and of unit base cross-sectional area. It can be seen that (except very near the summit where the zero temperature gradient causes a singularity in the differential emission measure) a more divergent loop has more of its emission at higher temperatures due to a greater amount of plasma existing at these higher temperatures. This is partly because the geometry allows a larger volume, and partly due to the smaller temperature gradients giving a more isothermal central region within the loop. The correspondingly greater base temperature gradients result in a depreciated emission near 10^6 K. These effects are seen as a greater emission-measure gradient, denoted as b in Equation (3.1.1).

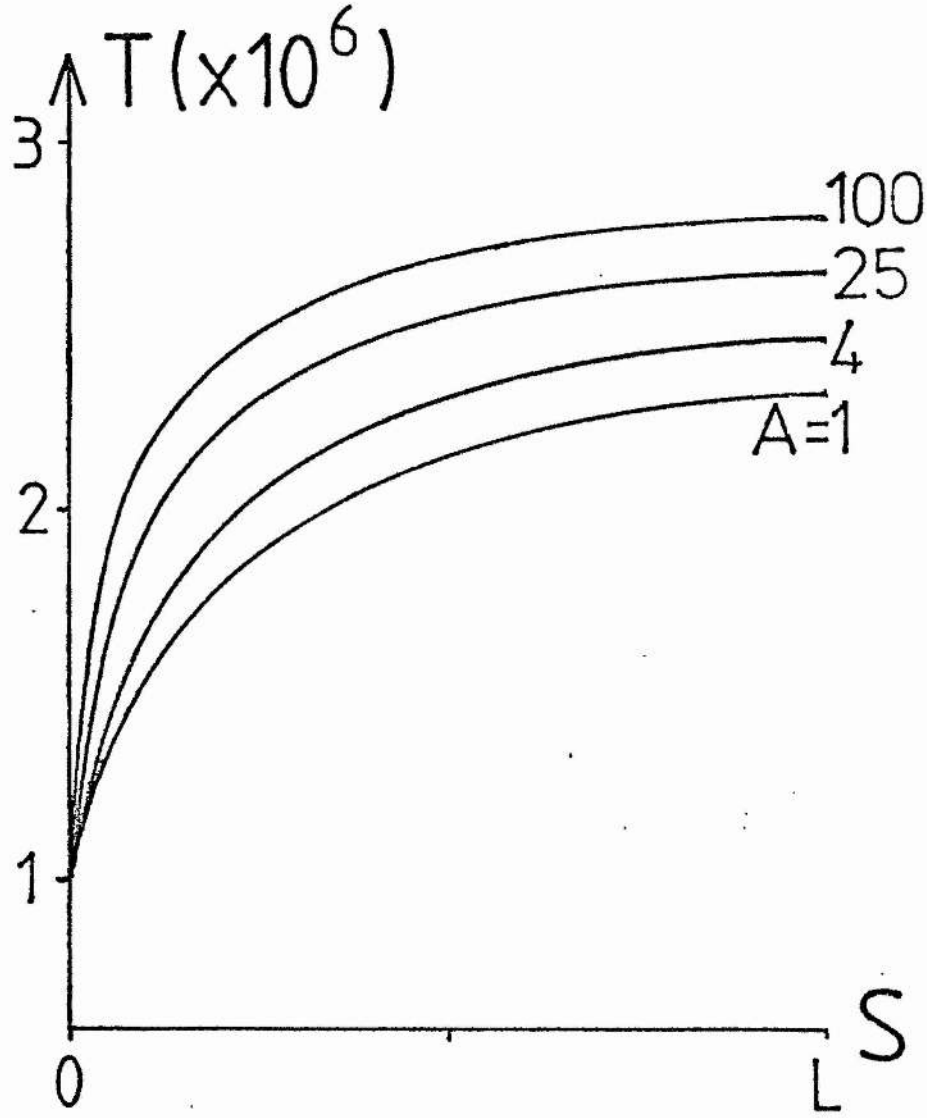

Figure 3.16a The effect of the loop divergence on the temperature profile for a semi-circular active-region loop of length 2L = 80 Mm and heating $\bar{h}$ = 20. A is the ratio of summit area to base area.

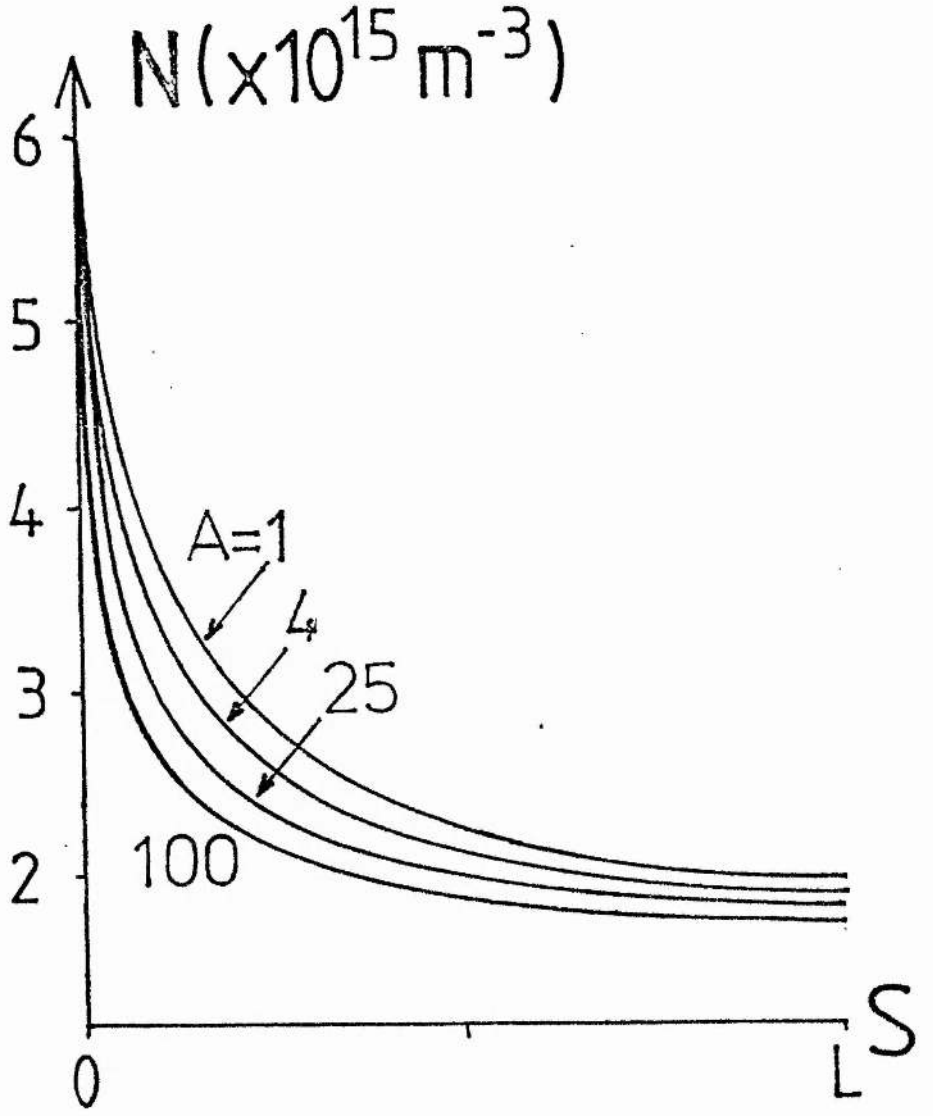

Figure 3.16b The effect of the loop divergence on the density profile for a loop of length 2L = 80 Mm and heating $\bar{h}$ = 20.

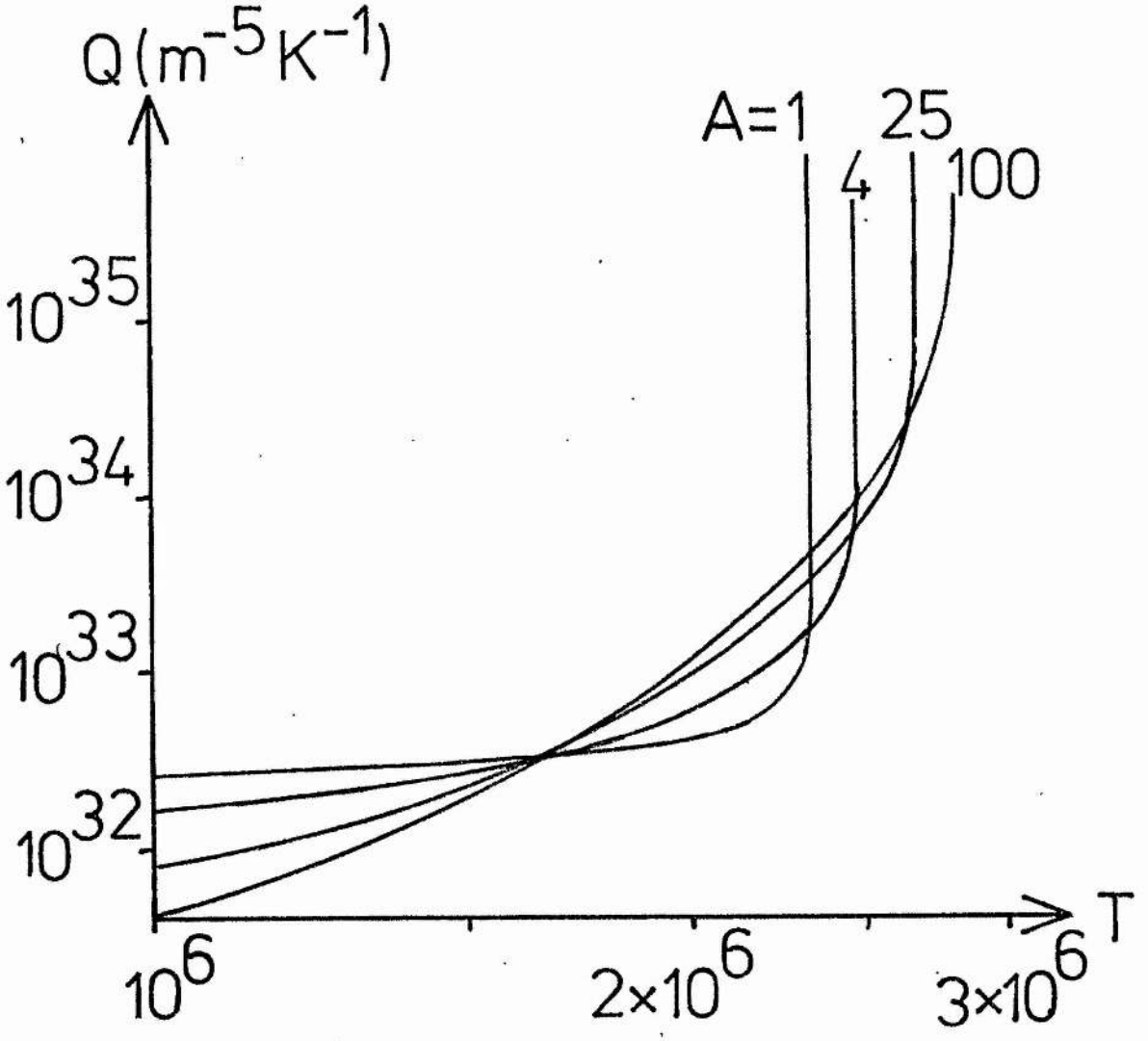

Figure 3.16c The differential emission measure (per unit cross-sectional base area) for a loop of length 2L = 80 Mm and heating $\bar{h}$ = 20, for various field-line divergences.

Of particular interest is the value at the base, 10^6 K. The network effect of a divergent transition-region field above the supergranular boundaries disappears well below 10^6 K and so the observed value of $b \approx 2.7$ (Jordan, 1976) may be reasonable at 10^6 K. If it is assumed that this holds for individual loops this may provide a method of selecting models that occur in practice. The feature of a larger gradient in the differential emission measure for a more divergent loop was also noted by Levine and Pye (1980). Their analysis was applied to loops of constant pressure and vanishing base flux, however.

It was also found that, near a critical point, increasing d is a stabilising factor in the sense of taking the equilibrium further away from critical conditions for non-equilibrium.

3.7.2 Loop Geometry

Now consider the effects of keeping d fixed equal to unity and varying r, the ratio of the height of the loop to half the footpoint separation (Figure 3.2). This results in the more complicated cosine term being used in the equation of hydrostatic equilibrium, as in Equation (3.2.2). The larger the value of r, the more the pressure decreases with altitude, although loops shorter than a scale height are insensitive to this effect. The value $r = 1$ gives a semicircular loop, whereas $r \ll 1$ corresponds to a low-lying loop for which the uniform-pressure results of Hood and Priest (1979) are valid. For large values of r the height is generally about a third of the length (2L).

Explicitly, for $r \geq 1$, the height is given by

$$\frac{1 + \left((r^2-1)/(r^2+1)\right)^{1/2}}{\pi + 2\tan^{-1}\left(\frac{1}{2}(r^2-1)/r\right)} L .$$

This equals $2L/\pi$ for both $r = 1$ and $r = \infty$ and has a maximum of $0.72L$ when r satisfies

$$\frac{r^2-1}{2r} = \tan^{-1}\left(r - \frac{\pi}{2}\right) ,$$

namely when $r \approx 2.3$.

The effect on the temperature and density profiles of varying r is shown graphically in Figures 3.17a and (b), and the differential emission measure in (c), for a typical interconnecting loop of length 225Mm. The heating is $\bar{h} = 7$, and base density 2×10^{16} m^{-3}. The temperature profile is found to vary only slightly with r. However, the density decreases markedly as the loop summit becomes higher with increasing r. The differential emission measure is seen to have a larger gradient where that part of the flux tube is nearly horizontal, namely throughout the length for the case $r = 0$, and near the base and summit but not inbetween if $r = 2.3$. In parts of a loop that are vertical, the fall off in density with height opposes any increase of emission measure with temperature.

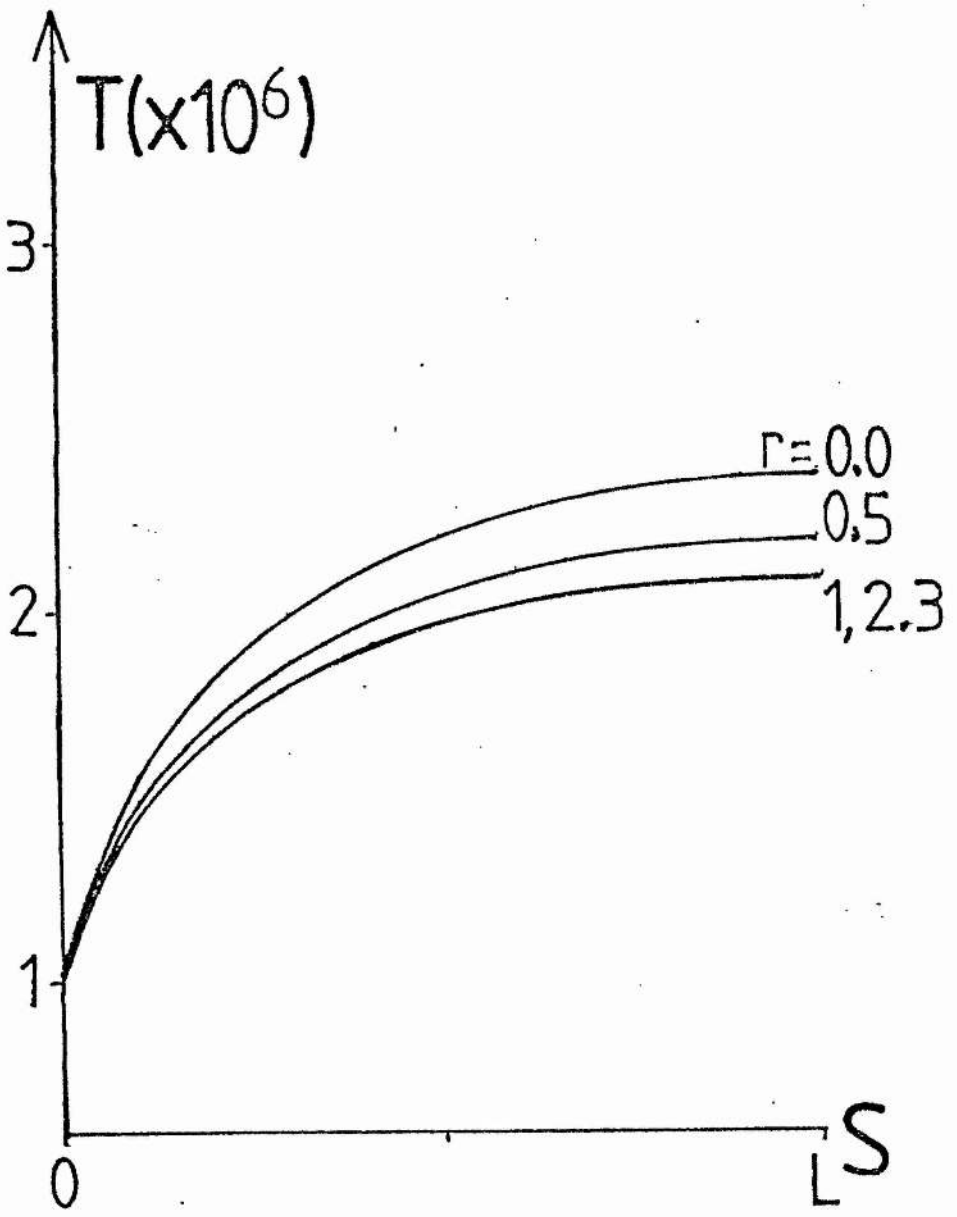

Figure 3.17a The effect of loop geometry on the temperature profile of an interconnecting loop of length 2L = 225 Mm and heating $\bar{h} = 7$. The ratio of the loop height to half its footpoint separation is denoted by r. r = 0 gives the uniform-pressure loop and r = 2.3 gives the loop of maximum height for a given length.

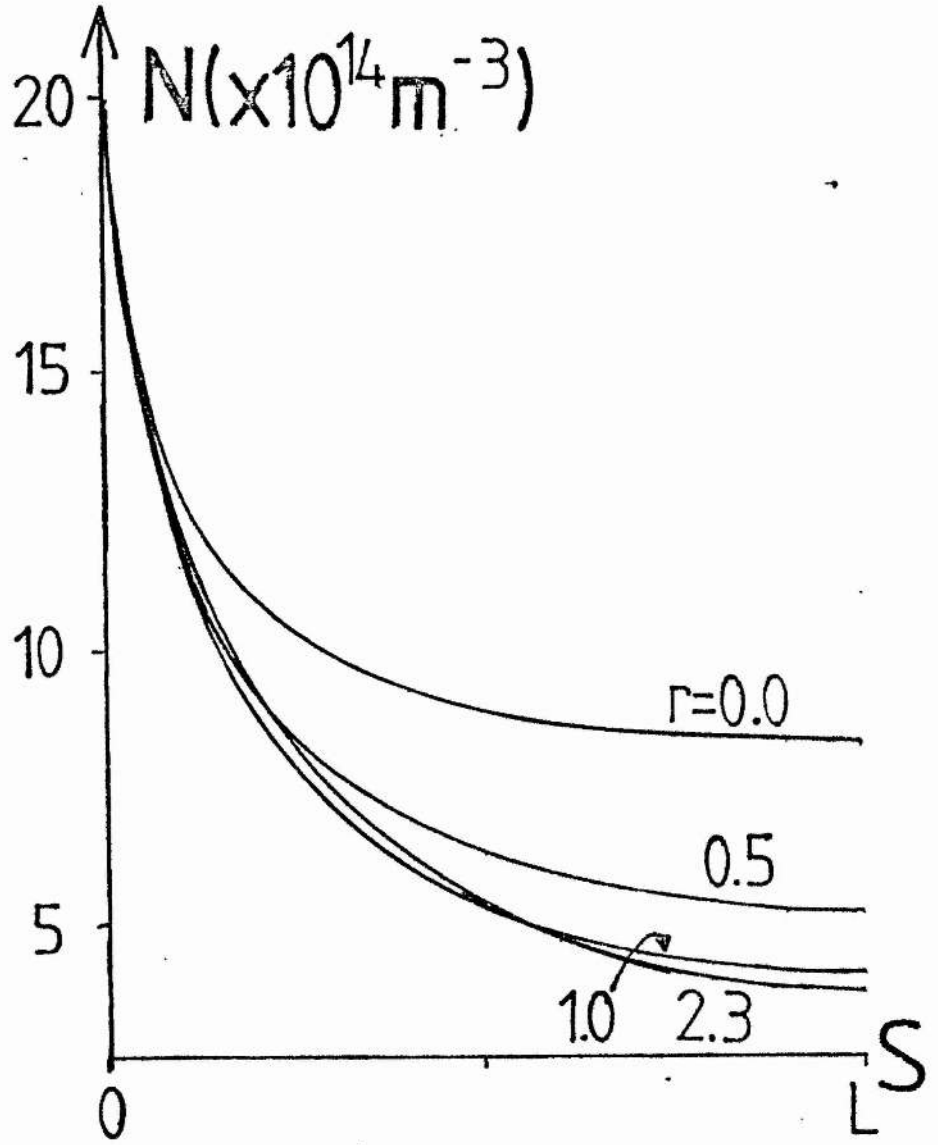

Figure 3.17b The effect of loop geometry on the density profile of an interconnecting loop of length 2L = 225 Mm and heating $\bar{h}$ = 7.

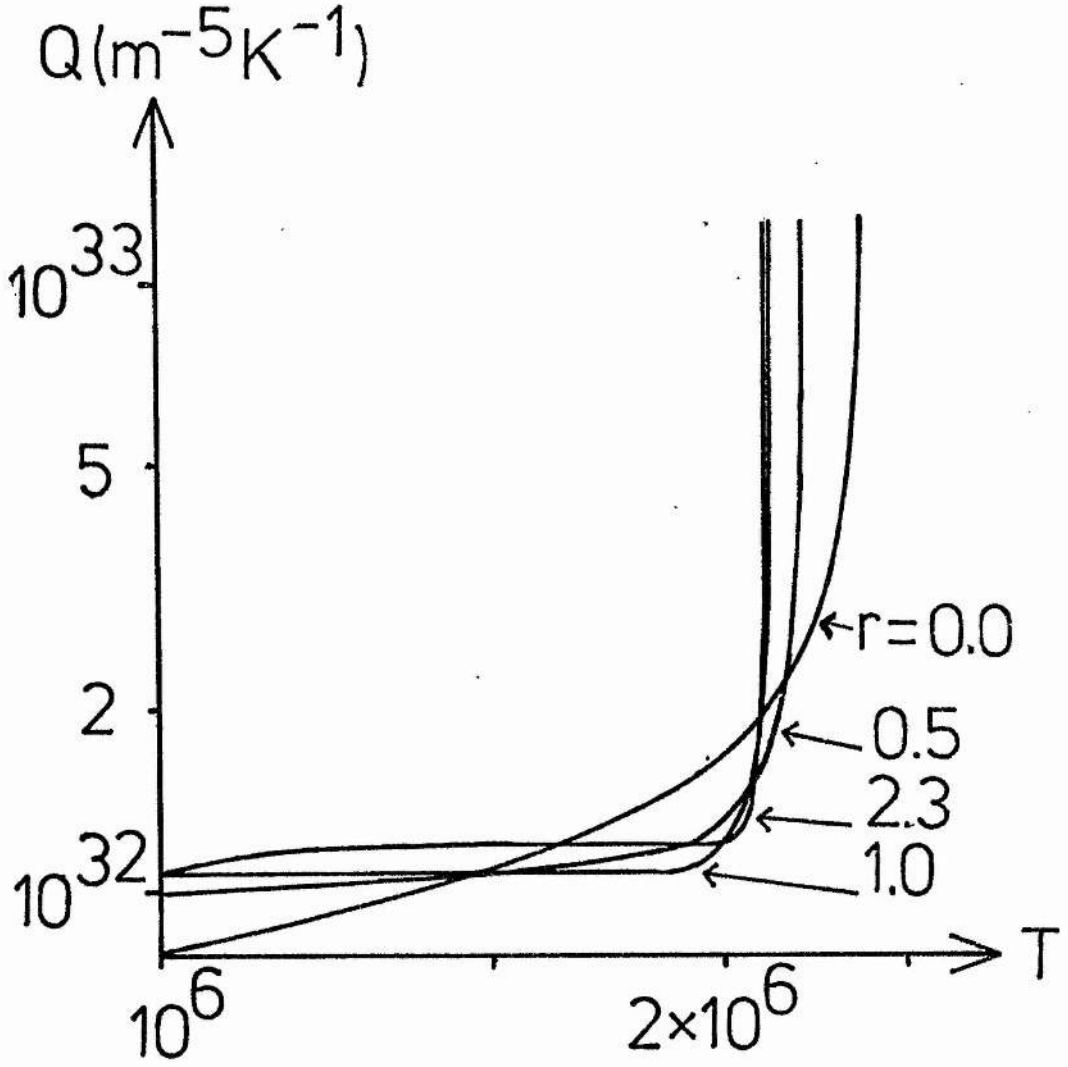

Figure 3.17c The effect of loop geometry on the differential emission measure of an interconnecting loop of length 2L = 225 Mm and heating $\bar{h}$ = 7.

3.8 SUMMARY

The present chapter has modelled a coronal loop by a single field line, along which the plasma is in both thermal and hydrostatic equilibrium. The simplest case is a thermally isolated loop for which the conductive flux vanishes both at the loop summit and at the loop base, taken at 2×10^4 K. The loop density can fall off by an order of magnitude or more, which is more than in the previous uniform-pressure approximation. The temperature is seen to be less than the uniform-pressure case, by as much as a factor of two for long loops of low density. The order-of-magnitude scaling law for loops whose summit is lower than a scale height (so that the pressure is uniform) is

$$T_1 \approx 9 \times 10^3 (L p_o)^{1/3}.$$

Gravity modifies this to

$$\exp\left(10^{-2} \frac{L}{T_1} \right) T_1^3 = 6 \times 10^{11} p_o L. \qquad (3.8.1)$$

As L increases, the temperature initially rises, but then reaches a maximum and eventually (for very long loops) falls again. For moderately long loops, near this maximum, Equation (3.8.1) may be approximated by

$$T_1 \approx 7 \times 10^6 p_o^{1/2}.$$

The limitations of the thermally-isolated approximation have been pointed out by Hood and Priest (1979). For example,

sometimes such loops appear to be thermally unstable and the transition region may not be modelled satisfactorily by the same equations with the same heating form as the corona.

Models have also been considered that start from higher in the atmosphere at a temperature of 10^6 K and have allowed the pressure there to be varied independently of the loop length and heating. In other words, it is supposed that the chromospheric pressure is governed by processes largely independent of the coronal heating and loop length. This approach exhibits the potential character of the solutions to the energy balance equations, although in practice there may be some subtle link between the parameters. The main results are as follows.

The order-of-magnitude scaling law for hot loops with uniform heating $\bar{E}_H$ per unit volume is

$$T_1 \sim (\bar{E}_H L^2)^{2/7},$$

and the density is given by

$$N = \frac{p_0}{2kT} \exp\left\{-4\times10^{-2}\,\frac{L}{T_1}\left[\frac{\pi}{4} - \tan^{-1}\left(1-\frac{s}{L}\right)\right]\right\}.$$

The numerical results for the variation of summit temperature and density with length, heating and density are presented in Figures 3.6 to 3.8. The effect of gravity is to lower the summit pressure, which decreases the radiation more than the heating and so raises the summit temperature above the uniform-pressure value. If the loop is very long, $L \gtrsim 200$Mm, the decrease in density is so severe in both the radiation and heating terms that the temperature actually falls below its uniform-pressure value.

Numerical results for the effect of changing the loop divergence and geometry are given in Figures 3.16 and 3.17. As the loop diverges more, so the temperature gradient decreases and the summit temperature rises while the density falls. As the height of a loop increases while its length remains constant, so the temperature changes only slightly and the density falls substantially.

Hood and Priest (1979) discovered that a lack of equilibrium could occur if the density were too high or the heating too low for a given loop length, the result being that the plasma in the core of the loop cools down. This feature has been confirmed by the present analysis. (However, a new result evident from Figure 3.10 is that, for a given heating, there exists a minimum density, below which the hot equilibria always exist, regardless of the loop length.) The lack of equilibrium may well explain the remarkable results from the Skylab Active Region Workshop (Krieger, 1980) that coronal loops cooler than 2×10^6 K possess cores at a lower temperature, while loops hotter than 2×10^6 K possess no such core. It can be seen from Figure 3.7a that loops between 10^6 K and 2×10^6 K require a coronal base density of between 2×10^{15} m^{-3} and 2×10^{16} m^{-3} for the onset of cooling by non-equilibrium in their cores; however, loops that are hotter than this require unreasonably large densities for cooling and so are likely to remain in hot equilibrium throughout.

It has been seen clearly in this chapter how the relationship between the physical parameters, namely

density, temperature and energy input is indeed complicated. A popular subset of these solutions has been the thermally isolated loops. These are re-examined in the following chapter, where a further comparison with scaling laws is sought, and the question of uniqueness is followed up.

4. THERMALLY ISOLATED LOOPS

4.1 INTRODUCTION

One question bypassed in the previous chapter was: what combinations of parameters - base density, loop length, energy input and base flux - occur in practise on the Sun? It was pointed out that only a small range of base flux values may be allowable, but the truth of that doesn't explain the situation. Many authors have assumed zero base conductive flux at the bottom of the transition region. Obviously the flux is very much reduced here, but a model of the type in Chapter 3 with vanishing flux has one less degree of freedom, and its validity is debatable.

An interesting loop model was proposed by Giovanelli (1975), assuming a zero temperature gradient at 2×10^4 K. If this is the case, then how is the interdependence between the parameters worked out by the Sun? Giovanelli suggested it is brought about by a automatic adjustment of the position of the base of the transition region, and hence the thickness of the chromosphere. If there is excess heat deposited in the corona, then the temperature near the base of the transition region will rise, causing the position where $T = 2 \times 10^4$ K (defined to be the base of the loop) to penetrate further down into the chromosphere, where the pressure is higher. The chromospheric region was assumed isothermal at $T = 2 \times 10^4$ K for convenience.

By implication, there was then just enough heat generated to balance the radiation there. Thus in his model, there existed a relation between the base density and length, while the exact value of each is determined by the energy input.

Interestingly, though, Giovanelli was also able to prescribe a density at the base of the chromosphere. Since also he imposed the overall length (to the base of the chromosphere), it would seem to suggest that vanishing base flux has been set without losing a degree of freedom. However, in Giovanelli's model he also allowed for a great divergence of field lines above a supergranular cell boundary, but the amount of this which occurs within his loop depends on the position of the base and hence on the length. Thus the automatic change of base position has a compound effect. It alters the length, although this is by only a few percent and probably not significant. It also changes the base density; this significantly changes the total amount of mass in the loop, since the density near the base is over two orders of magnitude larger than in the vicinity of the summit. Thirdly, it considerably alters the amount of field-line divergence within the loop, which can have a large effect on the rate of change of conductive flux near the base. It might just be that this variability in the divergence of the conductive flux acts, in practice, as a free parameter, justifying the approach of the work of Hood and Priest (1979), and of Chapter 3.

In Giovanelli's model, he assumed heating either uniform in volume or localised at the summit of the loop.

It was found that a greater heat input gives a larger coronal temperature, with a larger maximum if the heating is localised at the summit. A greater density at the base of the chromosphere only significantly alters the position of the base of the loop. Oscillatory solutions were found, similar to those discarded by Hood and Priest (1979) and Chapter 3.

Because of the interest in thermally isolated loops, they are re-examined in the present chapter. In Chapter 3 the scaling law derived by order of magnitude was compared with the full numerical solution. This is taken up further in Section 4.2, and the differential emission measure is plotted for a range of models. Although zero base flux has been assumed, it should be noted that moderate departures from a vanishing temperature gradient at 2×10^4 K make little difference to the results; enormous temperature gradients are necessary to change the conductive flux significantly at such low temperatures.

In Section 4.3 a thermally isolated loop of a given fixed mass is considered. Craig (1981) and Craig and McClymont (1981) modelled time-dependent flow in a similar situation, and observed a dynamical progression between apparently different static equilibria. This led them to suspect that several static equilibria may be possible, but they were unable to reproduce more than one from static equations. The question of the existence of mutiple solutions is, therefore, investigated here.

4.2 LOOPS IN HYDROSTATIC EQUILIBRIUM

The equations of energy balance and hydrostatic equilibrium,

$$\frac{d}{ds}\left(K_0 T^{5/2}\frac{dT}{ds}\right) = N^2\chi T^{\alpha} - hN\,, \qquad (4.2.1)$$

$$\frac{dp}{ds} = -Nm_p g\cos\left(\frac{\pi s}{2L}\right), \qquad (4.2.2)$$

were solved in Chapter 3, subject to the boundary conditions

$$\begin{aligned} &T = T_0\,, \quad N = N_0 \quad \text{at} \quad s = 0\,, \\ &\frac{dT}{ds} = 0 \qquad \text{at } s = L\,, \end{aligned} \qquad (4.2.3)$$

with T_0 chosen to be equal to 10^6 K. Solutions were found for a range of values of L, N_0 and h, and the value of dT/ds at the base was deduced. For thermally isolated loops, the boundary conditions (4.2.3) are supplemented by the extra constraint

$$\frac{dT}{ds} = 0 \qquad \text{at} \quad s = 0,$$

and so L, N_0 and h become interdependent, any two prescribing the third.

Assume constant pressure, $T_1 \gg T_0$, and $\alpha = -\frac{1}{2}$. Then, if the conduction and radiation terms are of the same order of magnitude, (4.2.1) gives at the summit,

$$K_0\frac{T_1^{7/2}}{L^2} \approx \frac{p_0^2}{4k^2T_1^2}\chi T_1^{-1/2}$$

or

$$T_1 \approx C_1 (p_o L)^{1/3} \qquad (4.2.4)$$

where $C_1 = (\chi/(4k^2\kappa_o))^{1/6}$ is approximately 11300, with $\chi = 10^{-31.8}$.

At constant pressure Equation (4.2.4) can be derived analytically when $\alpha = -\frac{1}{2}$. Substituting for N $(= p/(2kT))$ in Equation (4.2.1), multiplying by $T^{5/2}\, dT/ds$ and integrating from the loop summit yields

$$\frac{1}{2}\kappa_o \left(T^{5/2}\frac{dT}{ds}\right)^2 = \int_{T_1}^{T} T^{5/2}\left(\frac{p_o^2 \chi}{4k^2} T^{-5/2} - \frac{h p_o}{2k} T^{-1}\right) dT,$$

so that

$$\frac{1}{2}\kappa_o T^5 \left(\frac{dT}{ds}\right)^2 = \frac{p_o^2 \chi}{4k^2}(T - T_1) - \frac{h p_o}{5k}(T^{5/2} - T_1^{5/2}). \qquad (4.2.5)$$

When $T_1 \gg T_o$ this may be evaluated at the base, so that

$$h = \frac{5}{4}\frac{p_o \chi}{k} T_1^{-3/2}. \qquad (4.2.6)$$

Substituting for h into (4.2.5) and taking the square root then yields

$$T^2 \frac{dT}{ds} = \left(\frac{p_o^2 \chi}{2k^2 \kappa_o}\right)^{1/2} \left(1 - \frac{T^{3/2}}{T_1^{3/2}}\right)^{1/2},$$

which may be integrated to give

$$T_1 = C_2 (p_o L)^{1/3}, \qquad (4.2.7)$$

where

$$C_2 = \left(\frac{\chi}{2k^2 \kappa_o}\right)^{1/6} I^{-1/3}$$

and

$$I = \int_0^1 t^2 (1 - t^{3/2})^{-1/2} \, dt .$$

Numerically, $I \approx 0.89$ and $C_2 \approx 12200$, just 8% larger than the constant C_1 in Equation (4.2.4). The case of uniform heating has been calculated in a similar way in Hood and Priest (1979) and Rosner, et al.(1978).

Expression (4.2.4) was found in Chapter 3, with an alternative form for larger loops, and compared with the full numerical solution in Figure 3.5. Here the more accurate form (4.2.7) has been analytically derived and is compared along with the former. (The corresponding results of Chapters 3 and 4 differ in the choice of χ_0 which was taken as 3×10^{-11} in Chapter 3 only.)

The computer code originally used for Chapter 3 has been run for thermally isolated loops, with $T_0 = 2 \times 10^4$ K for a wide range of values of L and N_0. The heating was taken to be either proportional to density or uniform in space. For the case of heating proportional to density, Figure 4.1 shows the summit temperature plotted against $N_0 L$ on log-log scales. the dashed line gives the scaling law in (4.2.4), while the dotted line shows (4.2.7). Each curve shows the variation with L for a different fixed value of N_0. It can be seen that the small values of L give excellent agreement with (4.2.7), (dotted). For longer loops gravity becomes important, particularly for small values of N_0, and so T diverges away from the scaling-law approximation, reaching a maximum value and then

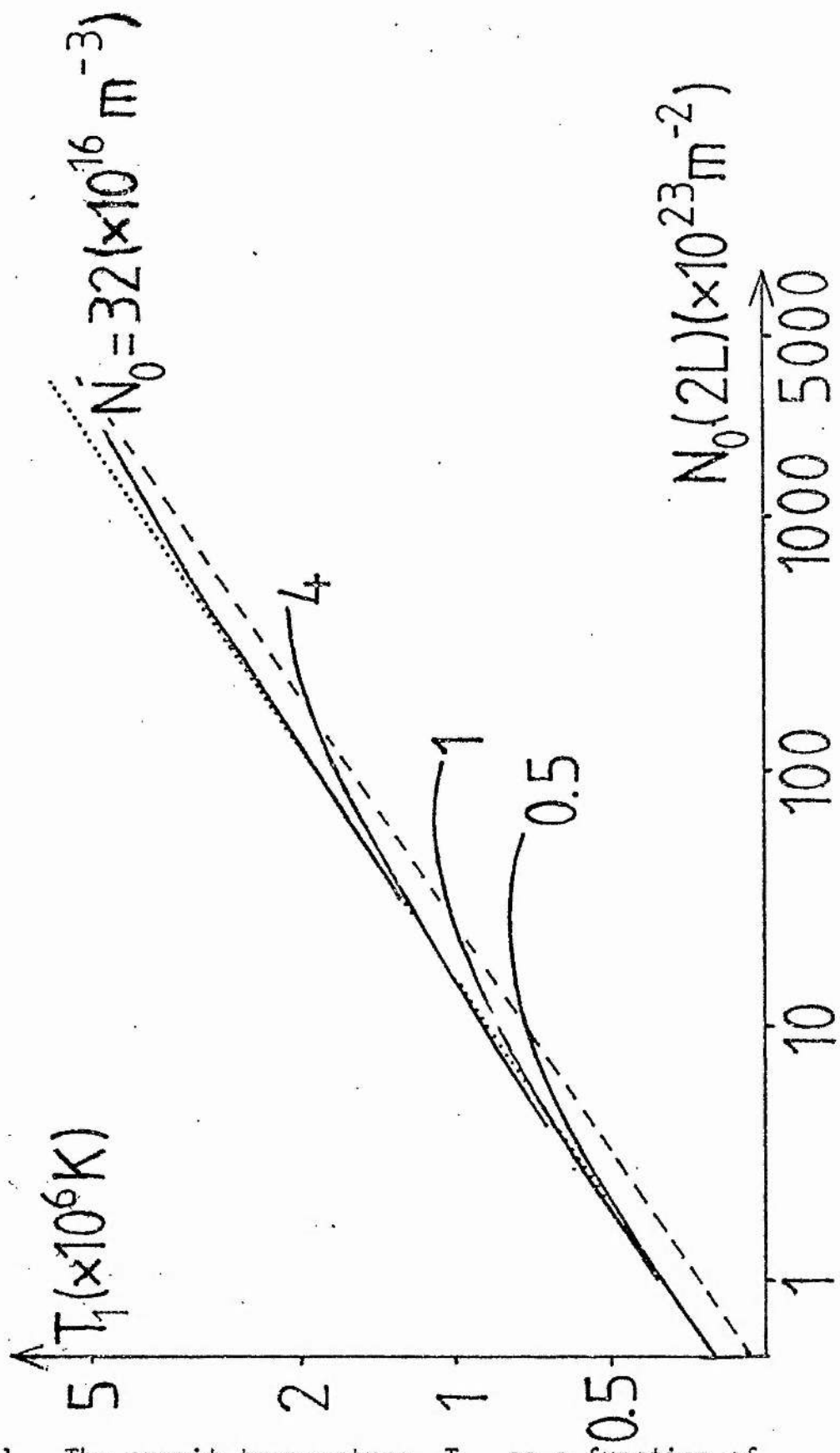

Figure 4.1 The summit temperature T_1 as a function of $N_0(2L)$, for various base densities N_b. The dashed line gives the $T \sim (N_0(2L))^{1/3}$ scaling law (4.2.4), while the dotted line gives the more accurate analytic derivation of it, (4.2.7).

falling. Also, the first order-of-magnitude approximation (4.2.4) (dashed) can be seen to be a reasonable approximation in its own right. The fact that as the length increases, the summit temperature becomes lower than the scaling-law value is to be expected, since a better approximation than (4.2.4) or (4.2.7) is

$$T_1 \sim (p_1 L)^{1/3},$$

and gravity has the effect of lowering the summit pressure (p_1) below the base value (p_0). For small loops the pressure is uniform and the curves for different densities coalesce, because the solution to (4.2.1) is unchanged by a transformation of s, N_0 and h to βs, N_0/β, h/β.

Uniform heating was also considered but the corresponding graph to Figure 4.1 gives little divergence from a simple $T_1 \sim (p_0 L)^{1/3}$ power law, even as the lengths were increased to large values. This is because while radiation dominates near the base, near the summit the heating and conduction balance while the radiation is much smaller. Although the pressure, and hence density, decrease with height due to gravity, the amount of heating is not reduced correspondingly, as in the former case.

It appears that the more the heating decreases with height (as in the case of heating proportional to density), the greater is the deviation of the temperature away from $T_1 \sim (p_0 L)^{1/3}$. Indeed, it was seen in Chapter 2, that for an open atmosphere the heating must decrease faster than N^2 beyond the temperature maximum in order to stop the

temperature falling to zero.

For a thermally isolated loop, the heating is determined in terms of the density and length. When the loop is short, and so gravity is unimportant, this is expressed by a scaling law which is

$$h = 4.78 \times 10^{-16} (p_o/L)^{1/2} \qquad (4.2.8)$$

when the heating is proportional to density.

This is obtained simply by equating the heating and radiation terms in (4.2.1) and using (4.2.4) to eliminate T_1. Again this can be derived analytically, merely by substituting for T_1 from Equation (4.2.7) into (4.2.6), so that

$$h = 1.07 \times 10^{-15} (p_o/L)^{1/2}. \qquad (4.2.9)$$

A graph of h against N_o/L is shown in Figure 4.2, with both scaling laws for comparison; the law (4.2.8) is dashed while (4.2.9) is dotted. Here h is plotted in units of the radiation at the standard coronal temperature and density of 10^6 K and 5×10^{14} m^{-3}, respectively; it is denoted by $\bar{h}$ so that $h = \bar{h} \times 7.42 \times 10^{-21}$. It can be seen that the relation (4.2.9) is a very good approximation for about half of the cases considered; yet it is up to a factor of 5 too small for long, rare loops (e.g. $N_o \approx 5 \times 10^{15}$ m^{-3}, $2L \approx 700$ Mm). Equation (4.2.8) is seen to be reasonable, about a factor of 2 smaller than (4.2.9). Using the same argument as above, it is easily seen that for uniform heating, N_o can be

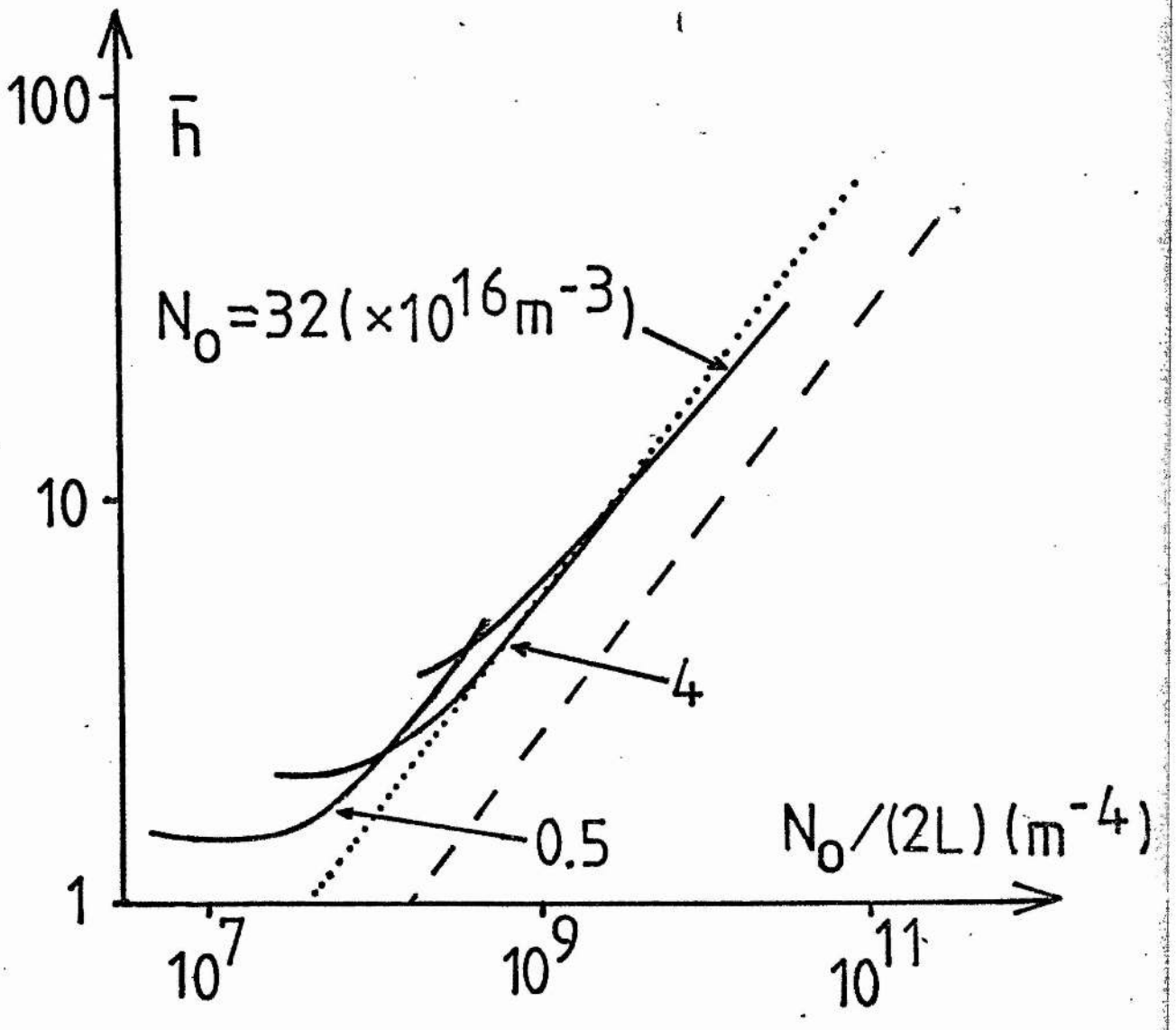

Figure 4.2 The heating $\bar{h}$ as a function of $N_o(2L)^{-1}$ for different values of N_o. The scaling law (4.2.8), $\bar{h} \sim (N_o(2L)^{-1})^{1/2}$, is shown dashed, and the analytic form of this, (4.2.9) is dotted.

eliminated to yield

$$E_H \sim T_1^{7/2}/L^2 .$$

However, Figure 4.1 reveals that the expression (4.2.4) for T_1 can be a factor of two too high, and so $T_1^{7/2}$ can be an order of magnitude too great. Consequently, this scaling law does not give good agreement with the numerical results.

The differential emission measure has been plotted for a range of the numerical solutions. Figures 4.3a and 4.3b show the cases when the base density is 10^{16} m^{-3} and 10^{17} m^{-3}, respectively, each for a range of lengths. These can be taken as typical densities for a quiet and an active region. In the lower transition region, below a temperature of about 3×10^5 K, the curves for different lengths are indistinguishable. It can be seen that between about 2×10^5 K and 2×10^6 K the differential emission measure is fairly constant. However, above 10^6 K in Figure 4.3a, or 2×10^6 K in 4.3b, the emission falls off rapidly with increasing temperatures. This is due to the decrease of pressure with height. A horizontal loop ($\bar{g} \ll 1$) is shown dotted for comparison for the case $N_o = 10^{16}$ m^{-3}, $2L = 200$ Mm where it is seen that the feature of reduced emission above 10^6 K is absent. This shows that it is necessary to use the equation of hydrostatic equilibrium (rather than constant pressure) while calculating the differential emission measure for the coronal temperatures of such loops. Typically, a loop need not have a great

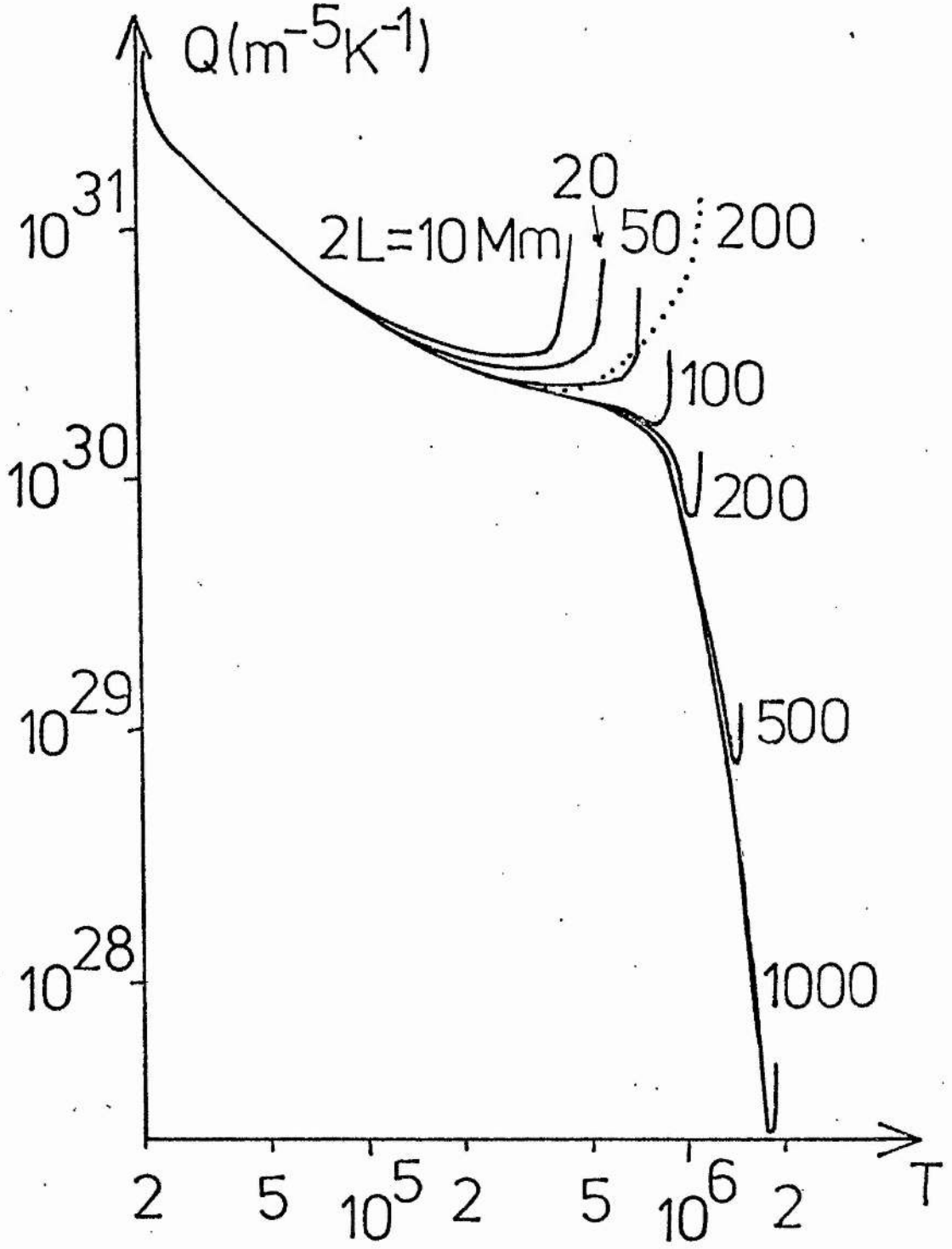

Figure 4.3a The differential emission measure (per unit cross-sectional area) for a thermally isolated loop of base density $N_o = 10^{16}$ m^{-3}. The dotted line refers to a uniform-pressure loop of length $2L = 200$ Mm.

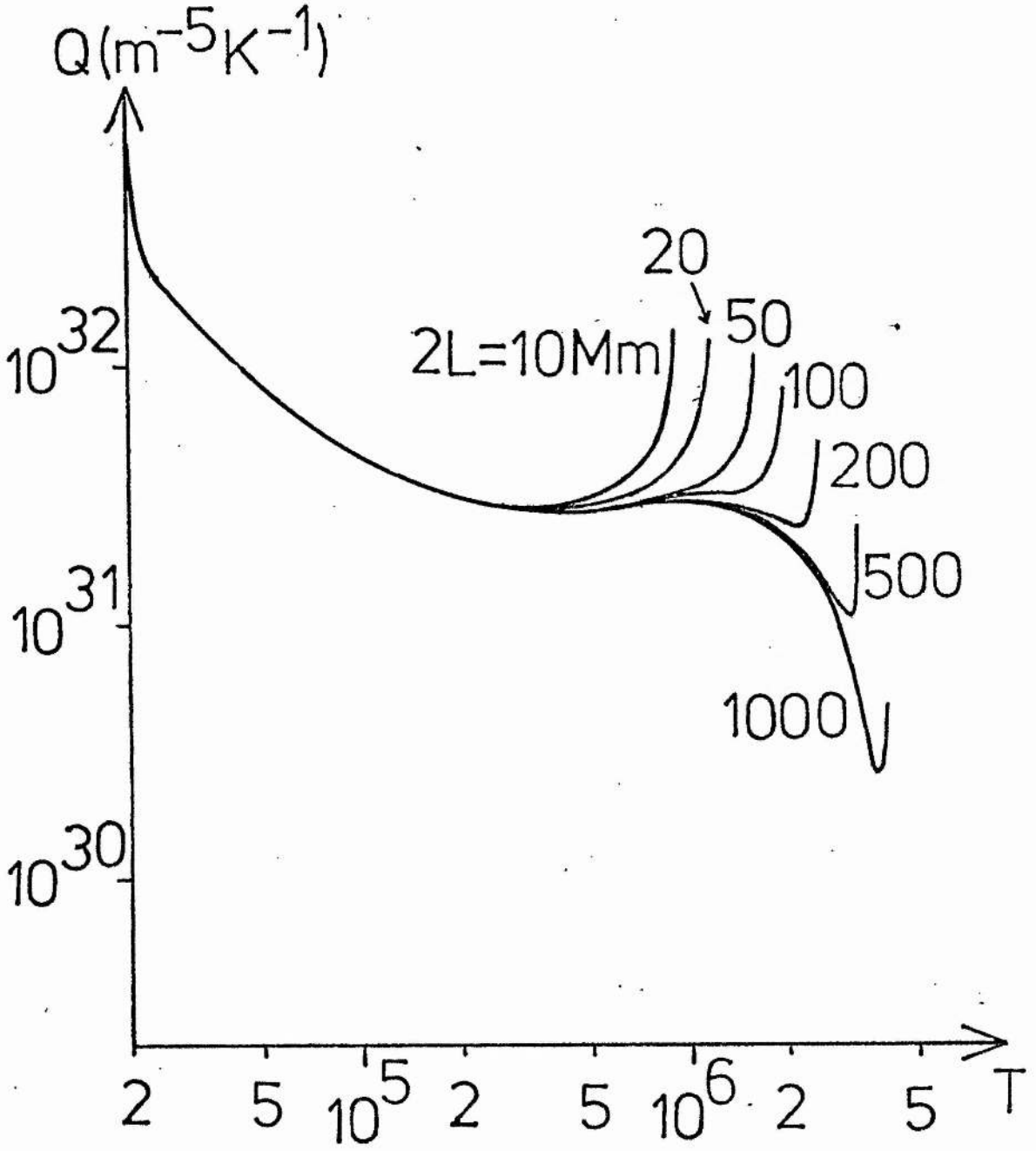

Figure 4.3b The differential emission measure (per unit cross-sectional area) for a thermally isolated loop of base density $N_o = 10^{17}$ m^{-3}.

excess of emission at its summit temperature because the pressure is reduced there, causing a decrease of typically an order of magnitude in the emission there.

Another observation from Figure 4.3 is that, except very near summit temperatures, where the vanishing temperature gradient causes a singularity in the emission, the curves for different lengths coalesce despite a variation in the spatial structure.

4.3 LOOPS WITH A FIXED MASS

Craig (1981) and Craig and McClymont (1981) have studied the dynamical formation of thermally isolated loops with fixed mass, assuming gravity negligible so that the pressure is uniform. They started with a uniform loop and, after giving it a transient impulsive heating, they observed its evolution towards a new static solution. They then gave it another impulse in heating and found that the loop settled down to a second, different solution (Figure 4.4). Craig and McClymont's dynamical solutions eveolved to include a small chromospheric region at the base, where the temperature is constant (of the order of 1000 km thick). To a certain extent this acted as a source/sink of mass for the corona.

They found that they could reproduce the first non-uniform state, using the static equations, to within 10%, but they were suspicious of the validity of further states.

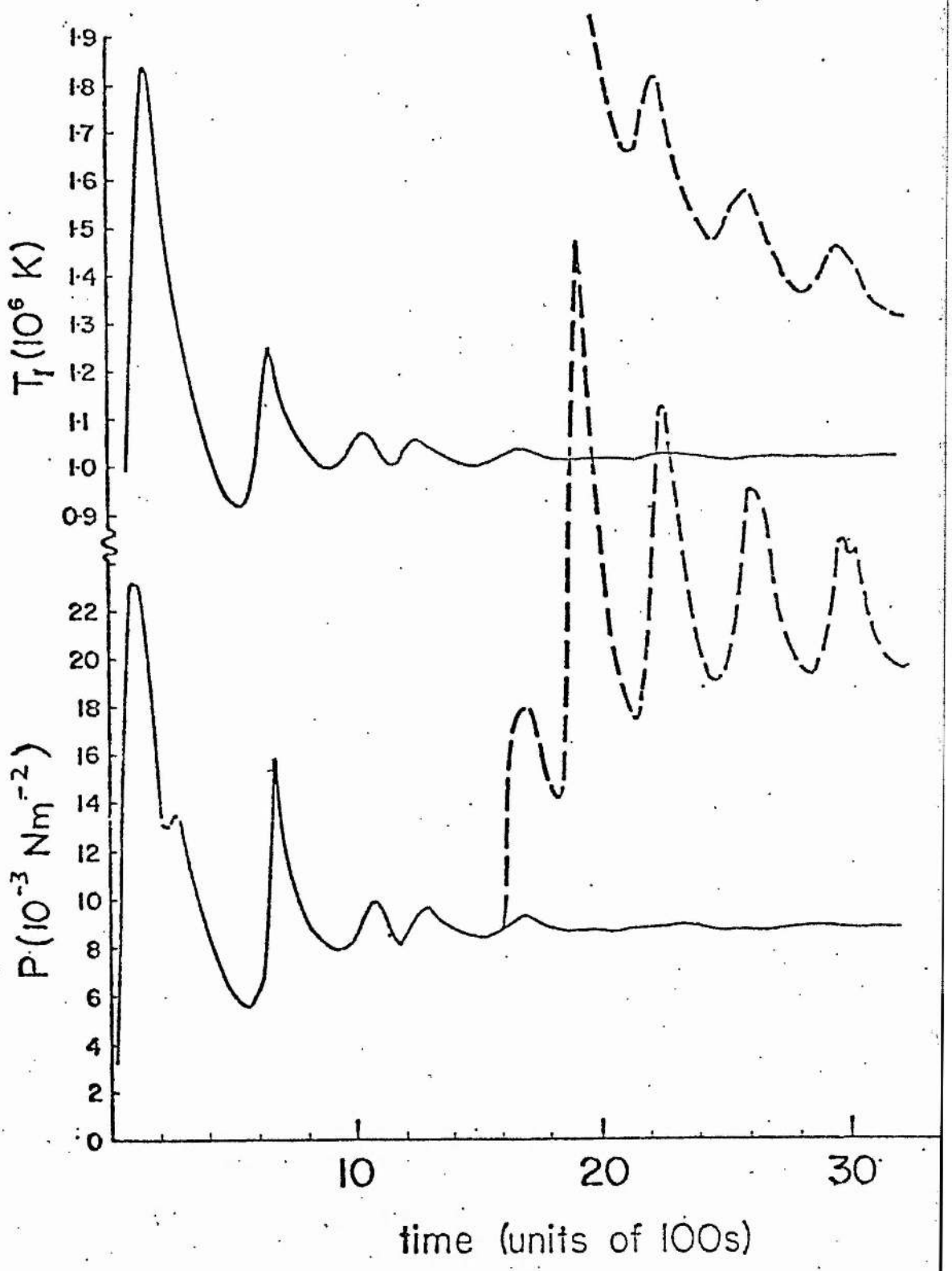

Figure 4.4 The summit temperature T_1 and pressure P_1 as a function of time. The dashed lines show the response to a second transient impulsive heating at $t = 1600$ s. (From Craig and McClymont, 1981.)

To investigate the problem further, accurate static solutions are sought with the same boundary conditions as Craig and McClymont. The problem modelled here is of basic interest but is not exactly comparable with theirs because no chromospheric interface is enforced.

At uniform pressure, so that $N = p/2kT$, Equation (4.1.1) becomes

$$\frac{d}{ds}\left[\chi_0 T^{5/2}\frac{dT}{ds}\right] = \frac{p^2 \alpha T^{\alpha-2}}{4k^2} - \frac{hp}{2kT} \qquad (4.3.1)$$

when the heating is proportional to density. The initial configuration is taken as a uniform plasma with

$$T_i = 6 \times 10^4 \text{ K},$$

$$N_i = 10^{-15} \text{ m}^{-3},$$

$$L = 33 \text{ Mm},$$

for which Craig and McClymont solved the usual hydrodynamic equations (Craig and McClymont, 1976). In terms of these parameters the mass M_i of the loop (per unit area) is given by

$$M_i = 2N_i L,$$

and the magnitude of the heating h is given from Equation (4.3.1) as

$$h = N_i \alpha_i T_i^{\alpha_i}.$$

The loop is isolated in the sense that no mass or heat flux are allowed through the base. In other words, it is

supposed that

$$\frac{dT}{ds} = v = 0, \quad \text{at} \quad s = 0 \quad \text{and} \quad s = L,$$

for all time, where v is the plasma speed. This means that, a first and subsequently a second steady state are sought for which both the mass, length and also the heating have remained the same. In other words, for a fixed L, h and M_i, is there a uniform state and two distinct non-uniform steady-state solutions?

Once L and h have been prescribed, there are three degrees of freedom to the problem: one arises because the constant p (or equivalently the base temperature T_o) is free, and the other two because the differential equation (4.3.1) is of second order. These three degrees of freedom are determined by the three conditions that M_i be prescribed, and that

$$\frac{dT}{ds} = 0 \quad \text{at} \quad s = 0 \quad \text{and} \quad s = L. \qquad (4.3.2)$$

However, the question arises, does this lead to a unique solution or indeed to any solution at all? The answer is not trivial, since the energy equation is non-linear. The procedure that has been adopted to solve the problem is to solve Equation (4.3.1) subject to (4.3.2) in order to find the loop mass M as a function of T_o for the specified L and h above, and the boundary conditions (4.3.2). The object is then to determine how many values of T_o (if any) make $M = M_i$. In Craig and McClymont (1981)'s program

they were suspicious that the steepest part of the transition zone had not been resolved numerically. The program used here, on the other hand, has a variable step-length which guarantees that the transition region is treated adequately.

The loop mass M is given by

$$M = \int_0^{2L} N ds ,$$

and T_o is varied through all realistic values ($10^4 \lesssim T_o \lesssim 5 \times 10^5$ K). A graph of M against T_o is shown in Figure 4.5. For a given loop length, the required base temperatures (denoted by large dots) are given by the intersection of the curve with $M = M_i$. The half-length of $L = 33$ Mm taken by Craig and McClymont clearly gives no static solution. The fact that a solution was obtained by Craig and McClymont must be due to the chromospheric layer that was included, which cushions the rigid requirement of a fixed mass, or possibly to lack of numerical resolution or optically thick modifications to the radiation near the base.

Other lengths have been considered as well; the curve for $L = 10$ Mm also gives no static solution, but interestingly it has a minimum around $T_o = 2 \times 10^4$ K, whereas the curves for $L = 33$ Mm and 100 Mm are monotonically increasing. (For loops with a half-length longer than 10 Mm to have non-uniform solutions, matter must be brought into the loop somehow during its evolution from the uniform to the non-uniform state.) In order to

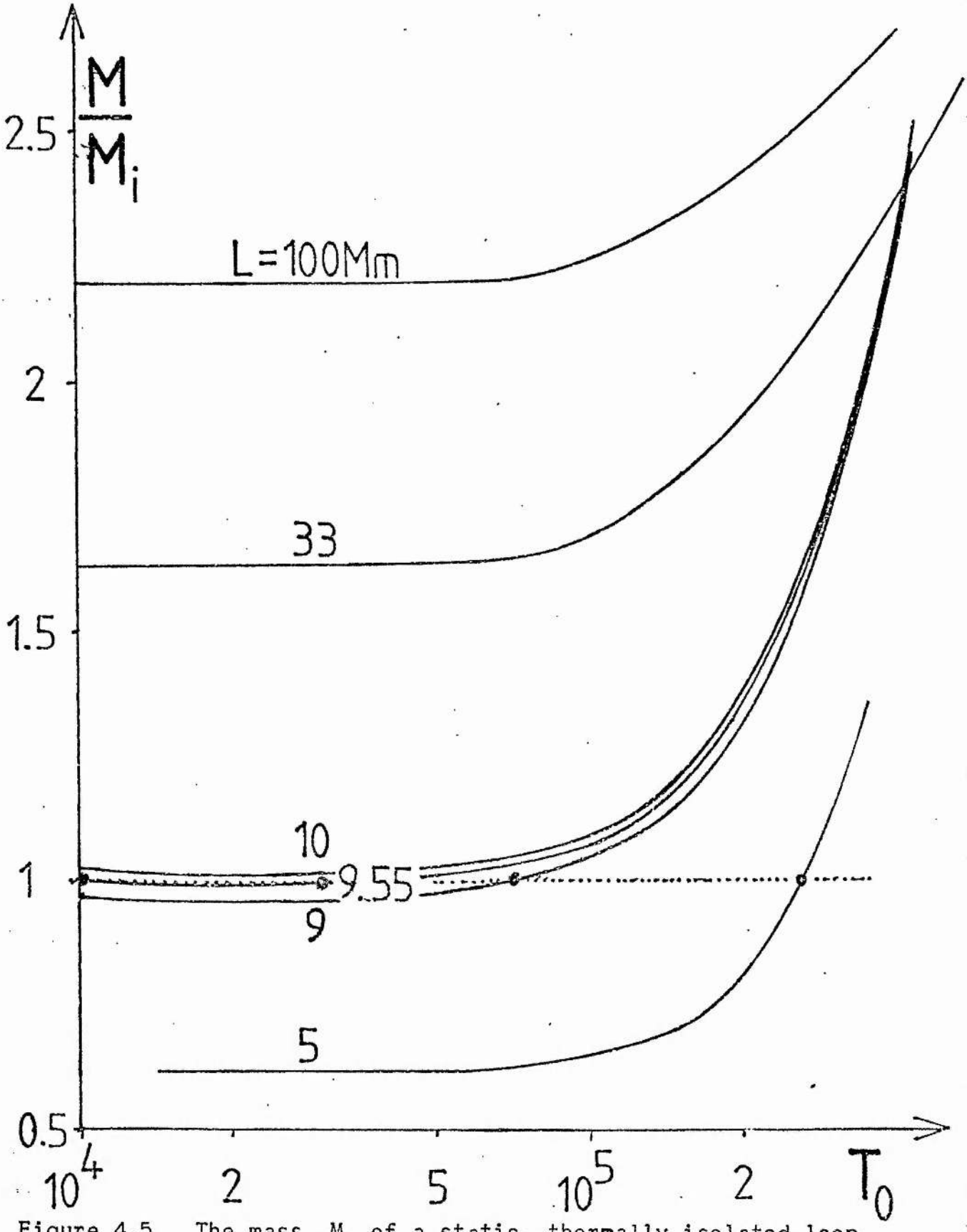

Figure 4.5 The mass M of a static, thermally isolated loop as a function of T_o, for a given heating and loop half-length. The static solutions with constant mass have $M = M_i$ and are denoted by large dots. The half-length L which Craig and McClymont took is 33 Mm.

obtain non-uniform solutions, L must be less than 9.61 Mm. For half-lengths less than 9.55 Mm, the curve of M against T_o crosses $M = M_i$ only once above 10^4 K and so gives only one possible non-uniform profile of the same mass. At a half-length L of about 4 Mm, the loop becomes isothermal and has a temperature of about 3×10^5 K, but smaller loops than this give no non-uniform solution. In the very small range $9.55 \leqslant L \leqslant 9.61$, there exist two non-uniform solutions, but this allowable range of L is rather insignificant. Furthermore, it should be noted that a curve crosses $M = M_i$ at most twice and so a natural speculation that there be an infinite number of static solutions is false.

It may be noted that, while T_o for these calculations was varied throughout an order of magnitude or more (i.e. 10^4 K to $> 10^5$ K), both p and T_1 were very insensitive to these changes, changing only by a few precent.

Figure 4.6 shows the dependence of T_o on L. No solution exists when L exceeds 9.61 Mm, while solutions with realistic base temperatures (lower than 10^5 K) have half-lengths aroung 9.5 Mm. It can be seen that there is only a very small range of L which give two solutions, namely from 9.55 Mm to 9.61 Mm, where the curve bends back.

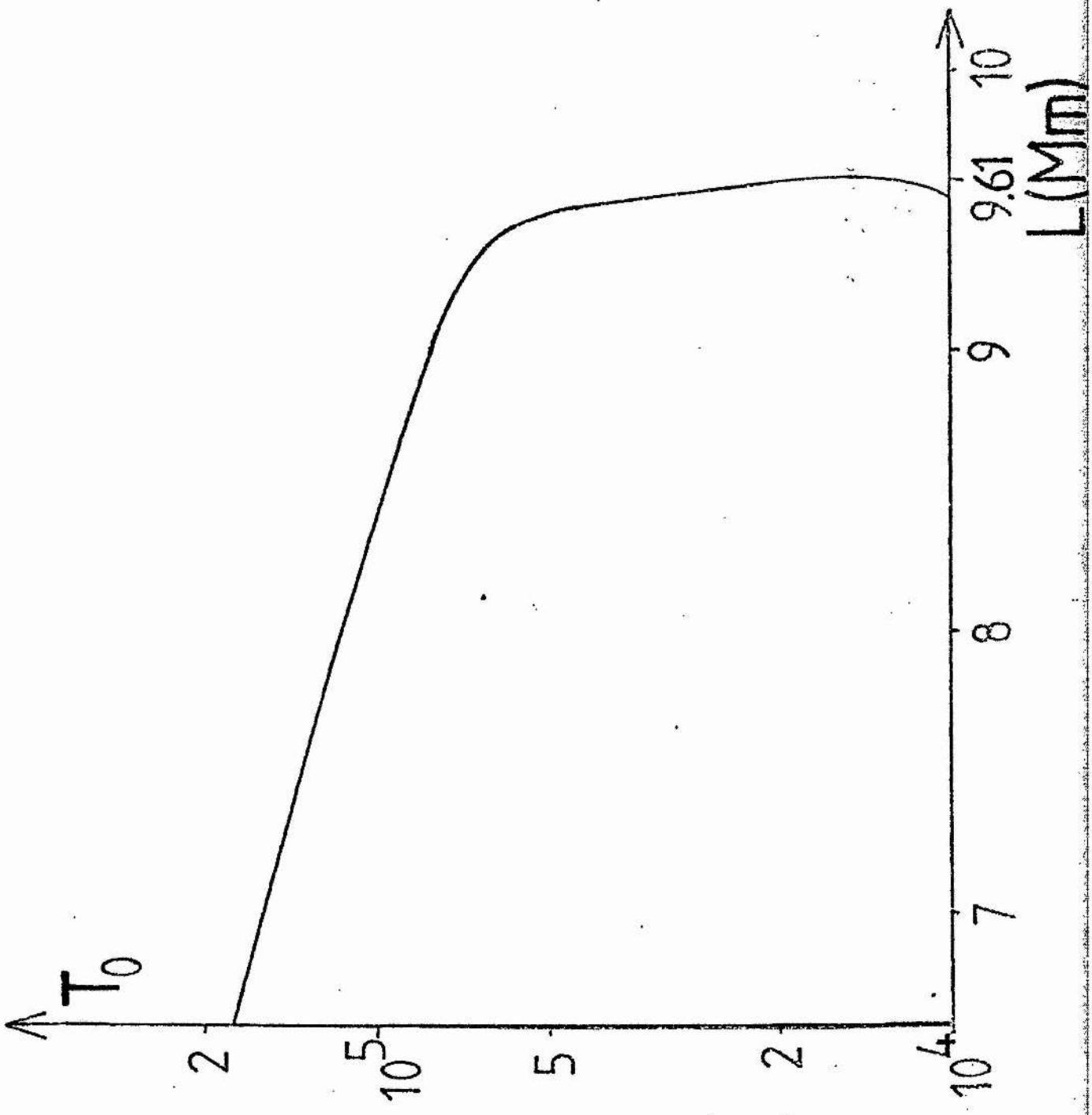

Figure 4.6 The base temperature T_o as a function of L. No solution exists for $L \gtrsim 9.61$ Mm.

4.4 SUMMARY

Thermally isolated static loops are the ones that have been considered most often, and the scaling law for the summit temperature $T_1 \sim (p_0 L)^{1/3}$ gives a reasonable fit (to within a factor two) to the X-ray observations (Rosner, et al., 1978). It is natural therefore to consider their properties in more detail. Two aspects have been treated here.

The analytically derived scaling law is found to give excellent agreement with the numerical solutions of the equations of energy balance and hydrostatic equilibrium, provided the loop is short and its density high. However, for sufficiently long (or rare) loops, the temperature may be lower by a factor or two or so, and increasing the length too much may actually cause the temperature to decline. The resulting values for the heating also agree well for short dense loops, while for longer or rarer ones the heating can be up to a factor 5 greater than the scaling law predicts.

The differential emission measure has been plotted for a range of models. A discrepancy of an order of magnitude in the coronal emission is seen if the assumption of constant pressure is used for long loops. The profiles of the emission curve below the summit temperature is seen to be insensitive to the length of the loop.

A static (non-uniform) thermally isolated loop of fixed mass can evolve from an isothermal state only if its half-length lies within critical values (here 4 Mm and 9.61 Mm). In general, one non-uniform solution can evolve for small

loops while large loops require a mass flow through the base. Two solutions are possible for only a tiny range of L near the upper limit. Mainly, just one set of initial conditions has been considered, namely $T_i = 6 \times 10^4$ K and $N_i = 10^{15}$ m^{-3}, but there is no reason to suspect that an alternative set will give different qualitative conclusions. Finally, it should be noticed that only static solutions have been considered, but the possibility of non-linear oscillatory solutions is intriguing and should certainly be investigated in future.

Equilibrium models have been studied in these last two chapters. Their stability will now be determined in Chapter 5.

5. THERMAL STABILITY OF CORONAL LOOPS

5.1 INTRODUCTION

With loop models so popular, it became important to consider their thermal stability. Several stability analyses have been developed (Priest, 1981). Rosner, et al. (1978) put forward the suggestion that the coronal part of a loop that is thermally isolated would be unstable if the temperature maximum was not located at the summit. Hood and Priest (1980) and Antiochos (1979) have each independently performed a linear stability analysis. Antiochos assumed uniform pressure, no area divergence, and both radiation and heating proportional to some power of temperature. For the equilibria, he imposed a zero base conductive flux, symmetry in temperature, and he specified the half-length and the ratio T_1/T_o. For his perturbation, he assumed zero pressure, velocity and heat flux at each footpoint. The first implies no pressure deviation throughout the loop, while the latter two imply that T and N vanish at the summit for his fundamental mode. His conclusion was that the stability of a loop depends on the base heat flux. If the base flux is much less than its maximum coronal or transition-region value, then the loop is unstable. In particular, thermally isolated loops with these boundary conditions are unstable. He suggested that static models

can be suitable for the corona and upper transition region, but that the lower transition region may have an oscillatory behaviour, and in such a case static models might possibly give a time-averaged representation of the structure.

Hood and Priest (1980) came to much the same conclusions by considering a variety of boundary conditions. In one case they imposed vanishing temperature and pressure perturbation at the base and vanishing temperature gradient at the summit (giving symmetry). Two alternative sets of boundary conditions on the perturbation were also considered. In one case zero temperature at the summit with zero temperature gradient at the footpoints were set, and in another, the temperature was imposed zero at one footpoint, while the temperature gradient vanished at the other. (This latter choice corresponds to a perturbation whose wavelength is 4 times the length of the loop.)

Hood and Priest (1980) found that equilibrium solutions on the upper branch of Figure 3.3 are stable while the middle branch comprise only unstable solutions to their first set of boundary conditions. All thermally isolated loops, with uniform pressure, are situated on the intermediate branch and so are immediately unstable. The intermediate branch has a base heat flux lower than that of the hot branch, and so there is agreement with Antiochos that loops are stable for suffiently high base flux.

Chiuderi, et al.(1981) have also analysed the problem, and found stable loops in abundance, even when thermally isolated. They suggested this is because they took a

detailed approximation to the radiative loss function (whereas Antiochos took only a single power low), but this is unlikely to be the cause of the difference. They took the same boundary conditions as Antiochos except for imposing a zero base temperature perturbation in place of his zero base flux perturbation. These boundary conditions may now not be a good choice, since their most unstable mode is exactly the same as Hood and Priest's first harmonic. This is often stable when Hood and Priest's fundamental mode is unstable. Thus the reason why Chiuderi, et al. found stable loops so freely was because they were not considering the most unstable mode. The question as to which approach is more relevant hinges on how restrictive the photosphere-corona interface is on the base boundary conditions in practice.

In each of these previous analyses, thermally isolated loops were found to be the most unstable type, and so they are reconsidered in the present chapter. In particular the basic state is assumed to be in hydrostatic equilibrium rather than having a uniform pressure. This extension is of fundamental importance because now the pressure perturbation does not identically vanish, and so the temperature and density perturbations need not merely be multiples of each other.

Several approaches suggest analytically that the presence of gravity is a stabilising factor (Section 5.4), and in Section 5.5 the numerical solutions show when this is so important that stability indeed occurs. First, however,

in Section 5.2, a local stability analysis is performed, which confirms the possibility of stable structures in a uniform plasma.

5.2 LOCAL STABILITY ANALYSIS

A local stability analysis can be performed as follows, under the simplifying assumption that the corona is uniform. The basic equations are

$$\frac{dN}{dt} + N\nabla.\mathbf{v} = 0, \tag{5.2.1}$$

$$m_p N \frac{d\mathbf{v}}{dt} + \nabla p = \mathbf{0}, \tag{5.2.2}$$

$$\frac{1}{\gamma-1}\frac{dp}{dt} - \frac{\gamma}{\gamma-1}\frac{p}{N}\frac{dN}{dt} + N m_p \mathcal{L} - \nabla.(\kappa\nabla T) = 0, \tag{5.2.3}$$

$$p = 2NkT, \tag{5.2.4}$$

where γ is the ratio of specific heats, for numerical calculations taken as 5/3, and $\mathcal{L}$ is the generalised heat loss function, (Field, 1956).

If $N = N_0$, $T = T_0$, $v = 0$ and $\mathcal{L}(N_0, T_0) = 0$ characterise the basic state, and their variables are written in the form

$$f(s,t) = f^{(0)}(s) + f^{(1)} \exp(\sigma t + i\mathbf{l}.\mathbf{s}), \tag{5.2.5}$$

the resulting linearised perturbed equations are

$$\sigma N^{(1)} + N^{(0)} i\boldsymbol{\ell}.\mathbf{v}^{(1)} = 0, \tag{5.2.6}$$

$$\sigma N^{(0)}\mathbf{v}^{(1)} + i\boldsymbol{\ell} p^{(1)} = \mathbf{0}, \tag{5.2.7}$$

$$\frac{\sigma}{\gamma-1} P^{(1)} - \frac{\sigma\gamma p^{(0)}}{(\gamma-1)N^{(0)}} N^{(1)} + N^{(0)} \frac{d\mathcal{L}}{dN} N^{(1)} + N^{(0)} \frac{d\mathcal{L}}{dT} T^{(1)} + \chi \ell^2 T^{(0)5/2} T^{(1)} = 0, \tag{5.2.8}$$

$$\frac{p^{(1)}}{p^{(0)}} = \frac{N^{(1)}}{N^{(0)}} + \frac{T^{(1)}}{T^{(0)}}. \tag{5.2.9}$$

For a non-trivial solution the determinant of coefficients of Equations (5.2.6 - 9) must vanish, which gives a cubic for the growth-rate σ, namely

$$\sigma^3 + \sigma^2 c\left(\ell_T + \frac{\ell^2}{\ell_K}\right) + \sigma c^2 \ell^2 + \frac{c^3 \ell^2}{\gamma}\left(\ell_T - \ell_N + \frac{\ell^2}{\ell_K}\right) = 0, \tag{5.2.10}$$

where c $(=(\gamma p^{(0)}/(N^{(0)} m_p))^{1/2})$ is the Laplacian sound speed, and ℓ_N, ℓ_T and ℓ_K are wave numbers defined as

$$\ell_N = \frac{m_p(\gamma-1)N^{(0)}}{2kcT^{(0)}} \frac{d\mathcal{L}}{dN}, \qquad \ell_T = \frac{m_p(\gamma-1)}{2kc} \frac{d\mathcal{L}}{dT},$$

$$\ell_K = \frac{2kcN^{(0)}}{(\gamma-1)\chi}.$$

A real positive root of Equation (5.2.10) corresponds to instability, while a complex root with a positive real part implies overstability. Thus for the system to be stable to <u>any</u> perturbation, all roots must have a negative real part. This is so (see Field, 1956), when

$$\ell_T + \frac{\ell^2}{\ell_K} - \ell_N > 0 \quad \text{and} \quad \ell_T + \frac{\ell^2}{\ell_K} + \frac{\ell_N}{\gamma-1} > 0. \tag{5.2.11}$$

Inequalities (5.2.11) are equivalent to

$$\frac{d\mathcal{L}}{dT} + \frac{\ell^2 \mathcal{K}}{m_p N^{(o)}} - \frac{N^{(o)}}{T^{(o)}} \frac{d\mathcal{L}}{dN} > 0 \qquad (5.2.12a)$$

and

$$\frac{d\mathcal{L}}{dT} + \frac{\ell^2 \mathcal{K}}{m_p N^{(o)}} + \frac{1}{\gamma - 1} \frac{N^{(o)}}{T^{(o)}} \frac{d\mathcal{L}}{dN} > 0 . \qquad (5.2.12b)$$

For a coronal loop to have a perturbation vanishing at its footpoints, a sinusoidal perturbation would need to have a wavelength no greater than 4L (twice the loop length), so that

$$\ell \geq \pi / 2L . \qquad (5.2.13)$$

Thus, if the other parameters (i.e. $N^{(o)}$ and $T^{(o)}$) are prescribed, the length 2L needs to be small enough that ℓ satisfies Equations (5.2.12) and (5.2.13). In other words

$$\frac{d\mathcal{L}}{dT} + \frac{\pi^2 \mathcal{K}}{(2L)^2 m_p N^{(o)}} - \frac{N^{(o)}}{T^{(o)}} \frac{d\mathcal{L}}{dN} > 0 \qquad (5.2.14a)$$

and

$$\frac{d\mathcal{L}}{dT} + \frac{\pi^2 \mathcal{K}}{(2L)^2 m_p N^{(o)}} + \frac{3}{2} \frac{N^{(o)}}{T^{(o)}} \frac{d\mathcal{L}}{dN} > 0 . \qquad (5.2.14b)$$

In the transition region or corona $\mathcal{K} = \mathcal{K}_o T^{5/2}$ and the function $\mathcal{L}$ is usually taken to be of the form

$$m_p N \mathcal{L} = N^2 \chi T^{\alpha} - H ,$$

with a balance between radiation and heating, H. In the corona α lies typically between 0 and -1; H, in this thesis, is either taken as uniform (denoted by E_H), or

proportional to density (hN). For either of these cases $d\mathcal{L}/dN$ is positive and so inequality (5.2.14b) is redundant.

If heating is proportional to density (hN) then stability is ensured provided

$$2L < \frac{\pi T^{7/4}}{N}\left(\frac{\kappa_0}{\chi T^{\alpha}(1-\alpha)}\right)^{1/2} . \qquad (5.2.15)$$

For typical coronal values of $T = 2 \times 10^6$ K, $N = 10^{15}$ m^{-3} and $\alpha = 0$, Equation (5.2.15) reduces to

$$2L < \frac{\pi T^{7/4}}{N}\left(\frac{\kappa_0}{\chi}\right)^{1/2} \simeq 99\ Mm. \qquad (5.2.16)$$

If heating is uniform in space the factor $(1-\alpha)^{-1/2}$ in (5.2.15) is replaced by $(2-\alpha)^{-1/2}$, and so for $\alpha = 0$ the loop length 2L needs to exceed 70 Mm for instability. For $\alpha = -1$ this value reduces to 57 Mm.

The equilibrium conditions assumed here, namely $\mathcal{L} = 0$ with uniform temperature and density may be reasonable approximations over small length-scales in the corona, and so the above result suggests that small loops may be stable. However, loop inhomogeneities would be important over large distances, and so it cannot be concluded that loops over 100 Mm long, say, are unstable. In the lower transition region α is again zero or negative (see Figure 1.1). If typical transition-region temperatures and densities are substituted into inequality (5.2.15) it gives $2L < 16$ km for stability! It would be fallacious to suggest, however, that this implies the transition region is unstable, since $\mathcal{L}$ is not zero there;

i.e. heating is very unlikely to balance radiation there, and in any case the validity of the equations begins to break down near the base of the transition region, due to incomplete ionisation and optically thick effects.

For a general heating term of the form $H = hN^{\beta}T^{\delta}$ (e.g. Roberts and Frankenthal, 1981), the inequality (5.2.15) is simply changed by replacing the factor $(1 - \alpha)^{-\frac{1}{2}}$ by $(2 + \delta - \alpha - \beta)^{-\frac{1}{2}}$ if $\beta < 2$, or by $(3/2\beta + \delta - \alpha - 3)^{-\frac{1}{2}}$ if $\beta > 2$. In the following sections of this chapter, the above analysis is generalised from a uniform medium to a non-uniform region.

5.3 THE EQUATIONS

The basic equations used in the previous chapters have been those of energy balance and hydrostatic equilibrium, namely

$$\frac{d}{ds}\left(\kappa_0 T^{5/2}\frac{dT}{ds}\right) = N^2\chi T^{\alpha} - E_H \,, \qquad (5.3.1a)$$

$$\frac{dp}{ds} = -m_p N g f(s) \,, \qquad (5.3.1b)$$

subject to the prescribed boundary conditions $T = T_0$ and $N = N_0$ at the base $s = 0$, $dT/ds = 0$ at the base and the summit ($s = L$) with the length held fixed. These determine the summit values T_1, N_1 and p_1, and the rate of heating E_H, here assumed constant in volume. $f(s)$ is the component of gravity parallel to the field lines at

any point s. The radiative loss function, which is uncertain to within a factor of 2 due to uncertainties in the solar abundance of elements, is approximated by the piecewise continuous curve χT^{α} of Table 1.

Equations (5.3.1) model the static basic state, and the more general time-dependent equations of energy, state momentum and continuity (Equations (1.2.21) to (1.2.24)) are used for a possible growth from the equilibrium. These are

$$-\frac{N^{\gamma}}{\gamma-1}\left[v\frac{\partial}{\partial s}\left(\frac{p}{N^{\gamma}}\right)+\frac{\partial}{\partial t}\left(\frac{p}{N^{\gamma}}\right)\right]+\frac{\partial}{\partial s}\left(\chi_0 T^{5/2}\frac{\partial T}{\partial s}\right)=N^2\chi T^{\alpha}-E_H, \quad (5.3.2)$$

$$p = 2NkT, \quad (5.3.3)$$

$$m_p N\left(\frac{\partial v}{\partial t}+v\frac{\partial v}{\partial s}\right) = -\frac{\partial p}{\partial s}-m_p N g f(s), \quad (5.3.4)$$

$$\frac{\partial N}{\partial t}+\frac{\partial}{\partial s}(Nv)=0. \quad (5.3.5)$$

It is convenient to introduce the following non-dimensional parameters,

$$s=\bar{s}L, \quad T=\bar{T}T_c, \quad N=\bar{N}N_c, \quad p=\bar{p}p_c, \quad v=\bar{v}c_s/\gamma^{\frac{1}{2}},$$

$$t=\tau_{rad}\bar{t}, \quad E_H=\bar{E}_H(N_c^2\chi_c T_c^{\alpha_c}), \quad \varepsilon=\frac{\tau_s}{\tau_{rad}},$$

$$\bar{\chi}=\frac{\chi T_c^{\alpha}}{\chi_c T_c^{\alpha_c}}, \quad \bar{L}=\frac{p_c L^2/(\chi_0 T_c^{7/2})}{p_c/(N_c^2\chi_c T_c^{\alpha_c})}, \quad \tau_s=\frac{L\gamma^{1/2}}{c_s},$$

$$\bar{g}=\frac{Lgm_p}{kT_c}, \quad \tau_{rad}=\frac{p_c}{N_c^2\chi_c T_c^{\alpha_c}}, \quad c_s^2=\frac{\gamma p_c}{m_p N_c},$$

where $T_c = 10^6$ K , $N_c = 5 \times 10^{14}$ m^{-3} are the standard coronal values used in the previous chapters. χ_c is the value of χ at a temperature of T_c. The coronal radiative time-scale is thus about one and a half hours. The resulting dimensionless equations become

$$-\frac{\bar{N}^{\gamma}}{\gamma-1}\left[\frac{\bar{v}}{\varepsilon}\frac{\partial}{\partial\bar{s}}\left(\frac{\bar{p}}{\bar{N}^{\gamma}}\right)+\frac{\partial}{\partial\bar{t}}\left(\frac{\bar{p}}{\bar{N}^{\gamma}}\right)\right]+\frac{1}{\bar{L}^2}\frac{\partial}{\partial\bar{s}}\left(\bar{T}^{5/2}\frac{\partial\bar{T}}{\partial\bar{s}}\right)$$
$$=\bar{N}^2\bar{\chi}\bar{T}^{\alpha}-\bar{E}_H\,, \qquad (5.3.6)$$

$$\bar{p}=\bar{N}\bar{T}\,, \qquad (5.3.7)$$

$$\varepsilon\bar{N}\frac{\partial\bar{v}}{\partial\bar{t}}+\bar{N}\bar{v}\frac{\partial\bar{v}}{\partial\bar{s}}=-\frac{\partial\bar{p}}{\partial\bar{s}}-\bar{N}\bar{g}\bar{f}(\bar{s})\,, \qquad (5.3.8)$$

$$\varepsilon\frac{\partial\bar{N}}{\partial\bar{t}}+\frac{\partial}{\partial\bar{s}}(\bar{N}\bar{v})=0\,. \qquad (5.3.9)$$

By perturbing all variables in the form

$$\bar{F}(\bar{s},\bar{t})=\bar{F}^{(0)}(\bar{s})+\bar{F}^{(1)}(\bar{s})e^{\sigma\bar{t}}\,,$$

with σ assumed real, the following linearised equations may be obtained, (where a dash $'$ denotes $d/d\bar{s}$).

$$-\frac{\bar{L}^2}{\gamma-1}\left[\frac{\bar{v}^{(1)}}{\varepsilon}\left(\bar{p}^{(0)\prime}-\gamma\bar{T}^{(0)}\bar{N}^{(0)\prime}\right)+\sigma\left(\bar{p}^{(1)}-\gamma\bar{T}^{(0)}\bar{N}^{(1)}\right)\right]+\left(\bar{T}^{(0)5/2}\bar{T}^{(1)}\right)''$$
$$=\bar{L}^2\bar{\chi}\left(\alpha\bar{N}^{(0)2}\bar{T}^{(0)\alpha-1}\bar{T}^{(1)}+2\bar{N}^{(0)}\bar{N}^{(1)}\bar{T}^{(0)\alpha}\right), \qquad (5.3.10)$$

$$\frac{\bar{p}^{(1)}}{\bar{p}^{(0)}}=\frac{\bar{T}^{(1)}}{\bar{T}^{(0)}}+\frac{\bar{N}^{(1)}}{\bar{N}^{(0)}}\,, \qquad (5.3.11)$$

$$\bar{N}^{(0)}\varepsilon\sigma\bar{v}^{(1)}=-\bar{p}^{(1)\prime}-\bar{g}\bar{N}^{(1)}\bar{f}(\bar{s})\,, \qquad (5.3.12)$$

$$\varepsilon\sigma\bar{N}^{(1)}+(\bar{N}^{(0)}\bar{v}^{(1)})'=0\,. \qquad (5.3.13)$$

If $\sigma \ll 1/\varepsilon$ is assumed, the term on the left-hand side of Equation (5.3.12) may be neglected so that the sound modes are filtered out.

Letting $V = (\bar{T}^{(0)5/2}\bar{T}^{(1)})'$ and using (5.3.11) to eliminate $\bar{p}$ in terms of $\bar{N}$ and $\bar{T}$, four first-order differential equations result, namely

$$V' = \bar{L}^2\left[\bar{\chi}\left(\alpha \bar{N}^{(0)2}\bar{T}^{(0)\alpha-1}\bar{T}^{(1)} + 2\bar{N}^{(0)}\bar{N}^{(1)}\bar{T}^{(0)\alpha}\right)\right. \tag{5.3.14}$$
$$\left. + \frac{\bar{v}^{(1)}}{\varepsilon}\left(\frac{\bar{N}^{(0)}\bar{T}^{(0)\prime}}{\gamma-1} - \bar{N}^{(0)\prime}\bar{T}^{(0)}\right) + \sigma\left(\frac{\bar{N}^{(0)}\bar{T}^{(1)}}{\gamma-1} - \bar{N}^{(1)}\bar{T}^{(0)}\right)\right],$$

$$\bar{T}^{(1)\prime} = \frac{V}{\bar{T}^{(0)5/2}} - \frac{5}{2}\frac{\bar{T}^{(0)\prime}\bar{T}^{(1)}}{\bar{T}^{(0)}}, \tag{5.3.15}$$

$$\bar{N}^{(1)\prime} = \frac{-1}{\bar{T}^{(0)}}\left[\bar{N}^{(0)\prime}\bar{T}^{(1)} + \bar{N}^{(0)}\bar{T}^{(1)\prime} + \bar{N}^{(1)}\bar{T}^{(0)\prime} + \bar{g}\bar{N}^{(1)}\bar{f}(\bar{s})\right], \tag{5.3.16}$$

$$\bar{v}^{(1)\prime} = \frac{-1}{\bar{N}^{(0)}}\left[\varepsilon\sigma\bar{N}^{(1)} + \bar{N}^{(0)\prime}\bar{v}^{(1)}\right]. \tag{5.3.17}$$

In the numerical calculations $\bar{f}(\bar{s})$ is again taken as $\cos(\pi\bar{s}/2)$, so that the loop has the shape of a semi-circle. These equations were then solved subject to a suitable choice of boundary conditions.

Many choices of boundary conditions are possible, but one would like to choose as unrestictive a set as possible. One reasonable assumption (for a purely thermal instability) is that any flows are along the field lines, i.e. the magnetic field is unperturbed. Also, in the uniform-pressure

analysis, the four variables T, T', N and v are related such that a given velocity drives a density variation (through the continuity equation), which in turn implies a temperature change (through the equation of state), while temperature implies the temperature gradient, and, to within constants of intergration, vice-versa. Thus, specifying the velocity everywhere would totally define the system. Once the boundary conditions on v have been imposed, those on N, T, and T' need to (and can) be chosen so as not to inhibit the system further. Chiuderi, et al. imposed $v^{(1)}(o) = O$, but also $N^{(1)}(o) = O$, which forces $v^{(1)'}(o) = O$ and so produces a more restrictive set of modes than Hood and Priest's (1980) first set. Antiochos took $v^{(1)} = O$ at each footpoint, so that a flow of matter is allowed across the summit from one leg to the other. Hood and Priest, by contrast, in their first set of boundary conditions, took $v = O$ at the summit, allowing a draining of material from the loop, or possibly a sucking up, sometimes referred to as evaporation. (Perhaps the observations of Levine and Withbroe (1977) refer to a process of this type.)

This set of boundary conditions of Hood and Priest are complementary to those taken by Antiochos, in the sense that, taken together they include any perturbation (on a scale no greater than twice the loop length).

Although things are not so neatly closed when pressure variations are allowed, because temperature and density perturbations need not be of the same form, it still remains

true that in essence, for a general perturbation, v and N should not be forced to vanish at the same point, and neither should T and T'.

It was decided here to generalise Hood and Priest's first set of boundary conditions, by imposing

$$T^{(1)} = N^{(1)} = 0 \quad \text{at} \quad s = 0 \quad \text{(base)}$$

and

$$T^{(1)\prime} = v^{(1)} = 0 \quad \text{at} \quad s = L \quad \text{(summit)},$$

Numerically, this involves a double interation, although a reasonable approximation for $v^{(1)}(o)$ can be gained from the integral of the continuity equation, given $v^{(1)}(1) = 0$. Thus, using $T^{(1)\prime}(o) = 1$ as a normalisation condition, $v^{(1)}(o)$ was easily iterated for each chosen σ, while σ was then iterated until $T^{(1)\prime}(1) = 0$.

5.4 APPROXIMATE SOLUTIONS

5.4.1 Analytic Approximations

Before turning to the numerical results, insight into the effect caused by gravity can be gained from some simplified analytic approaches. The radiative loss term (at constant pressure) is a decreasing function of T above 1.5×10^6 K, and so it is the term that tries to force instability. This is because an increase in temperature decreases the radiation, and so causes a further increase in temperature, and vice-versa. By its very nature, conduction tries to

smooth out irregularities, and thus, has a stabilising influence. The effect of heating depends on whether it is an increasing or decreasing function of temperature, but it is not as important as radiation in determining stability if (as is often assumed) its variation with temperature is less pronounced, so that the whole of the right-hand side of the energy equation (5.3.1) still decreases with increasing temperature. So, essentially, the question of stability is, in this simplistic view, governed by the relative importance of conduction and radiation. Now, the immediate effect of gravity is to decrease the coronal pressure (for a fixed p_o), which in turn primarily decreases the density (see Chapter 3). This decreases the magnitude of the radiation (by N^2), but not the conduction, thus making conduction relatively more important, with the loop as a whole becoming more stable.

It was seen in Section 3.7 that the "shape" of a loop, in terms of $f(s)$ is not critical to its structure. Suppose that, for a given solution, $f(s)$ had been set proportional to the temperature gradient,

$$f(s) = A \, dT/ds,$$

where A is a constant. This is seen to be zero at the summit, and so can be a physically realistic choice. (If the loop is thermally isolated, then the geometry is similar to that where the parameter r, in Section 3.7 is large.) The equation of hydrostatic equilibrium (5.3.1) then becomes

$$\frac{dp}{ds} = -N m_p \tilde{\mu} g \frac{dT}{ds} ,$$

whose intergral is

$$p = p_0 \left(\frac{T}{T_0} \right)^{-\delta g} ,$$

with δ given by

$$\delta = \frac{m_p \tilde{\mu} A}{2k}$$

and A is determined by

$$-\delta g = \log \left(\frac{T_0 p_1}{p_0 T_1} \right)$$

when the solution has been obtained. Thus Equation (5.3.1a) becomes

$$\frac{d}{ds} \left(\kappa_0 T^{5/2} \frac{dT}{ds} \right) = \frac{p_0^2}{4k^2} \left(\frac{T}{T_0} \right)^{-2\delta g} \chi T^{\alpha - 2} - E_H . \qquad (5.4.1)$$

This is essentially the same as the equation for constant pressure, except that the radiation term is multiplied by a different constant, and has a different value in the exponent of T, ($\alpha - 2 - 2\delta g$ rather than $\alpha - 2$). It can thus be solved in the same way as the constant pressure case, treated by Hood and Priest (1979). The effect of gravity on the stability of a loop can easily be seen, since the radiation term is now a factor $(T / T_0)^{2\delta g}$ smaller than in the uniform-pressure case. It is therefore less important, and so gravity has a stabilising influence.

5.4.2 Order of Magnitude

The order-of-magnitude method used to predict the static equilibria in Chapter 3 proved to be remarkably accurate, and it showed all the features of the full

numerical solutions. Thus it is reasonable to consider this type of approach to gain an analytical first approximation to the computed stability.

For this, Equations (5.3.6) to (5.3.9) may be used to eliminate N so that

$$-\frac{\bar{p}^{\gamma}}{\bar{T}^{\gamma(\gamma-1)}}\left[\frac{\bar{v}}{\varepsilon}\frac{\partial}{\partial\bar{s}}\left(\frac{\bar{T}^{\gamma}}{\bar{p}^{\gamma-1}}\right)+\frac{\partial}{\partial\bar{t}}\left(\frac{\bar{T}^{\gamma}}{\bar{p}^{\gamma-1}}\right)\right]+\frac{1}{\bar{L}^{2}}\frac{\partial}{\partial\bar{s}}\left(\bar{T}^{5/2}\frac{\partial\bar{T}}{\partial\bar{s}}\right)$$

$$=\bar{p}^{2}\bar{\chi}\,\bar{T}^{\alpha-2}-\bar{E}_{H}\,, \qquad (5.4.2)$$

$$\varepsilon\frac{\bar{\rho}}{\bar{T}}\frac{\partial\bar{v}}{\partial\bar{t}}+\frac{\bar{\rho}}{\bar{T}}\bar{v}\frac{\partial\bar{v}}{\partial\bar{s}}=-\frac{\partial\bar{p}}{\partial\bar{s}}-\frac{\bar{\rho}}{\bar{T}}\bar{g}_{\parallel}\,, \qquad (5.4.3)$$

$$\varepsilon\frac{\partial}{\partial\bar{t}}\left(\frac{\bar{\rho}}{\bar{T}}\right)+\frac{\partial}{\partial\bar{s}}\left(\frac{\bar{\rho}\bar{v}}{\bar{T}}\right)=0, \qquad (5.4.4)$$

where $\bar{g}_{\parallel}(\equiv\bar{g}\bar{f}(\bar{s}))$ is the component of $\bar{g}$ parallel to the field. All derivatives of products, e.g. $\partial/\partial\bar{s}(\bar{N}\bar{v})$ are evaluated as

$$\bar{N}\frac{\partial\bar{v}}{\partial\bar{s}}+\bar{v}\frac{\partial\bar{N}}{\partial\bar{s}}$$

before the spacial differencing is used, so that Equations (5.4.2) and (5.4.4) are re-written as

$$\frac{\partial\bar{p}}{\partial\bar{t}}+\frac{\bar{v}}{\varepsilon}\frac{\partial\bar{p}}{\partial\bar{s}}-\left[\frac{\gamma}{\gamma-1}\frac{\bar{p}}{\bar{T}}\left(\frac{\partial\bar{T}}{\partial\bar{t}}+\frac{\bar{v}}{\varepsilon}\frac{\partial\bar{T}}{\partial\bar{s}}\right)\right]+\frac{1}{\bar{L}^{2}}\frac{\partial}{\partial\bar{s}}\left(\bar{T}^{5/2}\frac{\partial\bar{T}}{\partial\bar{s}}\right)$$

$$=\bar{p}^{2}\bar{\chi}\,\bar{T}^{\alpha-2}-\bar{E}_{H} \qquad (5.4.5)$$

and

$$\varepsilon\frac{\partial\bar{p}}{\partial\bar{t}}-\varepsilon\frac{\bar{p}}{\bar{T}}\frac{\partial\bar{T}}{\partial\bar{t}}+\bar{p}\frac{\partial\bar{v}}{\partial\bar{s}}+\bar{v}\frac{\partial\bar{p}}{\partial\bar{s}}-\frac{\bar{p}\bar{v}}{\bar{T}}\frac{\partial\bar{T}}{\partial\bar{s}}=0\,. \qquad (5.4.6)$$

For spacial derivatives, a rough mesh of three points is used at $\bar{s} = 0, 1, 2$. To first order, about the summit, derivatives may be approximated by

$$\frac{\partial F}{\partial \bar{s}} = F_2 - F_0 \,, \qquad \frac{\partial^2 F}{\partial \bar{s}^2} = F_2 - 2F_1 + F_0 \,. \tag{5.4.7}$$

Boundary conditions (see Section 5.3) imply

$$\frac{\partial \bar{T}}{\partial \bar{s}} = \frac{\partial \bar{\rho}}{\partial \bar{s}} = 0 \quad \text{and} \quad \frac{\partial \bar{v}}{\partial \bar{s}} = -\bar{v}_0$$

at the summit, while

$$\frac{\partial^2 \bar{T}}{\partial \bar{s}^2} = 2(1 - \bar{T}_1) \,,$$

$$\frac{\partial^2 \bar{\rho}}{\partial \bar{s}^2} = 2(\bar{\rho}_0 - \bar{\rho}_1) \,,$$

$$\frac{\partial^2 \bar{v}}{\partial \bar{s}^2} = 0 \,.$$

After using these, Equations (5.4.5) and (5.4.6) reduce to

$$-\bar{\rho}_1' + \frac{\gamma}{\gamma - 1}\frac{\bar{\rho}_1}{\bar{T}_1}\bar{T}_1' = \frac{2\bar{T}_1^{5/2}}{\bar{L}^2}(1 - \bar{T}_1) - \bar{\rho}_1^2 \bar{\chi} \bar{T}_1^{\alpha - 2} - \bar{E}_H$$

and

$$\varepsilon \bar{\rho}_1' - \varepsilon \frac{\bar{\rho}_1}{\bar{T}_1}\bar{T}_1' - \bar{\rho}_1 \bar{v}_0 = 0 \,.$$

Because the momentum equation (5.4.3) is trivally satisfied, it may be differentiated with respect to $\bar{s}$ before being differenced. The non-zero terms give

$$\frac{\varepsilon \bar{\rho}}{\bar{T}}\frac{\partial}{\partial \bar{t}}\left(\frac{\partial \bar{v}}{\partial \bar{s}}\right) + \frac{\bar{\rho}}{\bar{T}}\left(\frac{\partial \bar{v}}{\partial \bar{s}}\right)^2 = -\frac{\partial^2 \bar{\rho}}{\partial \bar{s}^2} - \frac{\bar{\rho}\bar{g}}{\bar{T}}\frac{\partial \bar{f}}{\partial \bar{s}} \,,$$

from which

$$-\varepsilon\frac{\bar{p}_1}{\bar{T}_1}\bar{v}_0' + \frac{\bar{p}_1}{\bar{T}_1}\bar{v}_0^2 = -2(1-\bar{p}_1) - \frac{\bar{p}_1}{\bar{T}_1}\bar{g}_+ \qquad (5.4.8)$$

at the summit, ($\bar{g}_+ \equiv \bar{g}(d\bar{f}/d\bar{s})\big|_{\bar{s}=1}$ and, without loss of generality, $\bar{p}(0)$ is taken as one).

Equations (5.4.5), (5.4.6) and (5.4.8) reduce to the order-of-magnitude equations of Chapter 3 if the time derivatives are set equal to zero. They can also be used as follows to determine the effect of gravity on the stability. Perturb these equations, so that

$$\bar{v}_0 = \bar{v}^{(1)} e^{\sigma\bar{t}},$$

$$\bar{T}_1 = \bar{T}^{(0)} + \bar{T}^{(1)} e^{\sigma\bar{t}},$$

$$\bar{p}_1 = \bar{p}^{(0)} + \bar{p}^{(1)} e^{\sigma\bar{t}},$$

and, for the basic state of the momentum and energy equations, use the notation

$$\mathcal{M}(\bar{T}^{(0)}, \bar{p}^{(0)}) = 2(1-\bar{p}^{(0)}) + \bar{p}^{(0)}g_+/\bar{T}^{(0)} = 0,$$

$$\mathcal{E}(\bar{T}^{(0)}, \bar{p}^{(0)}) = 2\bar{T}^{(0)5/2}(1-\bar{T}^{(0)}) - \bar{L}^2(\bar{p}^{(0)2}\bar{\chi}\bar{T}^{(0)\alpha-2} - \bar{E}_H) = 0.$$

Then the linearised equations are

$$\varepsilon\sigma\bar{p}^{(1)} - \varepsilon\sigma\frac{\bar{p}^{(0)}}{\bar{T}^{(0)}}\bar{T}^{(1)} - \bar{p}^{(0)}\bar{v}^{(0)} = 0, \qquad (5.4.9)$$

$$\varepsilon\sigma\frac{\bar{p}^{(0)}}{\bar{T}^{(0)}}\bar{v}^{(1)} = -\frac{\partial\mathcal{M}}{\partial\bar{T}^{(0)}}\bar{T}^{(1)} - \frac{\partial\mathcal{M}}{\partial\bar{p}^{(0)}}\bar{p}^{(1)}, \qquad (5.4.10)$$

$$\bar{L}^2\left(-\sigma\bar{p}^{(1)} + \sigma\frac{\gamma}{\gamma-1}\frac{\bar{p}^{(0)}}{\bar{T}^{(0)}}\bar{T}^{(1)}\right) = \frac{\partial\mathcal{E}}{\partial\bar{T}^{(0)}}\bar{T}^{(1)} + \frac{\partial\mathcal{E}}{\partial\bar{p}^{(0)}}\bar{p}^{(1)}. \qquad (5.4.11)$$

If the inertial term on the left-hand side of Equation (5.4.10) is insignificant, it gives

$$\bar{p}^{(1)} = -\left(\frac{\partial \mathcal{M}}{\partial \bar{T}^{(0)}} \Big/ \frac{\partial \mathcal{M}}{\partial \bar{p}^{(0)}} \right) \bar{T}^{(1)} = c\bar{T}^{(1)}, \qquad (5.4.12)$$

where c is a positive constant, since

$$\frac{\partial \mathcal{M}}{\partial \bar{T}^{(0)}} = -\frac{\bar{p}^{(0)}}{\bar{T}^{(0)2}} \bar{g}_+ > 0 \quad \text{as} \quad \bar{g}_+ < 0,$$

and

$$\frac{\partial \mathcal{M}}{\partial \bar{p}^{(0)}} = -2 + \frac{\bar{g}_+}{\bar{T}^{(0)}} < 0.$$

Thus, after using Equation (5.4.12), the energy equation (5.4.11) can be written as

$$\sigma \bar{L}^2 \left(-c + \frac{\gamma}{\gamma - 1} \frac{\bar{p}^{(0)}}{\bar{T}^{(0)}} \right) = \frac{\partial \mathcal{E}}{\partial \bar{T}^{(0)}} + c \frac{\partial \mathcal{E}}{\partial \bar{p}^{(0)}}. \qquad (5.4.13)$$

The sign of the bracket on the left-hand side of Equation (5.4.13) is always positive, since $\bar{p}^{(0)}/\bar{T}^{(0)}$ is an upper bound on c. Hence the sign of σ depends on the sign of the right-hand side. The presence of gravity introduces the term

$$c \frac{\partial \mathcal{E}}{\partial \bar{p}^{(0)}}.$$

But

$$\frac{\partial \mathcal{E}}{\partial \bar{p}^{(0)}} = -2\bar{L}^{-2} \bar{p}^{(0)} \bar{\chi} \bar{T}^{(0)\alpha - 2}$$

is negative, and so finally it can be seen that gravity is stabilising.

5.5 NUMERICAL RESULTS

Figure 5.1 shows the growth-rate σ for a wide range of L and N_o. Three features are clearly present, each revealed within a different region of the $L - N_o$ plane. Most important is the region (b), where $2L \lesssim 300$ Mm and $N_o(2L) \gtrsim 1.25 \times 10^{23}$ m^{-2}. Here the growth-rate is dependent almost entirely on the length. It decreases from positive values (an unstable loop) for small lengths, through zero (at about $2L = 60$ Mm) to negative values (a stable loop), as the effect of gravity becomes more and more significant. This is in contrast to the case when gravity is neglected (valid for very low-lying loops) where a loop is unstable regardless of the length. Thus it is seen that in practice most loops which would appear to be unstable if the calculations were carried out neglecting gravity, are actually stable. This important result is a general conclusion, and is not offset by apparently different trends in regions (a) and (c) of Figure 5.1.

For $2L \gtrsim 300$ Mm (region (c)), as L continues to increase, σ appears to increase after having reached a minimum value. However, σ remains negative even at extremely large values of L. This decrease in the magnitude of σ is simply due to the large size of the loop, and it occurs whether the effect of gravity is included or not; i.e. if gravity is neglected, σ is positive and decreases as L increases. It can be seen in the simpler analytic case when gravity is absent that σ occurs in the

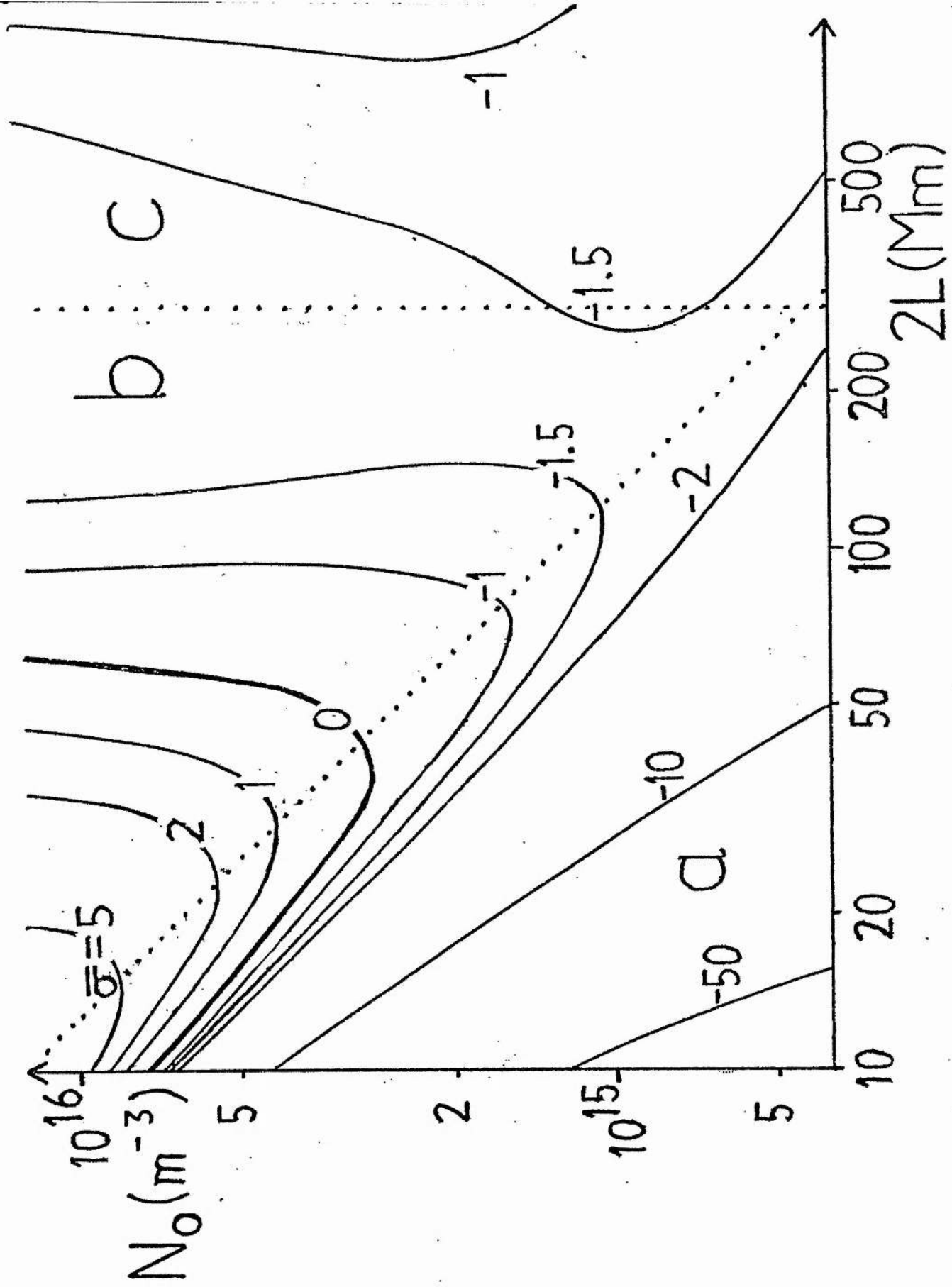

Figure 5.1 Contours of the growth-rate $\bar{\sigma}$ (= σ/5600) plotted in the N_o-L plane, where N_o is the base density and 2L the loop length. The dotted lines bound the regions (a), (b), (c) discussed in the text.

equations only in the combination $\bar{p}\bar{L}^2\sigma$ (Hood and Priest's, 1980, Equation 2.18).

Finally, if the product $N_o(2L)$ is too small, only the isothermal solution exists if the pressure is constant, and this, again for small enough $N_o(2L)$, is stable (Hood and Priest, 1980). With the inclusion of the gravity term the solution is almost isothermal when the size is much smaller than a scale height. Thus, the full solution must become stable if $N_o(2L)$ is small enough, as in region (a) of Figure 5.1. Although this appears to be so for a wide range of loops in Figure 5.1, it is merely because the base temperature has been chosen as high as 10^6 K. In practice, the feature can be neglected, because, for a base temperature of 2×10^4 K the region where only the isothermal solution exists is not of interest since $N_o(2L)$ is far too small, and in any case, loops with summit temperatures about 2×10^4 K are not of interest here.

Figure 5.2 shows the modification by gravity of the uniform-pressure case for a base density of 5×10^{15} m^{-3}. The top curve shows the uniform-pressure solutions, in which the continuous line refers to the non-isothermal solutions, while the dotted line denotes the isothermal ones (which exists for all lengths). The bottom curve includes the effect of gravity. This Figure shows the three features of Figure 5.1 that have been mentioned above. Firstly, for $2L \lesssim 30$ Mm only the isothermal solution exists at uniform pressure. It is stable ($\sigma<0$) for $2L \lesssim 13$ Mm, and the full solution approaches it for small L.

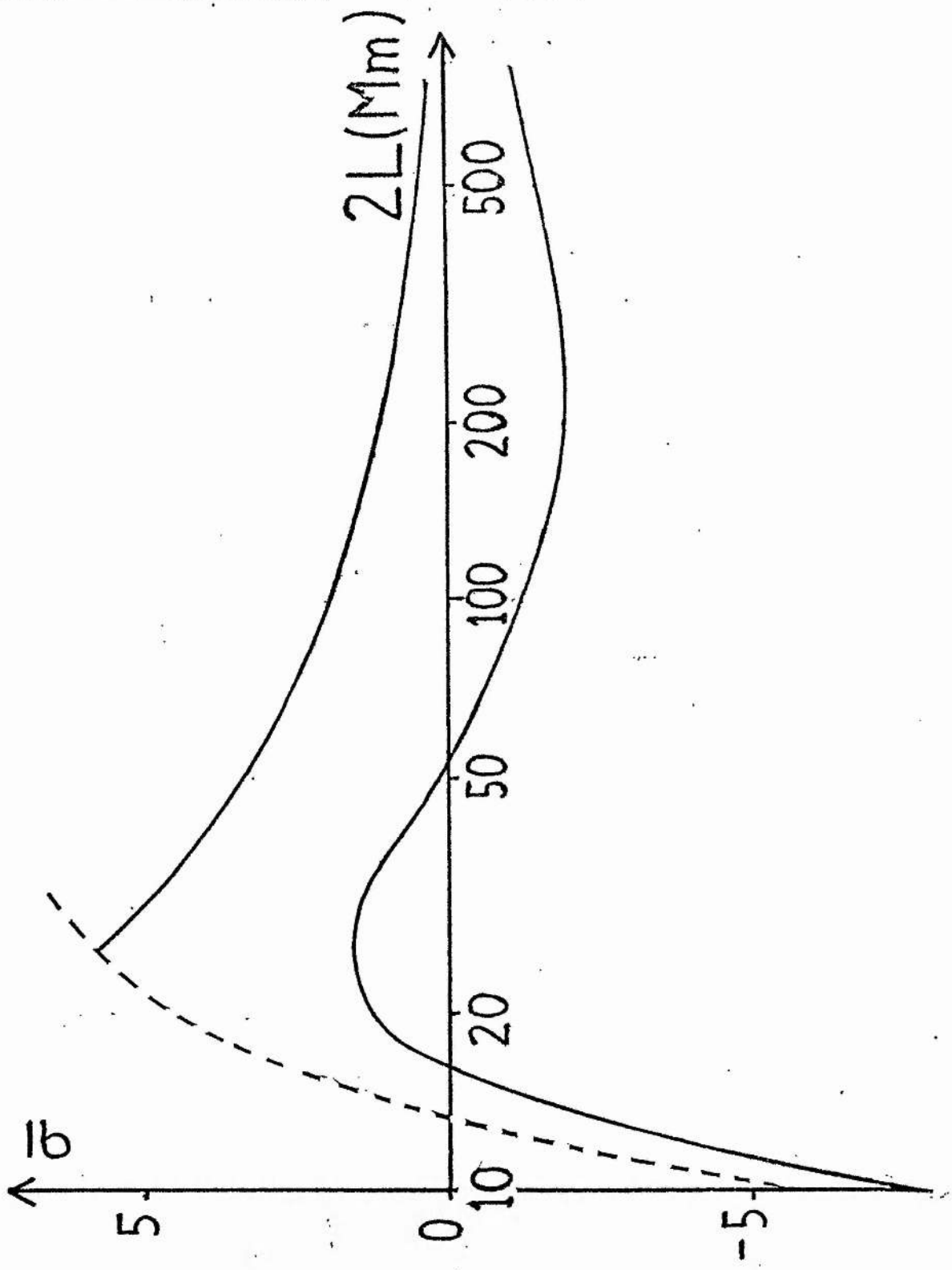

Figure 5.2 The growth-rate $\bar{\sigma}$ as a function of the length 2L for a fixed base density of $5 \times 10^{15}\ m^{-3}$. The bottom curve is for solutions in hydrostatic equilibrium ($g \neq 0$). The top curve is for uniform pressure ($g = 0$), with the dotted part referring to the isothermal solution (which exists for all lengths) and the solid part denoting the non-isothermal solution.

For $30 \lesssim 2L \lesssim 300$ Mm both curves decrease with increasing length, but σ for the full solution crosses zero at about 55 Mm, and thus the loop is stable for lengths in excess of this. For $2L \gtrsim 300$ Mm it can be seen that for both solutions σ decreases in magnitude with no change in sign.

For these results, the base temperature was kept fixed at 10^6 K. It would have been better to have chosen 2×10^4 K, but in this case numerical inaccuracies were unacceptably high. Thus, while the results for the two cases would be qualitatively similar, caution should be used before the absolute magnitudes of the results are applied to loops in practice.

Chiuderi, et al. (1981) criticised Antiochos (1979) for taking a constant temperature exponent in the radiative loss function (fixing α in Equation (5.3.10)). They suggested this as the reason Antiochos found all his thermally isolated loops to be unstable. It is clear, however, from Hood and Priest (1980), that Antiochos' loops at constant pressure are unstable for any reasonably chosen radiative loss function. The effect of different forms of radiation functions can be most easily seen by fixing α (over all temperatures) at different values. $-\frac{1}{2}$ is commonly used as a global approximation, although it is grossly inaccurate for the transition region. For the radiation fit used in this thesis $\alpha = 0$ at 10^6 K, and so if the summit temperature is not too much above this ($\lesssim 2 \times 10^6$ K) then $\alpha \equiv 0$. In Figure 5.3 the growth-rate as a function of α is shown for an average loop with

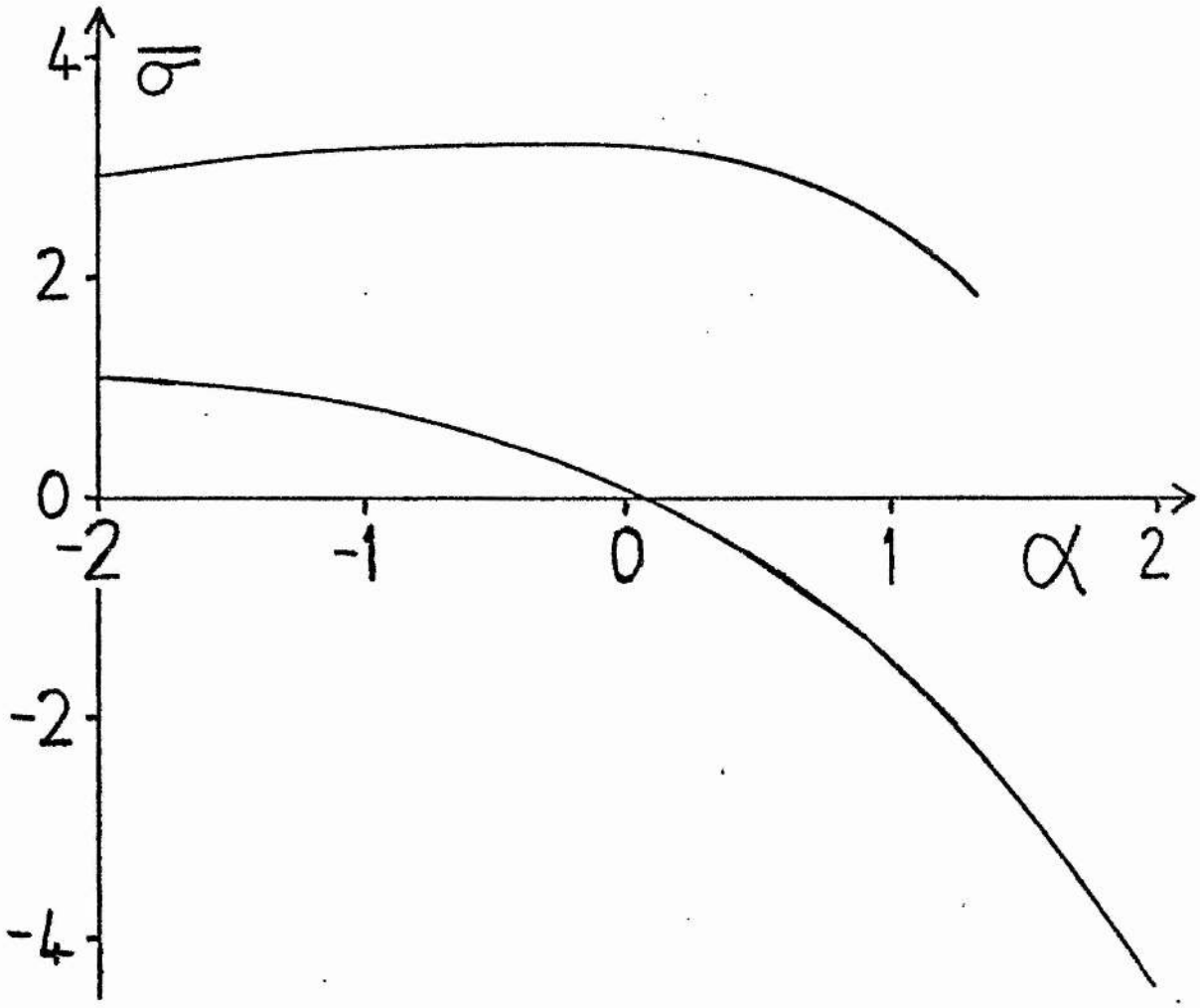

Figure 5.3 The effect on the growth-rate $\bar{\sigma}$ of the form of the radiative loss function through the power of temperature α. The lower curve gives the full solution, while the top curve is that for a low-lying loop with constant pressure.

$2L = 50$ Mm and $N_o = 5 \times 10^{15}$ m^{-3}, which is neither excessively stable nor unstable in the full solution. The top curve is for constant pressure and the one below is the full solution including gravitational effects. The growth-rate for the constant-pressure solution is not particularly dependent upon α ; if $\alpha = 2$ the loop is isothermal, and for this choice is stable, so the curve would have to become negative before $\alpha = 2$. The full solution can be seen to give a growth-rate significantly below the constant-pressure one, irrespective of α. Thus altering α would change slightly the contours of Figure 5.1, but not the qualitative appearance; no (sensible) choice would eliminate the wide range for stability.

5.6 DISCUSSION

For the uniform-pressure approximation, it was found that the domain of solutions trace curves similar to Figure 3.3. For these curves, all solutions on the top branch are stable, while all those on the intermediate branch are unstable, with marginal stability coinciding with the critical point. In that event, all thermally isolated loops were shown to be unstable because they always lie below the critical point. The method of proof used by Hood and Priest does not generalise straightforwardly when gravity is included, but the result is still seen to be the same, as follows. At marginal stability ($\sigma = 0$), the

(linearised) perturbation equations reduced to

$$\frac{d^2}{d\bar{s}^2}\left(\bar{T}^{(0)\,5/2}\bar{T}^{(1)}\right) = \bar{L}^2\bar{\chi}\left(\alpha\bar{N}^{(0)2}\bar{T}^{(0)\alpha-1}\bar{T}^{(1)} + 2\bar{N}^{(0)}\bar{N}^{(1)}\bar{T}^{(0)\alpha}\right), \tag{5.6.1a}$$

$$\frac{d\bar{P}^{(1)}}{d\bar{s}} = -\bar{g}\bar{N}^{(1)}\bar{f}(\bar{s}) \tag{5.6.1b}$$

and

$$\frac{\bar{P}^{(1)}}{\bar{P}^{(0)}} = \frac{\bar{T}^{(1)}}{\bar{T}^{(0)}} + \frac{\bar{N}^{(1)}}{\bar{N}^{(0)}}, \tag{5.6.1c}$$

which are again subject to the boundary conditions

$$\begin{aligned} &\bar{P}^{(1)} = 0, \quad \bar{T}^{(1)} = 0 \quad \text{at} \quad \bar{s} = 0, \\ &\bar{T}^{(1)\prime} = 0 \qquad\qquad\quad \text{at} \quad \bar{s} = 1. \end{aligned} \tag{5.6.2}$$

The equilibria are governed by

$$\frac{d}{d\bar{s}}\left(\bar{T}^{5/2}\frac{d\bar{T}}{d\bar{s}}\right) = \bar{L}^2\left(\bar{\chi}\bar{T}^{\alpha}\bar{N}^2 - \bar{E}_H\right) \tag{5.6.3a}$$

and

$$\frac{d\bar{P}}{d\bar{s}} = -\bar{g}\bar{N}\bar{f}(\bar{s}). \tag{5.6.3b}$$

Now consider a set of equilibrium variables T,N and p which satisfy Equation (5.6.3), and let (for a fixed $\bar{E}_H$), $\bar{T} + \bar{T}^+$, $\bar{N} + \bar{N}^+$, $\bar{p} + \bar{p}^+$ be a neighbouring solution. Then, since $\bar{E}_H$ is fixed, these two solutions will represent neighbouring points on an "S" curve, such as Figure 3.3. Since $\bar{T}^+$, $\bar{N}^+$ and $\bar{p}^+$ are small, to first order, Equations (5.6.3) give

$$\begin{aligned} &\frac{d\bar{P}^+}{d\bar{s}} = -\bar{g}\bar{N}^+\bar{f}(\bar{s}), \\ &\frac{d^2}{d\bar{s}^2}\left(\bar{T}^{5/2}\bar{T}^+\right) = \bar{L}^2\bar{\chi}\left(\alpha\bar{T}^{\alpha-1}\bar{T}^+\bar{N}^2 + 2\bar{T}^{\alpha}\bar{N}\bar{N}^+\right). \end{aligned} \tag{5.6.4}$$

Now suppose boundary conditions (5.6.2) apply. If that is so, the two systems of Equations (5.6.1) and (5.6.4) are identical with similar boundary conditions, and hence have the same solution. Thus the critical point is also the point of marginal stability, and from continuity it can be concluded that solutions on the upper branch are stable while those below the critical point are unstable.

This was checked numerically for solutions each side of the $\sigma = 0$ contour of Figure 5.1. From Figure 5.1, the solution for $2L = 20$ Mm, $N_o = 5 \times 10^{15}$ m^{-3} is unstable. In this case $\bar{E}_H = 20$. This solution is just the particular point on the "S" curve (Figure 3.3) for $2L = 20$ Mm, $\bar{E}_H = 20$ which has $T'(o) = 0$. The critical point occurs when $N_o = N_{crit} = 6 \times 10^{15}$ m^{-3}, and the base conductive flux at N_{crit} is positive, implying that the thermally-isolated solution must be below N_{crit}, on the intermediate branch as required. On the other hand, Figure 5.1 shows that the loop whose length and base density are $2L = 20$ Mm, $N_o = 3 \times 10^{15}$ m^{-3} is stable. Here $\bar{E}_H = 5$, and the critical solution in this case occurs at $N_o = 3.1 \times 10^{15}$ m^{-3}. At this critical point the base conductive flux is negative, forcing the thermally-isolated solution onto the top branch where it is stable. In this case there are stable oscillatory solutions when N_o lies in the range $3 - 3.1 \times 10^{15}$ m^{-3}.

A further deduction was verified numerically as follows. Given a thermally isolated loop which is <u>unstable</u>, then it is assumed to lie below T_{crit}. If this is so,

then there must be a different, hotter solution with the same length, base density and heating, lying on the upper branch. Similarly a stable solution ought to have a cooler (unstable) one with the same parameters. Two cases were investigated. First a loop whose length, density and heating are $2L = 20$ Mm, $N_o = 5 \times 10^{15}$ m^{-3}, $\bar{E}_H = 79$ is thermally isolated and unstable. If these parameters are fixed and the base flux varied, then T_1 changes and a vertical line is traversed in Figure 3.3. The intersections of this vertical line with the solution curve give the allowable loop solutions for which $T_1' = 0$. In this case vanishing base flux gives a solution, for which $T_1 = 1.08 \times 10^6$ K. There are no solutions for positive base flux, since T_1' is always positive. If the base flux is decreased from zero, T_1 increases and T_1' initially becomes negative but then is positive, yielding another solution as T_1' passes through zero. This occurs at $T_1' = 0.03$ K m^{-1} and the summit temperature is now $T_1 = 1.20 \times 10^6$ K, a hotter solution. Likewise, an example of a stable thermally isolated loop is $2L = 50$ Mm, $N_o = 2 \times 10^{15}$ m^{-3}, $\bar{E}_H = 9.9$. The summit temperature for this loop is $T_1 = 1.12 \times 10^6$ K. Here increasing T_o' from zero gives no solution, but decreasing it decreases T_1, and another solution is found (where $T_1' = 0$), cooler than the original, with a temperature $T_1 = 0.98 \times 10^6$ K, and with $T_o' = -0.01$ K m^{-1}.

These examples agree with the analytic conclusion that coronal loops are stable if and only if they rest on

the upper branch of the solution curves. Analytically, the choice of base temperature is arbitrary and so this is one way of extending the results of this chapter down to lower base temperatures, such as 2×10^4 K.

5.7 SUMMARY

The stability of coronal loops has been studied. A local analysis showed that at uniform temperature and density, for coronal radiation and typical heating functions, stability is ensured provided the length scale considered is smaller than a critical amount. This result is necessary for the existence of stable coronal loops, but the instability of large volumes of uniform material is not relevant to the more complex loops with non-uniform structure. Thus, a full linear analysis was performed, allowing for variations in both temperature and pressure in the basic state. Temperature variations alone had been treated before, but it has been shown here that in many cases these gave misleading results.

For thermally isolated loops, stability depends almost entirely on the length of a particular loop, independent of its density. For small lengths the loops are unstable (although an extremely small loop would tend towards being isothermal and isobaric, and so be stable). Longer loops are stable, due primarily to the decrease in pressure with height caused by gravity.

The result here that long loops should be stable and short ones unstable agrees with the observed properties of loops (Withbroe, 1980) that bright points and short loops tend to show fluctuations over a short time-scale, whereas the intensity of larger loops is steady over much longer times.

The result that loops on the top branch of the solution curves for constant length and heating are stable, while those on the lower branch are unstable, generalises from the uniform-pressure analysis, and so one way of determining the stability of thermally isolated loops is merely to see on which part of these curves they lie.

6. CONCLUSIONS

The preceeding four chapters have sought to model the solar transition region and corona using the equations of continuity, momentum, state and energy balance detailed in Chapter 1. The results of altering the amount of heating, flow and field-line divergence on a given solution have been assessed as follows:

(i) Heating

Locally, an excess of heating over radiation reduces the conductive flux with height, so making the temperature profile more concave. If boundary conditions on temperature and conductive flux are imposed at just one point, as in most models for an open atmosphere in Chapter 2, then an increase in heating leads to a decrease in temperature, and a lowering of the height for the temperature maximum. If heating is absent then the temperature rises indefinitely and no temperature maximum will exist.

For a two-point boundary value problem the opposite effect must occur, provided at least one of the boundary conditions prescribes the temperature rather than the conductive flux. This is because a greater amount of heating causes the temperature, at a fixed distance away from the temperature maximum, to be reduced relative to that maximum; in other words, there is a relatively hotter maximum compared to that fixed point. The main set of coronal loop models of Chapter 3, and the alternative sets

of boundary conditions (Section 2.4.1) for an open atmosphere were modelled in this way.

Although at first sight the result that a greater heating warrants a higher temperature might seem aesthetically correct, it is easy to see that this need not be so. For example, if an atmosphere, such as a thermally isolated loop, has a prescribed energy input, which it must radiate away, then to radiate away more energy would require the coronal temperature to be decreased.

(ii) Field-line Divergence

Field-line divergence decreases the magnitude of the conductive flux. Where the temperature is increasing with height this has qualitatively a similar effect to raising the heating; it was found that, for the base boundary conditions of an open region, a greater divergence reduces the temperature (Section 2.4.4), while for the two-point boundary conditions of coronal loops it increases it (Section 3.7.1). However, a temperature maximum cannot be caused by field-line divergence alone, and an isothermal atmosphere will be unaffected. It is expected that the network effect (in the transition region) would have a more profound effect than a coronal divergence because the conductive flux is so much greater in the transition region.

(iii) Subsonic Flows

A steady flow transports matter, and thus energy, along a field line. If the temperature increases with height, at each point a downflow deposits more heat there than is being carried away. This corresponds to an energy

input (locally), and so it has a similar effect to heating (Section 2.4.5). An upflow shows the opposite effect. As with field-line divergence, the effect is proportional to the conductive flux, and so it makes no impression on an isothermal atmosphere. Again, a temperature maximum cannot be created by a flow in the absence of heating.

In order to avoid confusion, it is important to relate given results to the prescribed boundary conditions; for example, a greater area divergence increases the temperature if the parameters L, N_o and $\bar{h}$ are kept fixed, while if the loop is thermally isolated (with the magnitude of the heating dependent upon L and N_o) then the opposite effect, a lower temperature, manifests itself.

In Section 2.4.5 it was shown that a maximum steady upflow exists, beyond which point a catastrophe occurs; for a steady, hot upflow to exist, conduction must be important. This gives a maximum on the temperature of a coronal model.

The different transition-region models do not transmit their differences through to the corona to any great extent (Section 2.4), except that there will be a certain amount of flexibility in the conductive flux at the base of the corona (defined here as where $T = 10^6$ K, Section 3.2). Indeed, part of this flexibility may be inherited from the bottom of the transition region (Section 4.1).

A range of equilibrium solutions for coronal loops showed the general trends that in most ranges not only is the summit temperature greater for a greater heating, but

also for a greater length or base density.

A striking result from Chapter 3 (Section 3.5) is the existence of non-equilibrium. There are ranges of the parameters L, N_o and $\bar{h}$, usually N_o large, $\bar{h}$ small or L within some interval, for which no hot equilibrium solution exists. If this region is entered, for example by a loop gradually being stretched by the magnetic-field configuration at constant N_o and $\bar{h}$, the loop will cool down and develop flows, possibly giving birth to a so-called cool loop.

If flare loops exhibit a quasi-static nature for part of their evolution this may be adequately explained in terms of a greater heat input (Section 3.6).

The differential emission measure was plotted for loops with various area divergences (Section 3.7.1) and geometries (Section 3.7.2). One way of deciding which range of coronal models can be matched onto the transition region might be by observing the slope of the differential emission measure at 10^6 K, as it is found to vary over a large range for different rates of field-line divergence (Figure 3.16c). However, the effect of the inclusion of many different loops is difficult to analyse.

If the base flux is assumed to be insignificant, then a loop is said to be thermally isolated. In the simplest view, this makes the length, base density and heating interdependent. Several scaling laws have been derived for such loops, both in this thesis and by other authors, and their agreement with the full numerical

solution has been checked (Sections 3.3.1 and 4.2). The greatest discrepancy is in long loops, due to the assumption of constant pressure by many authors.

Loops with a fixed mass were studied (Section 4.3). A static thermally isolated loop was shown to be capable of evolving from a uniform state to a non-uniform state provided its length is not too large. Usually this non-uniform state is unique.

The full set of solutions presented in Chapter 3 lie on "S" shaped curves (Figure 3.3). Solutions on the top branch are always thermally stable while those on the intermediate branch are always unstable (Section 5.7). Loops whose pressure is constant were always found to lie on the intermediate branch, and so they are immediately unstable. However, when hydrostatic equilibrium is assumed instead, some thermally isolated loops migrate to the upper branch. Contrary to the then accepted belief, it seems that these loops may yet be stable. Chapter 5 followed up this investigation. A <u>local</u> stability analysis (Section 5.2) showed that a uniform plasma will be stable provided the length scale is not too great. This result is necessary but not sufficient for the stability of coronal loops. A <u>global</u> analysis (Section 5.5) showed that the stability of a thermally isolated loop is almost entirely dependent upon its length. For small lengths the pressure is close to being constant, and the loop is unstable. For larger loops the summit pressure is significantly reduced and stability is ensured.

The importance of assuming hydrostatic equilibrium rather than constant pressure has been revealed in several situations throughout the last few chapters. Equilibrium loop models often give qualitative similar results, with the feature of non-equilibrium being present in both instances. However, the presence of gravity aids an → equilibrium in the sense that all choices of parameters which give a static constant-pressure loop also give one in hydrostatic equilibrium, whereas sometimes a solution exists only for the case of hydrostatic equilibrium (Section 3.3.2).

The temperature structure is not greatly affected by gravity; for loops near a critical point the temperature is raised, while those that are far from a critical point, including thermally isolated loops, become more isothermal and slightly cooler. Long interconnecting loops, however, can now exist at realistic temperatures independent of their length (Figure 3.12a). The density, on the other hand, declines to a much greater extent when gravity is included, with the result that the differential emission measure can have a considerably different slope (Figure 3.17c, here $r = 0.0$ corresponds to constant pressure), and it can be typically an order of magnitude lower at coronal temperatures (Section 4.2, Figure 4.3a).

Another effect is that the gravitational scale height is smaller at a lower temperature, and so at large heights the pressure has diminished so much that a lower temperature gives a lower density, and the density profiles are seen

to cross over (Section 2.4.5 and 3.5). Also, as mentioned above, the effect of gravity on the stability of loops may well be small, but it can result in the difference between stability and instability.

REFERENCES

Antiochos, S.K.:1979, Astrophys. J. 232 L125

Athay, R.G. and White, O.R.:1978, Astrophys. J. 226 1135

Basri, G.S., Linsky, J.L., Bartoe, J.-D.F., Breuckner, G. and Van Hoosier, M.E.:1979, Astrophys. J. 230 924

Bohlin, J.D. and Sheeley, N.R.(Jr.):1978, Solar Phys. 56 125

Brabban, D.H.:1974, Solar Phys. 38 449

Bruner, E.C.(Jr.):1978, Astrophys. J. 226 1140

Cargill, P.J. and Priest, E.R.:1980, Solar Phys. 65 251

Cargill, P.J. and Priest, E.R.:1981, submitted.

Chapman, G.A. and Broussard, R.M.:1977, Astrophys. J. 216 940

Chase, R.C., Krieger, A.S., Švestka, Z. and Vaiana, G.S.: 1976, Space Reseach 16 917

Cheng, C., Smith, J.B.(Jr.) and Tandberg-Hanssen, E.: 1980, Solar Phys. 67 259

Chiuderi, C. and Riani, I.:1974, Solar Phys. 34 113

Chiuderi, C., Einaudi, G. and Torricelli-Ciamponi, G.: 1981, Astron. Astrophys.

Cox, D.P. and Tucker, W.H.:1969, Astrophys. J. 157 1157

Craig, I.J.D.:1981, in Solar Flare MHD. (ed. E.R. Priest) Gordon and Breach, London.

Craig, I.J.D. and McClymont, A.N.:1976, Solar Phys. 50 133

Craig, I.J.D. and McClymont, A.N.:1981, Solar Phys. 70 97

Craig, I.J.D., McClymont, A.N. and Underwood, J.H.:1978, Astron. Astrophys. 70 1

Davis, J.M., Gerassimenko, M., Krieger, A.S. and Vaiana, G.S. :1975, Solar Phys. 45 393

Doschek, G.A., Feldman, U., and Bohlin, J.D.:1976, Astrophys. J. 205 L177

Dupree, A.K., Huber, M.C.E., Noyes, R.W., Parkinson, W.H., Reeves, E.M. and Withbroe, G.L.:1973, Astrophys. J. 182 321

Emslie, A.G. and Machado, M.E.:1979, Centre for Astrophys. Preprint No. 1034 Unpublished.

Field, G.B.:1965, Astrophys. J. 142 531

Foukal, P.V.:1975, Solar Phys. 43 327

Foukal, P.V.:1976, Astrophys. J. 210 575

Foukal, P.V.:1978, Astrophys. J. 223 1046

Gabriel, A.H.:1976, I.A.U. Colloquium 36 375

Gabriel, A.H.:1976, Phil. Tran. R. Soc. Lond. A. 281 339

Gabriel, A.H. and Jordan, C.:1975, Mon. Not. R. Astr. Soc. 173 397

Gibson, E.G.:1973, The Quiet Sun, NASA, Washington.

Gingerich, O., Noyes, R.W. and Kalkofen, W.:1971, Solar Phys. 18 347

Giovanelli, R.G.:1975, Solar Phys. 44 315

Harvey, J.W. and Sheeley, N.R.(Jr.):1979, Space Science Reviews 23 139

Hollweg, J.V.:1978, Solar Phys. 56 305

Hollweg, J.V. and Lillequest, C.G.:1978, J. of Geophys. Res. 83 2030

Hood, A.W. and Priest, E.R.:1979, Astron. Astrophys. 77 233

Hood, A.W. and Priest, E.R.:1980, Astron. Astrophys. 87 126

Howard, R. and Švestka, Z.:1977, Solar Phys. 54 65

Jordan, C.:1975, I.A.U. Symposium 68 109

Jordan, C.:1976, Phil. Trans. R. Soc. Lond. A. 281 391

Jordan, C.:1980, Astron. Astrophys. 86 355

Krieger, A.S.:1980, private communication to Priest, E.R.

Krieger, A.S., de Feiter, L.D. and Vaiana, G.S.:1976, Solar Phys. 47 117

Krieger, A.S., Vaiana, G.S. and Van Speybroeck, L.P.:1971, I.A.U. Symposium 43 397

Landini, M. and Monsignori-Fossi, B.C.:1975, Astron. Astrophys. 42 213

Landini, M. and Monsignori-Fossi, B.C.:1981, preprint

Leer, E. and Holzer, T.E.:1979, Solar Phys. 63 143

Levine, R.H.:1977, Astrophys. J. 218 291

Levine, R.H.:1978, J. of Geophysical Research 83 4193

Levine, R.H. and Pye, J.P.: 1980, Solar Phys. 66 39

Levine, R.H. and Withbroe, J.L.:1977, Solar Phys. 51 83

Levine, R.H., Altschuler, M.D., Harvey, J.W. and Jackson, B.V.: 1977, Astrophys. J. 215 636

Mariska, J.T., Feldman, U. and Doschek, G.A.:1981, Astrophys. J.

Maxson, C.W. and Vaiana, G.S.:1977, Astrophys. J. 215 919

McIntosh, P.S., Krieger, A.S., Nolte, J.T. and Vaiana, G.S.: 1976, Solar Phys. 49 57

McWhirter, R.W.P. and Wilson, R.:1975, Phil. Trans. R. Soc. Lond. A. 281 331

McWhirter, R.W.P., Thonemann, P.C. and Wilson, R.:1975, Astron. Astrophys. 40 63 and erratum (1977) 61 859

Neupert, W.M., Nakagawa, Y, and Rust, D.M.:1975, Solar Phys. 43 359

Nolte, J.T., Davis, J.M., Gerassimenko, M., Krieger, A.S. and Solodyna, C.V.:1978, Solar Phys. 60 143

November, L.J., Toomre, J. Gebbie, K.B., Simon, G.W., Bruner, E.C., Chipman, E.G., Lites, B.W., Orrall, F.G., Rottman, G.J., Shine, R.A., Athay, R.G. and White, O.R.: 1976, Bull. Am. Astron. Soc. 8 No.2, 148th Meeting of the Amer. Astron. Soc., Haverford.

Noyes, R.W., Withbroe, G.L. and Kirshner, R.P.:1970, Solar Phys. 11 388

Parkinson, J.H.:1973, Solar Phys. 28 487

Petrasso, R.D., Nolte, J.T., Gerassimenko, M, Krieger, A.S., Krogstad, R. and Soguin, F.H.:1979, Solar Phys. 62 133

Pick, M., Trottet, G. and MacQueen, R.M.:1979, Solar Phys. 63 369

Pneuman, G.W. and Kopp, R.A.:1977, Astron. Astrophys. 55 305

Pneuman, G.W. and Kopp, R.A.:1978, Solar Phys. 57 49

Pottash, S.R.:1965, Bull. Astron. Inst. Neth. 18 7

Priest, E.R.:1978, Solar Phys. 58 57

Priest, E.R.:1981, Chapter 9 of Skylab Workshop on Active Regions (ed. F. Orrall) Colo. Ass. Univ. Press

Pye, J.P., Evans, K.D., Hutcheon, R.J., Gerassimenko, M., Davis, J.M., Krieger, A.S. and Vesecky, J.F.:1978, Astron. Astrophys. 65 123

Raymond, J.C.:1978, private communication to Rosner, et al., 1978

Reeves, E.M., Foukal, P.V., Huber, M.C.E., Noyes, R.W., Schmahl, E.J., Timothy, J.G., Vernazza, J.E. and Withbroe, G.L.:1974, Astrophys. J. 188 L27

Roberts, B. and Frankenthal, S.:1980, Solar Phys. 68 103

Rosner, R., Tucker, W.H. and Vaiana, G.S.:1978, Astrophys. J. 220 643

Serio, S., Peres, G., Vaiana, G.S., Golub, L., and Rosner, R.:1981, Astrophys. J. 243 288

Sheeley, N.R.(Jr.):1980, Solar Phys. 65 229

Sheeley, N.R.(Jr.) and Harvey, J.W.:1978, Solar Phys. 59 159

Sheeley, N.R.(Jr.) and Harvey, J.W.:1980, Solar Phys. 70 237

Sheeley, N.R.(Jr.), Bohlin, J.D., Brueckner, G.E., Purcell, J.D., Scherrer, V. and Tousey, R.:1975, Solar Phys. 40 103

Spitzer, L.(Jr.):1962, Physics of Fully Ionised Gases, Interscience, New York

Stuhlinger, E.:1976, Space Research 16 849

Švestka, Z. and Howard, R.:1979, Solar Phys. 63 297

Švestka, Z., Krieger, A.S., Chase, R.C. and Howard, R.:1977, Solar Phys. 52 69

Švestka, Z., Solodyna, C.V., Howard, R. and Levine, R.H.: 1977, Solar Phys. 55 359

Timothy, A.F., Krieger, A.S. and Vaiana, G.S.:1975, Solar Phys. 42 135

Tousey, R., Bartoe, J.-D.F., Bohlin, J.D., Brueckner, G.E., Purcell, J.D., Scherrer, V.E., Sheeley, N.R.(Jr.), Schumacher, R.J. and Van Hoosier, M.E.:1973, Solar Phys. 33 256

Tucker, W.H. and Koren, M.:1971, Astrophys. J. 168 283

Underwood, J.H., Chapman, G.A., Janssens, T.J., Landecker, P.B., Mayfield, E.B., McKenzie, D.L., Vorpahl, J.A., Walker, A.B.C.(Jr.), Milligan, J.E., de Loach, A.C., Hoover, R.B., McGuire, J.G. and Wilson, R.M.:1974, I.A.U. COSPAR Symposium 68 179

Vaiana, G.S. and Rosner, R.:1978, Ann. Rev. Astron. Astrophys. 16 393

Vaiana, G.S., Davis, J.M., Giacconi, R., Krieger, A.S., Silk, J.K., Timothy, A.F. and Zombeck, M.:1973, Astrophys. J. 185 L47

Vaiana, G.S., Krieger, A.S. and Timothy, A.F.:1973, Solar Phys. 32 81

Vernazza, J.E. and Mason, H.E.:1978, Astrophys. J. 226 720

Vernazza, J.E. and Raymond, J.C.:1979, Astrophys. J. 228 L89

Vesecky, J.F., Antiochos, S.K. and Underwood, J.H.:1979, Astrophys. J. 233 987

Wentzel, D.G.:1974, Solar Phys. 39 129

Wentzel, D.G.:1976, Solar Phys. 50 343

Withbroe, G.L.:1970, Solar Phys. 11 42

Withbroe, G.L.:1980, private communication to Priest, E.R.

Withbroe, G.L. and Noyes, R.W.:1977, Ann. Rev. Astron. Astrophys. 15 363